LARGE DEFORMATION ANALYSIS OF LAMINATED COMPOSITE STRUCTURES BY A CONTINUUM-BASED SHELL ELEMENT WITH TRANSVERSE DEFORMATION

by

Pey M. Wung

Dissertation submitted to the Faculty of the

Virginia Polytechnic Institute and State University

in partial fulfillment of the requirements for the degree of

Doctor of Philosophy

in

Engineering Mechanics

APPROVED:

J.N. Reddy, Chairman

D. Post

D.T. Mook

Z. Gurdal

E. Green

June, 1989

Blacksburg, Virginia

LARGE DEFORMATION ANALYSIS OF LAMINATED COMPOSITE STRUCTURES BY A CONTINUUM-BASED SHELL ELEMENT WITH TRANSVERSE DEFORMATION

by

Pey M. Wung

J.N. Reddy, Chairman

Engineering Mechanics

(ABSTRACT)

In this work, a finite element formulation and associated computer program is developed for the transient large deformation analysis of laminated composite plate/shell structures. In order to satisfy the plate/shell surface traction boundary conditions and to have accurate stress description while maintaining the low cost of the analysis, a newly assumed displacement field theory is formulated by adding higher-order terms to the transverse displacement component of the first-order shear deformation theory. The laminated shell theory is formulated using the Updated Lagrangian description of a general continuum-based theory with assumptions on thickness deformation. The transverse deflection is approximated through the thickness by a quartic 1olynomial of the thickness coordinate. As a result both the plate/shell surface tractions (including nonzero tangential tractions and nonzero normal pressure) and the interlaminar shear stress continuity conditions at interfaces are satisfied simultaneously. Furthermore, the rotational degree of freedoms be-

come layer dependent quantities and the laminate possesses a transverse deformation capability(i.e the normal strain is no longer zero).

Analytical integration through the thickness direction is performed for both the linear analysis and the nonlinear analysis. Resultants of the stress integrations are expressed in terms of the laminate stacking sequence. Consequently, the laminate characteristics in the normal direction can be evaluated precisely and the cost of the overall analysis is reduced. The standard Newmark method and the modified Newton Raphson method are used for the solution of the nonlinear dynamic equilibrium equations.

Finally, a variety of numerical examples are presented to demonstrate the validity and efficiency of the finite element program developed herein.

Acknowledgements

To begin with, I like to express heartfelt thanks to my major advisor, Professor J. N. Reddy for his encouragement and valuable suggestions provided throughout this research work. Also I would like to thank Professors D. Post, D. Mook, Z. Gurdal and E. Green for serving as members of my thesis committee.

I am indebted to , (currently director of Engineering School of University of Texas at San Antonio) for his encouragement and support. The support of my education at VPI&SU from the Materials Division of the Office of Naval Research through Contract N00014-82-K-0185 is gratefully acknowledged.

I wish to express my deep appreciation and love to my father, mother, brothers, sister and two daughters. Without their love, encouragement and patience, my education at VPI&SU would never be completed.

Finally, special thanks are given to my wife, for her patience in waiting and working hard to support the family financially.

Table of Contents

INTRODUCTION

1.1 MOTIVATION

Composite materials have increasingly been accepted as ideal materials in the high-performance but weight-sensitive structures such as space vehicles and automobiles. This is due to the high strength-to-weight and high stiffness-to-weight ratios offered by composite materials. Laminated composite materials consist of two or more layers of different materials so as to achieve desired structural properties. Since laminated composite are made of different material layers, the material property is discontinuous through its thickness. The material miss-match across the laminate interfaces, bending-stretching coupling, and geometric nonlinear effects make the analysis of composite structures very complicated. Consequently, the old design procedures, traditional analysis methods and experimental experience obtained from isotropic materials can not be applied to composite materials directly. New design procedures, analysis methods and testing techniques should be developed to ensure the integrity of laminated composite structures.

Composite laminates place special kinematic modeling requirements because of their low modulus transverse to the plane of the laminae. The Kirchhoff plate theory, known as the classical laminate theory, underestimates the deflections and over predicts the natural frequencies and critical buckling loads [1]. The first-order shear deformation theory (FSDT), known as the Mindlin plate theory, gives excellent results for global response characteristics, such as displacements, natural frequencies and buckling loads. But this theory yields very poor results for the interlaminar shear stresses. The interlaminar shear stresses obtained from FSDT through the constitutive relations are discontinuous across the laminar interfaces [1]. Obviously these results can not satisfy the lamina interface continuity conditions and the equilibrium conditions, which are the major sources of layer debonding/delamination as proved by many micromechanics studies [2,3] of composite materials. The well-known free edge effect [4] is a good example of this category.

Many refined higher order shear deformation theories [5,6] were introduced to improve this defect. For instance, the most recent and probably the most advanced one is the Generalized Laminated Plate Theory (GLPT) developed by Reddy [7] and advanced by his colleagues [8]. This theory is based on an assumed layer-wise displacement field, and it yields accurate stresses, including the interlaminar shear stresses. However, nonzero plate/shell surface boundary conditions are not commonly satisfied by the existing theories in the literature. Furthermore, these theories often neglect the transverse normal stress.

Ignoring normal stress may not introduce any significant error in the linear analysis. However, in nonlinear analysis the situation is quite different; the tangential stiffness and the out-of-balance force vector are stress dependent quantities. Ignoring the

normal stress together with the unrealistic distribution of the in-plane shear stresses will slow the numerical convergence and yield less accurate results. Because of this reason there exists a need for an improved theory which can relax the Kirchhoff assumptions completely. Also, all plate and shell theories are based on certain assumptions concerning kinematics and/or stress distributions. In a continuum-based theories such assumptions are not required. Motivated by these observations, the present study was undertaken to develop a continuum-based shell finite element that accounts for transverse stresses, nonzero surface tractions, and large deflections. The literature reviewed in the next section forms a background for the present study.

1.2 LITERATURE REVIEW

The earliest need for shell structure design probably came with the development of the steam engine. However, it was not until 1888, that the first general theory was presented by Love. Surveys of various classical shell theories can be found in the works of Naghdi [9] and Bert [10,11]. These theories, known as the Love's first approximation theories [12], are expected to yield sufficiently accurate results when (i) the thickness-to-span ratio is small; (ii) the dynamic excitations are within the low-frequency range; (iii) the material anisotropy is not severe. However, application of such theories to layered anisotropic composite shell could lead to as much as 30% or more errors.

Ambartsumyan [13,14] was considered to be the first one to analyze laminates that incorporated the bending-stretching coupling. In 1962, Dong, Pister and Taylor [15] formulated a thin laminated anisotropic shells theory. Cheng and Ho [16] presented an analysis of laminated anisotropic cylindrical shells using Flugge's shell theory [17]. The first approximation theory for the unsymmetrical deformation of nonhomogeneous, anisotropic, elastic cylindrical shells was derived by Widera [18,19]. An exposition of various shell theories can be found in the article by Bert [20].

The effect of transverse shear deformation and transverse isotropy as well as thermal expansion through the shell thickness were considered by Gulati and Essenberg [21] and Zukas and Vinson [22]. Dong and Tso [23] presented a theory applicable to layered, orthotropic cylindrical shells. Whitney and Sun [24] developed a higher order shear deformation theory. This theory is based on a displacement field in which the displacements in the surface of the shell are expanded as linear function of the thickness coordinate. Reddy [25] presented a shear deformation version of the Sander's shell theory for laminated composite shells. As far as the finite element analysis of shells is concerned, the early works can be attributed to those by Dong [26], Dong and Selna [27], Wilson and Parsons [28], and Schmit and Monforton [29]. The studies of those works are confined to the analysis of the orthotropic shells of revolution. Other finite element analyses of laminated anisotropic composite shells include the works of Panda and Natarajan [30], Shivakumar and Krishna Murty [31], Rao [32], Seide and Chang [33], Venkatesh and Rao [34] and Reddy and his colleagues [35,36,37,38], among others.

Geometrically nonlinear laminated composite structure finite element analysis has recently been studied by quite a few researchers. For instance, Noor and his col-

leagues [39,40,41] investigated the static response of a nonlinear shell via mixed isoparametric elements. Chang and Swamiphakdi [42] presented a updated Lagrangian formulation of 3D degenerated shell element for geometrically nonlinear bending analysis of laminated composite shells. However no numerical results are given to laminated shell in their examples. Chao and Reddy [43] presented a total Lagrangian formulation for a 3D degenerated shell with application to composite shells. Liao and Reddy [45] extended the work done in [44] to develop a solid-shell transition element for geometrically nonlinear analysis of laminated composite structures [45].

In reviewing finite element applications, three approaches are used for analyzing a plate/shell type structures. The first one is the 2D shell element approach. For instance, Reddy [46] presented a generalization of Sander's shell theory(1959) to laminated, doubly curved anisotropic shell. In this approach, a well developed plate or shell theory is adopted. Through-the-thickness analytical integration together with the plate/shell assumptions reduce a 3D continuum field problem to a 2D one such that problems can be solved in a relatively simple and efficient way. However since a predefined plate/shell theory is being used, the geometrical shape can not be chosen arbitrarily. Only the theory specified shape can be used (to fit the theory) in this approach. Thus the application of this approach is limited. The element based on Sander's doubly curved shell theory is good for a plate surface, a cylindrical surface or a spherical surface. But it may not be good for a twisted surface or a distorted surface [1,47]. Another shortcoming of using this approach to a general three dimensional shell structure is the stiffness matrix transformation problem. Ideally, one can divide a general three-dimensional shell structure into a series of flat, cylindrical or even doubly curved surfaces such that plate element, cylindrical element and curved

element can be used to simulate their corresponding surfaces. However, a fictitious rotational stiffness should be introduced [47] in element stiffness assembly. Research conducted by Greene, Stome and Weikel [48] indicate that the accuracy of the analysis is controlled by the size of the fictitious rotational stiffness [47]. This means an iteration procedure should be used to decide the fictitious rotational stiffness before a final answer can be accepted. This shortcoming plus the increase of the problem size (from a 5-dof problem to a 6-dof problem) makes this approach almost impractical for a transient nonlinear structural analysis of a general three-dimensional shell. But it is a very ideal tool for structures which can nearly maintain its shape to the theory specified shape.

The second approach is to model shell with three-dimensional elements [49]. No particular plate/shell theory is followed in this approach. However, in this approach numerical integrations must be performed in all three dimensions. This shortcoming plus the high cost of a 3D modeling makes this approach relatively expensive, precludes its use in most composite structural analysis.

The third approach is the degenerated 3D approach. Ahmad [50] was considered to be the first one using this approach. It is called a degenerated 3D approach because a three-dimensional elasticity is degenerated to a 2D model [51]. In this approach, the structure can be directly discretized using 2D finite elements without applying any plate or shell theory. This feature coupled with the 2D finite element modeling enable the 3D degenerate element (or continuum based 2D element) to solve most shell structure. However, formulation of this approach is much complex than the other two. This element also requires numerical integration in all three dimensions [50,51], which means numerical integration through-the-thickness must be carried out. Re-

cent research by Chao and Reddy [43] indicates that in this approach there may exist a way to avoid the numerical integration through the thickness. Current work verified this concept and extended it into geometric nonlinear formulation. Mathematical formulations derived in section 5.3.2 of this work completes the required analytical integration quantities for laminated plate/shell structural analysis.

1.3 PRESENT WORK

The standard Kirchhoff assumptions are; (i) straight lines normal to the mid-surface remain straight and normal after deformation, (ii) the displacement gradients are small, (iii) the length of a normal remains unchanged, (iv) the effects of normal stress are small and it can be neglected. Thus the classical plate theory does not account for the transverse deformations. The first order shear deformation theory [FSDT] removes the normality assumption. Consequently it accounts for constant state of transverse shear stresses but does not satisfy the non-zero surface traction conditions. The refined higher order shear deformation theory including the latest Generalized Laminated Plate Theory can satisfy stress-free boundary condition and continuous shear stress distribution through the thickness. However, Kirchhoff's last assumption is still not removed in these theories.

In all the mentioned theories, improvements are made by adding higher order terms to the in-plane displacements. In this work, contrary to the traditional way, higher order terms are added to the out-of-plane displacement. The purpose of doing so is to relax the last two assumptions of Kirchhoff theory. As a result, boundary condi-

tions on the plate/shell surfaces and the interlaminar shear stress continuity conditions across the laminar interfaces are all satisfied simultaneously. In applying this new idea to the plate/shell structural analysis, the first order shear deformation theory (FSDT) is adopted as a base line in the current work.

The goal of this research is to develop a finite element program for general dynamic, geometrically nonlinear laminated composite structural analysis. This program has three features.

1. Generality

   A continuum based shell element approach is being used. Shape of the shell is not bounded by any plate or shell theory.

2. Computational Efficiency

   Using FSDT as a base line, refined displacement and stress fields are recovered. Thus the cost of the analysis is at the same level as the FSDT analysis. Besides, the integration through the shell thickness is performed analytically. Thus, the whole cost of analysis is relatively low.

3. Completeness

   Higher order terms are added to the out-of-plane displacement component such that the surface boundary conditions and the continuity conditions at the laminar interfaces are satisfied. As a result, the rotational degree of freedom become layer dependent quantities. This allows a more accurate description of the kinematics

and stress state in a composite laminate.

The finite element form of the equations of motion is derived in Chapter 2. A review of an orthotropic single-layer constitutive equations is presented in Chapter 3. In Chapter 4, a new set of higher-order displacement field and a stress recovery iteration technique are developed. This technique is used to recover the refined displacement fields of each layer and to satisfy all the laminate surface boundary conditions and the interface continuity conditions. In Chapter 5, a continuum-based shell element is developed for transient large deformation shell structural analyses, and analytical integrations through the shell thickness is performed. Several illustrative problems are presented in Chapter 6. Conclusions are presented in Chapter 7.

EQUATIONS OF MOTION

2.1 UPDATED LAGRANGIAN FORMULATION

By means of the principle of virtual displacements, the Updated Lagrangian description of the motion of a continuous body, can be expressed as [44,45]

$$\int_{t_V} {}^{t+\Delta t}_{t}S_{ij}\, \delta\, {}^{t+\Delta t}_{t}\varepsilon_{ij}\, d^tV = {}^{t+\Delta t}_{t}R \tag{2.1}$$

where S_{ij} are the 2nd Piola-Kirchhoff stress components and ε_{ij} are the Green-Lagrange strain tensor components. The 2nd Piola-Kirchhoff stress tensor relates to the Cauchy stress tensor τ by

$${}^{t+\Delta t}_{t}S_{ij} = \frac{{}^{t}\rho}{{}^{t+\Delta t}\rho}\, {}^{t}_{t+\Delta t}x_{i,m}\ {}^{t+\Delta t}\tau_{mn}\ {}^{t}_{t+\Delta t}x_{j,n} \tag{2.2}$$

where ρ represents the material density, and ${}^{t}_{t+\Delta t}x_{j,n} = \dfrac{\partial {}^{t}x_j}{\partial {}^{t+\Delta t}x_n}$.

The variation of the Green-Lagrange strain tensor is

$$\delta {}^{t+\Delta t}_{t}\varepsilon_{ij} = \delta \frac{1}{2}({}^{t+\Delta t}_{t}u_{i,j} + {}^{t+\Delta t}_{t}u_{j,i} + {}^{t+\Delta t}_{t}u_{k,i}\,{}^{t+\Delta t}_{t}u_{k,j}) \tag{2.3}$$

The applied load is

$${}^{t+\Delta t}R = \int_{0_V} {}^{t+\Delta t}_{0}f_i^B\,\delta u_i\,d^0V + \int_{0_A} {}^{t+\Delta t}_{0}T_i\,\delta u_i^S\,d^0A \tag{2.4}$$

when the loading is not a function of deformation, and

$${}^{t+\Delta t}R = \int_{t_V} {}^{t+\Delta t}_{t}f_i^B\,\delta u_i\,d^tV + \int_{t_A} {}^{t+\Delta t}_{t}T_i\,\delta u_i^S\,d^tA \tag{2.5}$$

if the loading is a function of deformation. Here f^B represents the body force, and T represents the surface traction.

In case of transient analysis, by means of D'Alembert's principle, the inertia force can be included as a part of the body force by

$$-\int_{t_V} {}^{t}\rho\,{}^{t}\ddot{u}_i\,\delta u_i\,d^tV \tag{2.6}$$

Hence, assuming that the applied loading is a function of deformation, the equations of motion for a large displacement and large rotation continuous body can be expressed in integral form

$$\int_{{}^tV} {}^t\rho\, {}^{t+\Delta t}\ddot{u}_i\, \delta u_i\, d^tV + \int_{{}^tV} {}^{t+\Delta t}_{\ t}S_{ij}\, \delta\, {}^{t+\Delta t}_{\ t}\varepsilon_{ij}\, d^tV = \int_{{}^tV} {}^{t+\Delta t}_{\ t}f_i^B\, \delta u_i\, d^tV + \int_{{}^tA} {}^{t+\Delta t}_{\ t}T_i\, \delta u_i^s\, d^tA \quad (2.7)$$

2.2 INCREMENTAL DECOMPOSITION

The 2nd Piola-Kirchhoff stress components with respect to current configuration (time = t) can be expressed as

$$ {}^{t+\Delta t}_{\ t}S_{ij} = {}^t_tS_{ij} + {}_tS_{ij} = {}^t\tau_{ij} + {}_tS_{ij} \quad (2.8)$$

where ${}^t_tS_{ij} \equiv {}^t\tau_{ij}$, ${}^t\tau_{ij}$ are the Cauchy stress components and ${}_tS_{ij}$ are the incremental stress components. The Green-Lagrange strains decomposed according to the equation

$$ {}^{t+\Delta t}_{\ t}\varepsilon_{ij} = \frac{1}{2}\left({}_tu_{i,j} + {}_tu_{j,i} + {}_tu_{k,i}\ {}_tu_{k,j}\right) = {}_te_{ij} + {}_t\eta_{ij} = {}_t\varepsilon_{ij}$$

in which the following notation is used

$${}_te_{ij} = \frac{1}{2}\left({}_tu_{i,j} + {}_tu_{j,i}\right) \text{ and } {}_t\eta_{ij} = \frac{1}{2}\,{}_tu_{k,i}\ {}_tu_{k,j} \quad (2.9)$$

where ${}_t\varepsilon_{ij}$ denotes the incremental Green-Lagrange strain components and ${}_te_{ij}$ and ${}_t\eta_{ij}$ denote the linear and nonlinear parts of ${}_t\varepsilon_{ij}$, respectively.

Recalling the stress and strain relationship ${}_tS_{ij} = {}_tC_{ijkl}\ {}_t\varepsilon_{kl}$, equation(2.8) can be written as

$${}^{t+\Delta t}_{t}S_{ij} = {}^{t}\tau_{ij} + {}_{t}S_{ij} = {}^{t}\tau_{ij} + {}_{t}C_{ijkl}\,{}_{t}\varepsilon_{kl}$$

Substituting this expression and equation (2.9) into equation (2.7), one obtains

$$\int_{{}^{t}V} \rho_o\, {}^{t+\Delta t}\ddot{u}_i\, \delta u_i\, d^{t}V + \int_{{}^{t}V} {}_{t}C_{ijkl}\, {}_{t}\varepsilon_{kl}\, \delta_{t}\varepsilon_{ij}\, d^{t}V + \int_{{}^{t}V} {}^{t}\tau_{ij}\, \delta_{t}\eta_{ij}\, d^{t}V = {}^{t+\Delta t}R - \int_{{}^{t}V} {}^{t}\tau_{ij}\, \delta_{t}e_{ij}\, d^{t}V \tag{2.10}$$

where ${}^{t+\Delta t}R$ is defined by either equation (1.4) or equation (1.5) depending on the loading conditions, and ${}^{t}\rho = \rho_0 =$ constant.

Using the approximation ${}_{t}S_{ij} \cong {}_{t}C_{ijkl}\, e_{kl}$ and $\delta_{t}\varepsilon_{ij} \cong \delta_{t}e_{ij}$, the equation of motion (2.10) can be simplified to

$$\int_{{}^{t}V} \rho_o\, {}^{t+\Delta t}\ddot{u}_i\, \delta u_i\, d^{t}V + \int_{{}^{t}V} {}_{t}C_{ijkl}\, {}_{t}e_{kl}\, \delta_{t}e_{ij}\, d^{t}V + \int_{{}^{t}V} {}^{t}\tau_{ij}\, \delta_{t}\eta_{ij}\, d^{t}V = {}^{t+\Delta t}R - \int_{{}^{t}V} {}^{t}\tau_{ij}\, \delta_{t}e_{ij}\, d^{t}V \tag{2.11}$$

This is the incremental Updated Lagrangian description of the equation of motion that a transient nonlinear continuum medium has to follow.

2.3 FINITE ELEMENT MODEL

Let

[H] = the displacement interpolation matrix ;

$\{u^e\}$ = nodal displacement vector of element "e"

ϕ_i = shape function of nodal point "i"

$\{{}^t\tau\}$ = stress vector (2.12)

$[{}^t\tau]$ = stress matrix

[L] = linear differential operator

[B] = [L][H] strain-displacement matrix

$\{\varepsilon\} = [B]\{u^e\}$ strain of any point inside element "e"

{u} = displacement vector of any point inside an element i.e $\{u\} = [H]\{u^e\}$,then the continuous incremental Updated Lagrangian description of equation of motion equation (2.11) can be replaced by a discretized finite element model

$$[{}_tM]\{{}^{t+\Delta t}\ddot{u}\} + ([{}_tK_L] + [{}_tK_{NL}])\{\delta u\} = \{{}^{t+\Delta t}R\} - \{{}^tU\} \tag{2.13}$$

The consistent mass matrix is

$$[{}_tM] = \int_{{}^tV} \rho\,[H]^T[H]\,d^tV \tag{2.14}$$

The linear stiffness matrix is

$$[{}_tK_L] = \int_{{}^tV} [{}_tB_L]^T[{}_tC][{}_tB_L]\,d^tV \tag{2.15}$$

The nonlinear stiffness matrix is

$$[{}_tK_{NL}] = \int_{{}_tV} [{}_tB_{NL}]^T [{}^t\tau][{}_tB_{NL}] d^tV \tag{2.16}$$

The stress induced reaction force is

$$\{{}^tU\} = \int_{{}_tV} [{}_tB_L]^T \{{}^t\tau\} d^tV \tag{2.17}$$

SINGLE PLY CONSTITUTIVE RELATIONS

3.1 ASSUMPTIONS

The macroscopic view of composite material [57] generally assumes that there is perfect bonding between the matrix and fiber, each ply is homogeneous and linearly elastic. It has three elastic symmetric planes perpendicular to each other which requires nine independent material constants to describe its constitutive behavior. Also, it is assumed to be free from any manufacturing defect and residual stresses. In this work, these assumptions are all accepted. Besides, the material's behavior is examined only as an average apparent properties of the composite layer. The effects of thermal, moisture and viscoelastic influences are ignored.

3.2 MATERIAL PROPERTIES IN PRINCIPAL COORDINATES

It has been proved in continuum mechanics [58] that an orthotropic material has three orthogonal elastic symmetrical planes with nine independent material properties. According to Hooke's law, in the material principal coordinates(1,2,3), the stress-strain relations are given by

$$\begin{Bmatrix} \varepsilon_{11} \\ \varepsilon_{22} \\ \varepsilon_{33} \\ \gamma_{23} \\ \gamma_{13} \\ \gamma_{12} \end{Bmatrix} = \begin{bmatrix} \frac{1}{E_1} & \frac{-\nu_{21}}{E_2} & \frac{-\nu_{31}}{E_3} & 0 & 0 & 0 \\ \frac{-\nu_{12}}{E_1} & \frac{1}{E_2} & \frac{-\nu_{32}}{E_3} & 0 & 0 & 0 \\ \frac{-\nu_{13}}{E_1} & \frac{-\nu_{23}}{E_2} & \frac{1}{E_3} & 0 & 0 & 0 \\ 0 & 0 & 0 & \frac{1}{G_{23}} & 0 & 0 \\ 0 & 0 & 0 & 0 & \frac{1}{G_{13}} & 0 \\ 0 & 0 & 0 & 0 & 0 & \frac{1}{G_{12}} \end{bmatrix} \begin{Bmatrix} \sigma_{11} \\ \sigma_{22} \\ \sigma_{33} \\ \sigma_{23} \\ \sigma_{13} \\ \sigma_{12} \end{Bmatrix} \tag{3.1}$$

$$\begin{Bmatrix} \sigma_{11} \\ \sigma_{22} \\ \sigma_{33} \\ \sigma_{23} \\ \sigma_{13} \\ \sigma_{12} \end{Bmatrix} = \begin{bmatrix} C_{11} & C_{12} & C_{13} & 0 & 0 & 0 \\ C_{12} & C_{22} & C_{23} & 0 & 0 & 0 \\ C_{13} & C_{23} & C_{33} & 0 & 0 & 0 \\ 0 & 0 & 0 & C_{44} & 0 & 0 \\ 0 & 0 & 0 & 0 & C_{55} & 0 \\ 0 & 0 & 0 & 0 & 0 & C_{66} \end{bmatrix} \begin{Bmatrix} \varepsilon_{11} \\ \varepsilon_{22} \\ \varepsilon_{33} \\ \gamma_{23} \\ \gamma_{13} \\ \gamma_{12} \end{Bmatrix} \tag{3.2}$$

where

$$C_{11} = \frac{E_1(1 - \nu_{23}\nu_{32})}{\Delta} \qquad C_{12} = \frac{E_1(\nu_{21} + \nu_{31}\nu_{23})}{\Delta}$$

$$C_{22} = \frac{E_2(1 - \nu_{13}\nu_{31})}{\Delta} \qquad C_{13} = \frac{E_3(\nu_{13} + \nu_{12}\nu_{23})}{\Delta}$$

$$C_{33} = \frac{E_3(1 - \nu_{12}\nu_{21})}{\Delta} \qquad C_{23} = \frac{E_3(\nu_{23} + \nu_{21}\nu_{13})}{\Delta}$$

$$C_{44} = G_{23} \quad C_{55} = G_{13} \quad C_{66} = G_{12} \qquad \Delta = 1 - \nu_{12}\nu_{21} - \nu_{23}\nu_{32} - \nu_{31}\nu_{13} - 2\nu_{21}\nu_{32}\nu_{13}$$

3.3 MATERIAL PROPERTIES IN PROBLEM COORDINATES

The transformation between the problem coordinate system (x,y,z) and the principal material coordinate system (1,2,3), as depicted in Figure 3.1, is

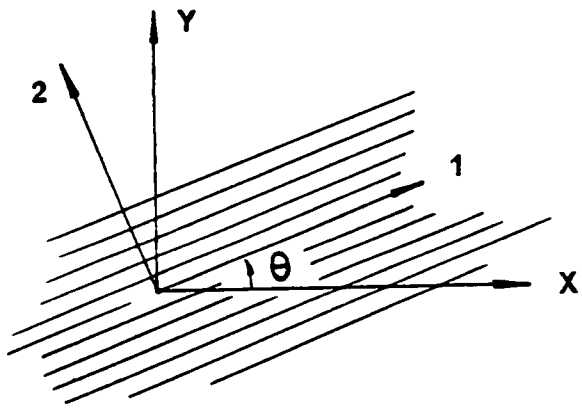

Figure 3.1 A single ply

$$\{\sigma\}_1 = [T_1]\{\sigma\}_x \tag{3.3}$$

$$\{\varepsilon\}_1 = [T_2]\{\varepsilon\}_x \tag{3.4}$$

where

$$[T_1] = \begin{bmatrix} m^2 & n^2 & 0 & 0 & 0 & 2mn \\ n^2 & m^2 & 0 & 0 & 0 & -2mn \\ 0 & 0 & 1 & 0 & 0 & 0 \\ 0 & 0 & 0 & m & -n & 0 \\ 0 & 0 & 0 & n & m & 0 \\ -mn & mn & 0 & 0 & 0 & m^2 - n^2 \end{bmatrix}$$

and $[T_2] = [T_1]^{-T}$ with the symbol $m = \cos\theta$, $n = \sin\theta$.

Substituting equation (3.1) into equation (3.3) and using equation (3.4), the transformed 3-D stiffness matrix $[\bar{C}]$ is obtained as

$$\{\sigma\}_x = [T_1]^{-1}\{\sigma_1\} = [T_1]^{-1}[C]\{\varepsilon_1\} = [T_1]^{-1}[C][T_2]\{\varepsilon\}_x = [\bar{C}]\{\varepsilon\}_x \tag{3.5}$$

Hence $[\bar{C}] = [T_1]^{-1}[C][T_2]$

$$= \begin{bmatrix} \overline{C}_{11} & \overline{C}_{12} & \overline{C}_{13} & 0 & 0 & \overline{C}_{16} \\ \overline{C}_{12} & \overline{C}_{22} & \overline{C}_{23} & 0 & 0 & \overline{C}_{26} \\ \overline{C}_{13} & \overline{C}_{23} & \overline{C}_{33} & 0 & 0 & \overline{C}_{36} \\ 0 & 0 & 0 & \overline{C}_{44} & \overline{C}_{45} & 0 \\ 0 & 0 & 0 & \overline{C}_{45} & \overline{C}_{55} & 0 \\ \overline{C}_{16} & \overline{C}_{26} & \overline{C}_{36} & 0 & 0 & \overline{C}_{66} \end{bmatrix}$$

where

$$\overline{C}_{11} = m^4 C_{11} + 2m^2 n^2 (C_{12} + 2C_{66}) + n^4 C_{22}$$

$$\overline{C}_{12} = m^2 n^2 (C_{11} + C_{22} - 4C_{66}) + (m^4 + n^4) C_{12}$$

$$\overline{C}_{13} = m^2 C_{13} + n^2 C_{23}$$

$$\overline{C}_{16} = mn[m^2 (C_{11} - C_{12} - 2C_{66}) + n^2 (C_{12} - C_{22} + 2C_{66})]$$

$$\overline{C}_{22} = n^4 C_{11} + 2m^2 n^2 (C_{12} + 2C_{66}) + m^4 C_{22}$$

$$\overline{C}_{23} = n^2 C_{13} + m^2 C_{23}$$

$$\overline{C}_{26} = mn[n^2 (C_{11} - C_{12} - 2C_{66}) + m^2 (C_{12} - C_{22} + 2C_{66})]$$

$$\overline{C}_{33} = C_{33}$$

$$\overline{C}_{36} = mn(C_{13} - C_{23})$$

$$\overline{C}_{44} = m^2 C_{44} + n^2 C_{55}$$

$$\overline{C}_{45} = mn(C_{55} - C_{44})$$

$$\overline{C}_{55} = n^2 C_{44} + m^2 C_{55}$$

$$\overline{C}_{66} = m^2 n^2 (C_{11} - C_{12} - C_{22}) + + C_{66} (m^2 - n^2)^2$$

3.4 REDUCED STIFFNESSES

The general three dimensional stress-strain relations defined in equation (3.5), can be simplified by rewriting it in two parts

$$\begin{Bmatrix} \sigma_x \\ \sigma_y \\ \sigma_z \\ \sigma_{xy} \end{Bmatrix} = \begin{bmatrix} \bar{C}_{11} & \bar{C}_{12} & \bar{C}_{13} & \bar{C}_{16} \\ \bar{C}_{12} & \bar{C}_{22} & \bar{C}_{23} & \bar{C}_{26} \\ \bar{C}_{13} & \bar{C}_{23} & \bar{C}_{33} & \bar{C}_{36} \\ \bar{C}_{16} & \bar{C}_{26} & \bar{C}_{36} & \bar{C}_{66} \end{bmatrix} \begin{Bmatrix} \varepsilon_x \\ \varepsilon_y \\ \varepsilon_z \\ \gamma_{xy} \end{Bmatrix} \tag{3.6}$$

and

$$\begin{Bmatrix} \sigma_{yz} \\ \sigma_{xz} \end{Bmatrix} = \begin{bmatrix} \bar{C}_{44} & \bar{C}_{45} \\ \bar{C}_{45} & \bar{C}_{55} \end{bmatrix} \begin{Bmatrix} \gamma_{yz} \\ \gamma_{xz} \end{Bmatrix} \tag{3.7}$$

from which the normal strain is defined by $\varepsilon_z = \frac{\sigma_z}{\bar{C}_{33}} - \frac{\bar{C}_{13}}{\bar{C}_{33}}\varepsilon_x - \frac{\bar{C}_{23}}{\bar{C}_{33}}\varepsilon_y - \frac{\bar{C}_{36}}{\bar{C}_{33}}\gamma_{xy}$.

Substituting last expression into equation (2.6) yields

$$\begin{Bmatrix} \sigma_x \\ \sigma_y \\ \sigma_z \\ \sigma_{xy} \end{Bmatrix} = \begin{bmatrix} \bar{C}_{11} & \bar{C}_{12} & \bar{C}_{13} & \bar{C}_{16} \\ \bar{C}_{12} & \bar{C}_{22} & \bar{C}_{23} & \bar{C}_{26} \\ \bar{C}_{13} & \bar{C}_{23} & \bar{C}_{33} & \bar{C}_{36} \\ \bar{C}_{16} & \bar{C}_{26} & \bar{C}_{36} & \bar{C}_{66} \end{bmatrix} \begin{Bmatrix} \varepsilon_x \\ \varepsilon_y \\ \frac{\sigma_z}{\bar{C}_{33}} - \frac{\bar{C}_{13}}{\bar{C}_{33}}\varepsilon_x - \frac{\bar{C}_{23}}{\bar{C}_{33}}\varepsilon_y - \frac{\bar{C}_{36}}{\bar{C}_{33}}\gamma_{xy} \\ \gamma_{xy} \end{Bmatrix} \tag{3.8}$$

Writing these stress components into a condensed form, equation (3.8) becomes

$$\begin{Bmatrix} \sigma_x \\ \sigma_y \\ \sigma_z \\ \sigma_{xy} \end{Bmatrix} = \begin{bmatrix} \bar{Q}_{11} & \bar{Q}_{12} & \bar{Q}_{13} & \bar{Q}_{16} \\ \bar{Q}_{12} & \bar{Q}_{22} & \bar{Q}_{23} & \bar{Q}_{26} \\ \bar{Q}_{13} & \bar{Q}_{23} & \bar{Q}_{33} & \bar{Q}_{36} \\ \bar{Q}_{16} & \bar{Q}_{26} & \bar{Q}_{36} & \bar{Q}_{66} \end{bmatrix} \begin{Bmatrix} \varepsilon_x \\ \varepsilon_y \\ 0 \\ \gamma_{xy} \end{Bmatrix} + \begin{Bmatrix} \bar{C}_{13}/\bar{C}_{33} \\ \bar{C}_{23}/\bar{C}_{33} \\ 1 \\ \bar{C}_{36}/\bar{C}_{33} \end{Bmatrix} \sigma_z \tag{3.9}$$

provided that

$$\bar{Q}_{13}\varepsilon_x + \bar{Q}_{23}\varepsilon_y + \bar{Q}_{36}\gamma_{xy} = 0 \tag{3.10}$$

where $\bar{Q}_{ij} = \bar{C}_{ij} - \bar{C}_{i3}\dfrac{\bar{C}_{3j}}{\bar{C}_{33}}$ (for i = 1,2,3,6 and j = 1,2,6).

Eliminating the normal stress σ_z, the generalized Hooke's law becomes :

$$\begin{Bmatrix} \sigma_x \\ \sigma_y \\ \sigma_{xy} \end{Bmatrix} = \begin{bmatrix} \bar{Q}_{11} & \bar{Q}_{12} & \bar{Q}_{16} \\ \bar{Q}_{12} & \bar{Q}_{22} & \bar{Q}_{26} \\ \bar{Q}_{16} & \bar{Q}_{26} & \bar{Q}_{66} \end{bmatrix} \begin{Bmatrix} \varepsilon_x \\ \varepsilon_y \\ \gamma_{xy} \end{Bmatrix} \tag{3.11}$$

and

$$\begin{Bmatrix} \sigma_{yz} \\ \sigma_{xz} \end{Bmatrix} = k^2 \begin{bmatrix} \bar{Q}_{44} & \bar{Q}_{45} \\ \bar{Q}_{45} & \bar{Q}_{55} \end{bmatrix} \begin{Bmatrix} \gamma_{yz} \\ \gamma_{xz} \end{Bmatrix} \tag{3.12}$$

where k^2 is the shear correction factor. Comparing equation (3.11) and equation (3.12) with equation (3.6) and equation (3.7), it is found that $\bar{Q}_{ij}$ are equal to or smaller than $\bar{C}_{ij}$. Thus they are called "reduced stiffnesses".

TRANSVERSE DEFORMATION THEORY TO PLATES

In this chapter, a first-order (for u and v) shear/fourth-order (for w) transverse deformation theory is introduced. Instead of using this theory directly to develop a finite element model, a technique is developed to recover all the "refined" generalized displacements for each individual layer after the FSDT "averaged" generalized displacements are obtained. As a part of the refined displacement recovery, the plate surface boundary conditions and the interlaminar interface continuity conditions are all satisfied identically. The following review of the existing theories provides a background for present theory.

4.1 A REVIEW OF PLATE THEORIES

A transversely and edge loaded plate is shown in Figure 4.1. The transient displacement components(u,v and w) at any location inside the plate are functions of the coordinates(x,y and z) and time(t). These displacement components can be expanded into Taylor's series about z :

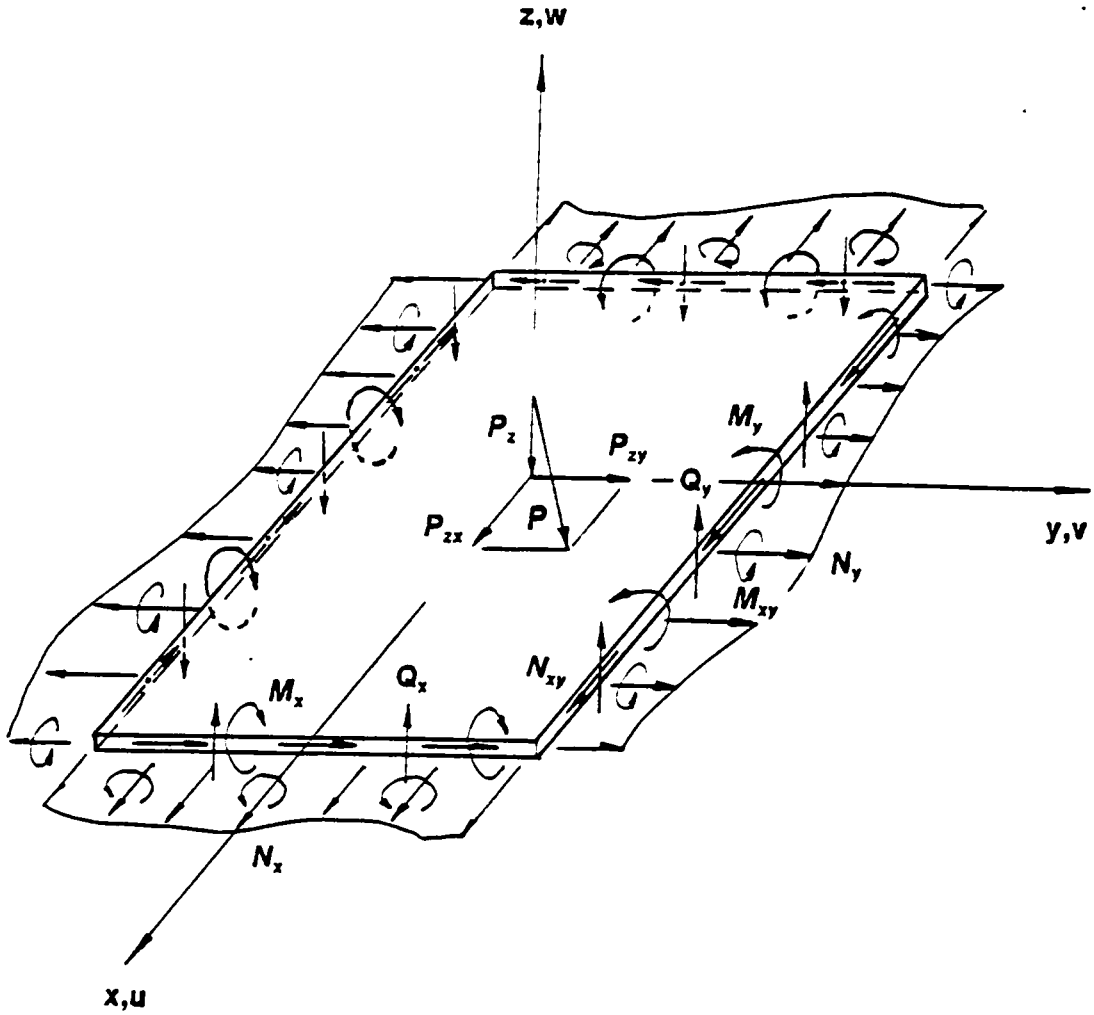

Figure 4.1 A loaded plate

$$
\begin{aligned}
u(x,y,z,t) &= u_o(x,y,t) + z\psi_x(x,y,t) + z^2\xi_x(x,y,t) + z^3\zeta_x(x,y,t) + ... \\
v(x,y,z,t) &= v_o(x,y,t) + z\psi_y(x,y,t) + z^2\xi_y(x,y,t) + z^3\zeta_y(x,y,t) + ... \\
w(x,y,z,t) &= w_o(x,y,t) + z\psi_z(x,y,t) + z^2\xi_z(x,y,t) + z^3\zeta_z(x,y,t) + ...
\end{aligned} \tag{4.1}
$$

where u_o, v_o, w_o, ψ_x, ξ_x, ζ_x, ψ_y, ξ_y, ζ_y, ψ_z, ξ_z and ζ_z..... are functions to be determined. In general, to find all these functions which can satisfy the equilibrium equations, compatibility conditions, boundary conditions and initial conditions is extremely difficult [75]. Finite expansions are used to develop plate theories. For instance the classical plate theory is based on the assumptions due to Kirchhoff [1]. The displacement field of the classical plate theory is

$$
\begin{aligned}
u(x,y,z) &= u_o(x,y) + z\frac{\partial w_o}{\partial x} \\
v(x,y,z) &= v_o(x,y) - z\frac{\partial w_o}{\partial y} \\
w(x,y,z) &= w_o(x,y)
\end{aligned} \tag{4.2}
$$

which contains only three unknowns u_0, v_0 and w_0 representing the mid plane displacement components. The displacement field yields zero transverse strains.

To include the transverse shear strains, one may write the simplest shear deformation displacement field by direct observation of a deformed plate, such as the one shown in Figure 4.2:

$$
\begin{aligned}
u(x, y, z) &= u_o(x, y) + z\theta_2(x, y) \\
v(x, y, z) &= v_o(x, y) - z\theta_1(x, y) \\
w(x, y, z) &= w_o(x, y)
\end{aligned} \tag{4.3}
$$

This displacement field contains five unknowns (u_o, v_o, w_o, θ_1 and θ_2), where θ_1 and θ_2 represent the shear deformations about the coordinates 1 and 2, respectively. Thus

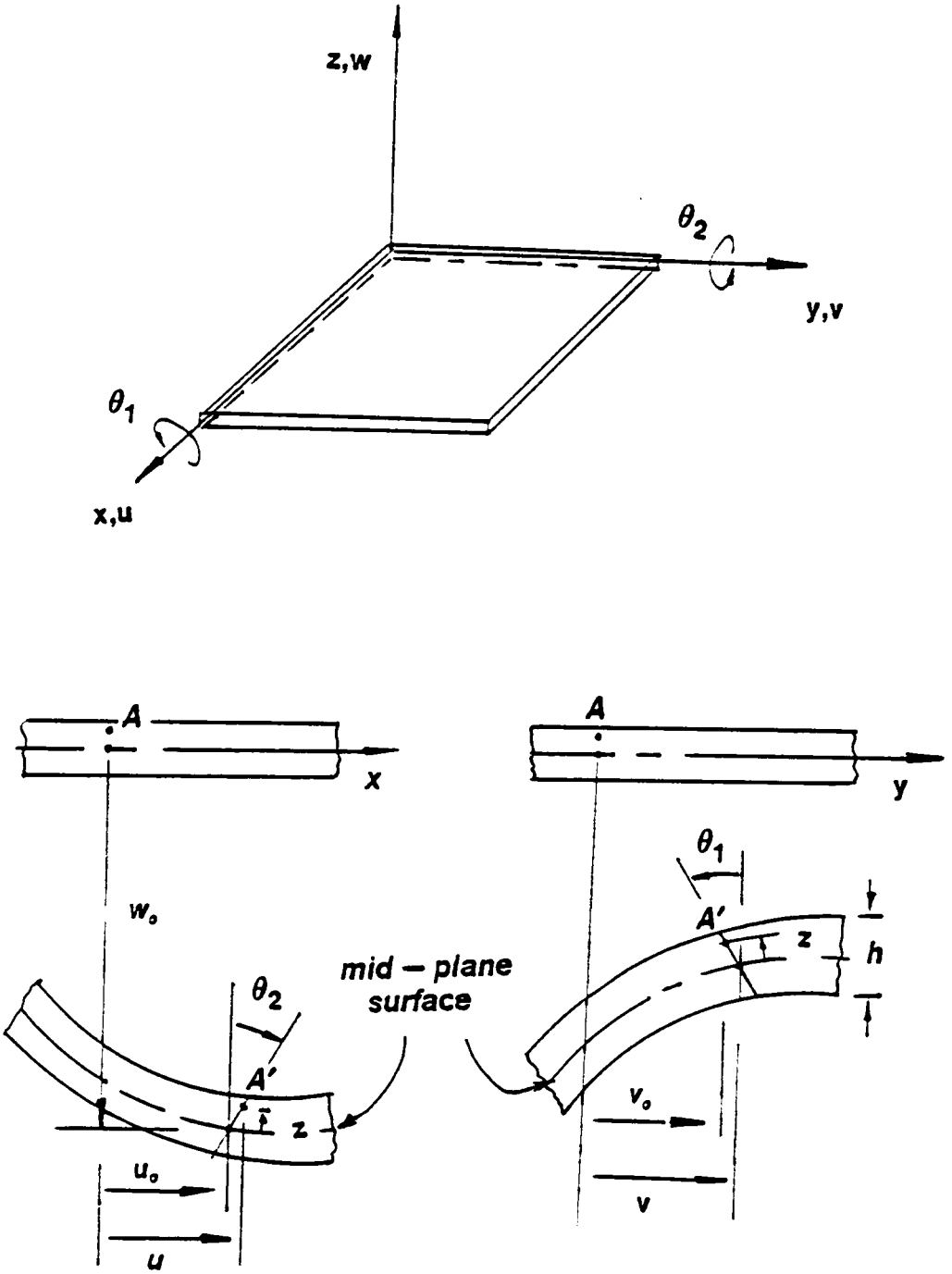

Figure 4.2 Notations used in plate deformation

this theory allows for constant state of transverse shear stresses. However, plate surface boundary conditions and interface continuity conditions for laminated composite plates, in general, are not satisfied by this theory.

By retaining higher-order terms of the expansion, one can write

$$\begin{aligned} u(x, y, z) &= u_o(x, y) + z\psi_1(x, y) + z^2\xi_1(x, y) + z^3\zeta_1(x, y) \\ v(x, y, z) &= v_o(x, y) + z\psi_2(x, y) + z^2\xi_2(x, y) + z^3\zeta_2(x, y) \\ w(x, y, z) &= w_o(x, y) \end{aligned} \tag{4.4}$$

After applying free surface boundary conditions, Reddy [1,5,6] proved that this displacement field can be simplified to

$$\begin{aligned} u(x, y, z) &= u_o(x, y) + z[\theta_2 - \frac{3}{4}(\frac{z}{h})^2(\theta_2 + \frac{\partial w_o}{\partial x})] \\ v(x, y, z) &= v_o(x, y) - z[\theta_1 + \frac{3}{4}(\frac{z}{h})^2(-\theta_1 + \frac{\partial w_o}{\partial y})] \\ w(x, y, z) &= w_o(x, y). \end{aligned} \tag{4.5}$$

All of the above mentioned theories do not account for the stretching of the transverse normals (i.e. $\varepsilon_z = 0$). But some higher-order theories containing higher-order terms in the out-of-plane displacement(w) can account for transverse deformation. For instance the displacement field given below is used for free edge effects [76] :

$$\begin{aligned} u(x,y,z) &= u_o(x,y) + z\psi_x(x,y) \\ v(x,y,z) &= v_o(x,y) + z\psi_y(x,y) \\ w(x,y,z) &= w_o(x,y) + z\psi_z(x,y) \end{aligned} \tag{4.6}$$

4.2 NEED FOR A REFINED TRANSVERSE DEFORMATION THEORY

There are quite a few physical conditions which can not be satisfied by the above reviewed plate theories. First, all of the plate theories (i.e. equations 4.2, 4.3 and 4.5) assume non-stretching of the transverse normals. This assumption results in ignorance of the transverse normal stress through out the entire plate. However transverse normal stress does exist in some loading conditions. For instance, in a pressurized vessel the radial stress has the same magnitude as the hoop stress. Inclusion of the radial stress is required in the failure analysis [59] of a pressurized vessel.

Second, non-zero surface traction (P_{zx} and P_{zy} of Figure 4.1) boundary conditions are not satisfied by the above mentioned plate theories. Existence of these non-zero surface tractions are found in many plate/shell contact surfaces. Example of these surfaces are: mechanical power transferred belt-pulley contact surfaces or rolling-drum contact surfaces or the external surfaces of a high-speed flying object such as missiles. Ignorance of these non-zero surface tractions also results in an incomplete stress field, and therefore the failure prediction could not be accurate. For example, the maximum principal stress criterion assumes that "tensile fracture surfaces will form in a previously uncracked isotropic material when the maximum principal stress reaches a limiting value in tension" [59]. From tensor analysis, it is known that the sum of the principal stresses is the first invariant of the stress tensor

$$\begin{bmatrix} \sigma_x & \sigma_{xy} & \sigma_{xz} \\ \sigma_{yx} & \sigma_y & \sigma_{yz} \\ \sigma_{zx} & \sigma_{zy} & \sigma_z \end{bmatrix} \tag{4.7}$$

According to maximum principal criterion, ignoring transverse normal stress σ_z from the stress tensor, definitely will yield incorrect principal stress. Similarly, the Tresca criterion states that " yielding of an isotropic material will begin when the maximum shear stress reaches a limiting value" [59]. From continuum mechanics [58], it is known that the maximum shear stress is defined by

$$\tau_{max} = \frac{\sigma_1 - \sigma_3}{2} \tag{4.8}$$

where σ_1 and σ_3 represent the largest and the smallest principal stresses respectively. According to this criterion, incorrect principal stresses will also result in an incorrect Tresca failure evaluation.

Third, a reasonable distribution of transverse shear stresses through the plate thickness can not be obtained by the above mentioned theories. The first order shear deformation theory (equation 4.3) yields constant state of transverse shear stresses and Reddy's higher order shear deformation theory (equation 4.4) yields parabolic transverse shear stresses with zero surface traction loading cases. None of the above mentioned plate theories can yield reasonable transverse shear stress distribution for non-zero surface tractions. Unrealistic state of transverse shear stresses does not only cause inaccurate failure prediction but also slow down the convergence rate in a nonlinear analysis. As demonstrated in Table 6.4 of Chapter 6, unrealistic

state of transverse shear stresses requires more iterations before an acceptable convergence criterion can be satisfied. Also it generates less accurate stress field.

Finally, the interlaminar shear stress continuity conditions are not satisfied in laminated composite plates and the peak value of the shear stresses can not be correctly predicted by the above mentioned theories. As pointed out by many composite structural micromechanics studies [2,3] the interlaminar shear stresses are usually responsible for the laminate debonding/delamination in laminated composite structures. Failure to predict the peak values of shear stresses represents a serious deficiency in laminated composite structural analyses. Therefore, a theory that overcomes the deficiencies of the existing theories is needed.

4.3 A PROCEDURE FOR STRESS RECOVERY

From last section, it is seen that a new theory is needed to improve the deficiencies of the existing plate theories. The conventional way of improvement is to retain higher order terms in the in-plane displacements (u and v). Effects of this improvement is too slow at considerable computational expense. In this work, a new higher order theory is proposed by retaining higher order terms in the out-of-plane displacement (w) only. Improvements of this new theory are remarkably good. To describe the new theory it is necessary to review the first order shear deformation theory (FSDT). The following review of the finite element model of FSDT provides a background for present theory.

The displacement field of FSDT is given by equation (4.3). The strain components at any point inside the plate are :

$$\begin{Bmatrix} \varepsilon_1 \\ \varepsilon_2 \\ \gamma_{23} \\ \gamma_{13} \\ \gamma_{12} \end{Bmatrix} = \begin{Bmatrix} u_{o,1} + z\theta_{2,1} \\ v_{o,2} - z\theta_{1,2} \\ -\theta_1 + w_{o,2} \\ \theta_2 + w_{o,1} \\ u_{o,2} + z\theta_{2,2} + v_{o,1} - z\theta_{1,1} \end{Bmatrix}$$

$$= \sum_{i=1}^{n} \begin{bmatrix} \phi_{i,1} & 0 & 0 & 0 & z\phi_{i,1} \\ 0 & \phi_{i,2} & 0 & -z\phi_{i,2} & 0 \\ 0 & 0 & \phi_{i,2} & -\phi_i & 0 \\ 0 & 0 & \phi_{i,1} & 0 & -\phi_i \\ \phi_{i,2} & \phi_{i,1} & 0 & -z\phi_{i,1} & z\phi_{i,2} \end{bmatrix} \begin{Bmatrix} u^i \\ v^i \\ w^i \\ \theta_1^i \\ \theta_2^i \end{Bmatrix} \tag{4.9}$$

where u_o, v_o, w_o, θ_1 and θ_2 represent the mid plane displacements before discretization, while u^i, v^i, w^i, θ_1^i and θ_2^i represent the mid plane displacements at the nodal point "i" after discretization, and ϕ_i are the interpolation functions. This expression can be written in a short form as;

$$\{\varepsilon\} = \sum_{i=1}^{n} [B_L^i]\{u_j^i\}$$

where n is the number of nodes per element (NPE) and u_j^i represent the generalized j-th displacement value at node i. Substituting $[B_L]$ into equation (1.15), the linear stiffness matrix is

$$[K_L] = \int_V [B_L]^T [\bar{Q}][B_L] dV$$

Substituting the strain-displacement matrix [B_L] defined in equation (4.9) into last equation, the linear stiffness matrix [K_L] becomes

$$[K_L] = \int_v [B_1]^T [\bar{Q}][B_1]\, dV + \int_v ([B_1]^T [\bar{Q}][B_2] + [B_2]^T [\bar{Q}][B_1])\, z\, dV + \int_v [B_2]^T [\bar{Q}][B_2] z^2\, dV \tag{4.10}$$

where $[B_L] = [B_1] + z[B_2]$ is a direct decomposition of equation (4.9),i.e.

$$[B_1] = \begin{bmatrix} \phi_{i,1} & 0 & 0 & 0 & 0 \\ 0 & \phi_{i,2} & 0 & 0 & 0 \\ 0 & 0 & \phi_{i,2} & -\phi_i & 0 \\ 0 & 0 & \phi_{i,1} & 0 & -\phi_i \\ \phi_{i,2} & \phi_{i,1} & 0 & 0 & 0 \end{bmatrix} \qquad [B_2] = \begin{bmatrix} 0 & 0 & 0 & 0 & \phi_{i,1} \\ 0 & 0 & 0 & -\phi_{i,2} & 0 \\ 0 & 0 & 0 & 0 & 0 \\ 0 & 0 & 0 & 0 & 0 \\ 0 & 0 & 0 & -\phi_{i,1} & \phi_{i,2} \end{bmatrix} \tag{4.11}$$

As illustrated in Figure 4.3, in the standard notation of a laminated plate, the laminate stiffness are

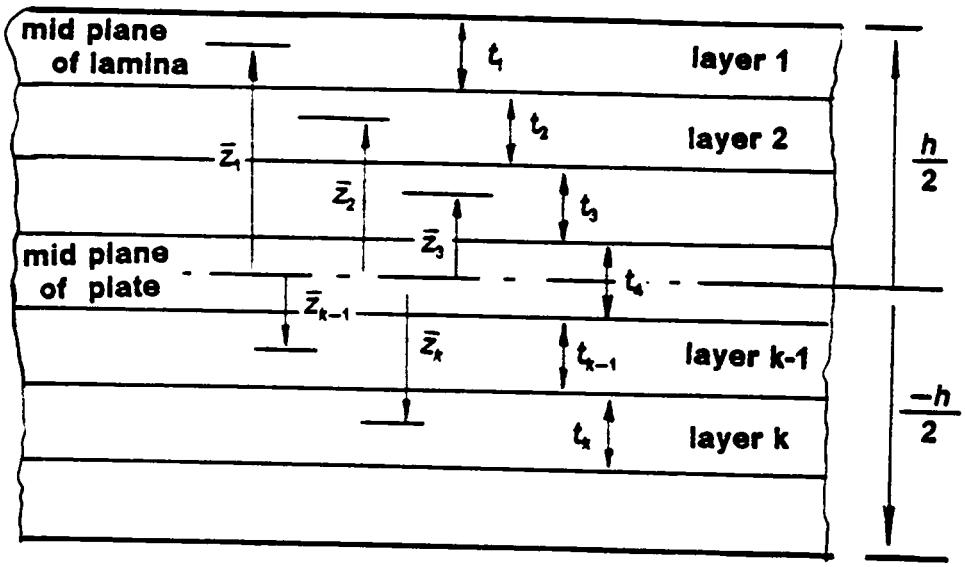

Where

t_k is the thickness of each layer and $\bar{z}_k$ is the height of middle plane of each layer to the middle plane of the laminated plate.

Figure 4.3 Laminated plate

$$[A_{ij}, B_{ij}, D_{ij}] = \int_{-h/2}^{h/2} [\bar{Q}_{ij}](1, z, z_3^2)\ dz$$
$$= \sum_{k=1}^{NLY} [\bar{Q}_{ij}^k](t_k, t_k\bar{z}_k, (\bar{z}_k t_k + \frac{t_k^2}{12})) \tag{4.12}$$

where t_k is the thickness of each layer for total number of NLY layers through the plate thickness and $\bar{z}_k$ is the height of middle plane of each layer to the middle plane of the plate. With these notations, the element linear stiffness matrix can be constructed easily. Equation (4.10) thus becomes

$$[K_L] = \begin{bmatrix} k_{11} & k_{12} & k_{13} & k_{14} & k_{15} \\ k_{12} & k_{22} & k_{23} & k_{24} & k_{25} \\ k_{13} & k_{23} & k_{33} & k_{34} & k_{35} \\ k_{14} & k_{24} & k_{34} & k_{44} & k_{45} \\ k_{15} & k_{25} & k_{35} & k_{45} & k_{55} \end{bmatrix} \tag{4.13}$$

where

$$k_{11} = A_{11}S_{11} + A_{16}(S_{12} + S_{21}) + A_{66}S_{22}$$

$$k_{12} = A_{12}S_{12} + A_{16}S_{11} + A_{26}S_{22} + A_{66}S_{21}$$

$$k_{13} = 0$$

$$k_{14} = -B_{12}S_{12} - B_{16}S_{11} - B_{26}S_{22} - B_{66}S_{21}$$

$$k_{15} = B_{11}S_{11} + B_{16}(S_{12} + S_{21}) + B_{66}S_{22}$$

$$k_{22} = A_{22}S_{22} + A_{26}(S_{12} + S_{21}) + A_{66}S_{11}$$

$$k_{23} = 0$$

$$k_{24} = -B_{22}S_{22} - B_{26}(S_{12} + S_{21}) - B_{66}S_{11}$$

$$k_{25} = B_{12}S_{21} + B_{26}S_{22} + B_{16}S_{11} + B_{66}S_{12}$$

$$k_{33} = A_{45}S_{12} + A_{44}S_{22} + A_{55}S_{11}$$

$$k_{34} = -A_{45}S_{12} - A_{44}S_{22}$$

$$k_{35} = A_{55}S_{10} + A_{45}S_{20}$$

$$k_{44} = A_{44}S_{00} + D_{22}S_{22} + D_{26}(S_{21} + S_{12}) + D_{66}S_{11}$$

$$k_{45} = -D_{12}S_{21} - D_{26}S_{22} - D_{16}S_{11} - D_{66}S_{12} - A_{45}S_{00}$$

$$k_{55} = A_{55}S_{00} + D_{11}S_{11} + D_{16}(S_{12} + S_{21}) + D_{56}S_{22}$$

in which the integration $S_{mn} = \int_A \phi_{i,m}\,\phi_{j,n}\,dxdy$ for i,j = 1,NPE and m,n = 1,2 (coordinate 1,2) has to be conducted numerically over the entire plate surface A. Once the stiffness matrix $[K_L]$ is determined, the whole problem is reduced to a finite element discretized system

$$[K_L]\{U\} = \{R\} \tag{4.14}$$

from which the generalized nodal displacements of the entire plate can be solved. Once displacement field is solved, the stress-strain relation can be used to solve for the stress components. For instance the stress components in the k-th layer are

$$\begin{Bmatrix} \sigma_{11} \\ \sigma_{22} \\ \sigma_{33} \\ \sigma_{23} \\ \sigma_{13} \\ \sigma_{12} \end{Bmatrix}_k = \sum_{j=1}^{n} \begin{bmatrix} \overline{Q}_{11} & \overline{Q}_{12} & \overline{Q}_{13} & 0 & 0 & \overline{Q}_{16} \\ \overline{Q}_{12} & \overline{Q}_{22} & \overline{Q}_{23} & 0 & 0 & \overline{Q}_{16} \\ \overline{Q}_{13} & \overline{Q}_{23} & \overline{Q}_{33} & 0 & 0 & \overline{Q}_{36} \\ 0 & 0 & 0 & k^2\overline{Q}_{44} & k^2\overline{Q}_{45} & 0 \\ 0 & 0 & 0 & k^2\overline{Q}_{45} & k^2\overline{Q}_{55} & 0 \\ \overline{Q}_{16} & \overline{Q}_{26} & \overline{Q}_{36} & 0 & 0 & \overline{Q}_{66} \end{bmatrix}_k \begin{Bmatrix} u^j_{,1} + z\theta^j_{2,1} \\ v^j_{,2} - z\theta^j_{1,2} \\ 0 \\ -\theta^j_1 + w^j_{,2} \\ \theta^j_2 + w^j_{,1} \\ u^j_{,2} + z\theta^j_{2,2} + v^j_{,1} - z\theta^j_{1,1} \end{Bmatrix} \tag{4.15}$$

where θ_{jm} $(m = 1,2)$ represent the averaged rotations at node j. From equation (3.8) to (3.10), it is understood that the normal stress is assumed to be zero. This is a result of Kirchhoff assumption. There are several features need to be noticed about the stresses of the first order shear deformation theory :

1. Surface boundary conditions

$$\begin{aligned} \sigma_{33}(x, y, \pm\frac{h}{2}) &= P_{33}(x, y, \pm\frac{h}{2}) \\ \sigma_{13}(x, y, \pm\frac{h}{2}) &= P_{13}(x, y, \pm\frac{h}{2}) \\ \sigma_{23}(x, y, \pm\frac{h}{2}) &= P_{23}(x, y, \pm\frac{h}{2}) \end{aligned} \tag{4.16}$$

   are not satisfied at the plate surfaces.

2. In-plane stresses σ_{11} and σ_{22} are symmetrical with respect to the $z = 0$ plane, which is not true in general.
3. Shear stresses σ_{13} and σ_{23} are independent of z such that the shear continuity conditions are not satisfied at the lamina interfaces.
4. Constant rotations θ_1 and θ_2 are assumed through out the whole plate thickness in spite of the fact that different material has been used for each layer. This means that the strains are not layer dependent quantities.

From elasticity solution [78], it is known that above mentioned features are not consistent with the physical conditions.

To improve the stress field of the FSDT, a new set of displacement field is proposed as following

$$
\begin{aligned}
u(x, y, z) &= u_o(x, y) + z\theta_2(x, y) \\
v(x, y, z) &= v_o(x, y) - z\theta_1(x, y) \\
w(x, y, z) &= w_o(x, y) + x(a_1 z + a_2 z^2) + y(b_1 z + b_2 z^2) + \frac{c_1}{3} z^3 + \frac{c_2}{4} z^4
\end{aligned}
\tag{4.17}
$$

Following the same procedure as used in obtaining equation (4.15), the stress-strain relations for the displacement field (4.17) are :

$$
\begin{Bmatrix} \sigma_{11} \\ \sigma_{22} \\ \sigma_{33} \\ \sigma_{23} \\ \sigma_{13} \\ \sigma_{12} \end{Bmatrix}_k = \sum_{j=1}^{n} \begin{bmatrix} \overline{Q}_{11} & \overline{Q}_{12} & \overline{Q}_{13} & 0 & 0 & \overline{Q}_{16} \\ \overline{Q}_{12} & \overline{Q}_{22} & \overline{Q}_{23} & 0 & 0 & \overline{Q}_{16} \\ \overline{Q}_{13} & \overline{Q}_{23} & \overline{Q}_{33} & 0 & 0 & \overline{Q}_{36} \\ 0 & 0 & 0 & \alpha^2\overline{Q}_{44} & \beta^2\overline{Q}_{45} & 0 \\ 0 & 0 & 0 & \beta^2\overline{Q}_{45} & \gamma^2\overline{Q}_{55} & 0 \\ \overline{Q}_{16} & \overline{Q}_{26} & \overline{Q}_{36} & 0 & 0 & \overline{Q}_{66} \end{bmatrix}_k \begin{Bmatrix} u^j_{,1} + z\theta^j_{2,1} \\ v^j_{,2} - z\theta^j_{1,2} \\ f_j(x, y, z) \\ -\theta^j_1 + w^j_{,2} + b^j_1 z + b^j_2 z^2 \\ \theta^j_2 + w^j_{,2} + a^j_1 z + a^j_2 z^2 \\ u^j_{,2} + z\theta^j_{2,2} + v^j_{,1} - z\theta^j_{1,1} \end{Bmatrix}_k \tag{4.18}
$$

where $f_j(x, y, z) = x(a^j_1 + 2a^j_2 z) + y(b^j_1 + 2b^j_2 z) + c^j_1 z^2 + c^j_2 z^3$, $n = NPE$ (nodes per element) and a^j_i, b^j_i and c^j_i (i = 1,2) are constants to be determined using surface and inter layer conditions.

It is important to note the difference between stress-strain relations (4.18) and those of the FSDT defined in equation (4.15). In equation (4.18) the subscript "k" at the right lower corner means that the strain is in the k-th layer, which indicates that all the generalized displacements are layer dependent quantities. In addition, the new shear correction factors(α^2, $\beta^2$and γ^2) can be defined by comparison with the exact solution.

There are too many unknowns in equation (4.17). It represents a very complex equation for solving. Although it is possible to solve all the unknowns directly, the cost would be high. Furthermore it is against the goal of computational efficiency to do so. Therefore, instead of solving for all unknowns directly, a fast displacement and stress recovery technique which allows all the generalized displacements at each layer to be recovered such that the surface boundary conditions and shear continuity conditions are all satisfied is proposed. The displacement and stress recovery techniques developed herein requires the solution of equation (4.15).

Denoting θ_1^k and θ_2^k the "refined" rotations of k-th layer, the shear stresses of each layer can be written as

$$\begin{aligned}\sigma_{23}^k &= \overline{Q}_{44}^k[-\theta_1^k + w_{,2} + b_1 z + b_2 z^2] + \overline{Q}_{45}^k[\theta_2^k + w_{,1} + a_1 z + a_2 z^2] \\ \sigma_{13}^k &= \overline{Q}_{45}^k[-\theta_1^k + w_{,2} + b_1 z + b_2 z^2] + \overline{Q}_{55}^k[\theta_2^k + w_{,1} + a_1 z + a_2 z^2]\end{aligned} \tag{4.19}$$

where the subscript "j" for each nodal point is omitted for simplicity. Applying the plate surface traction boundary conditions, it is found that

$$\begin{aligned}\sigma_{23}^1(x, y, +\frac{h}{2}) &= \tau_{23}^T(x, y) \\ \sigma_{13}^1(x, y, +\frac{h}{2}) &= \tau_{13}^T(x, y) \\ \sigma_{23}^N(x, y, -\frac{h}{2}) &= \tau_{23}^B(x, y) \\ \sigma_{13}^N(x, y, -\frac{h}{2}) &= \tau_{13}^B(x, y)\end{aligned} \tag{4.20}$$

in which τ^T and τ^B represent the specified shear stresses at plate top surface and bottom surface, respectively. Write equation (4.20) in terms of the constants a_1, a_2, b_1 and b_2 ,

$$\begin{bmatrix} H\,C_5 & H^2C_5 & H & H^2 \\ -H\,C_6 & H^2C_6 & -H & H^2 \\ H & H^2 & H\,C_7 & H^2C_7 \\ -H & H^2 & -H\,C_8 & H^2C_8 \end{bmatrix} \begin{Bmatrix} a_1 \\ a_2 \\ b_1 \\ b_2 \end{Bmatrix} = \begin{Bmatrix} \bar{\tau}_{23}^{T} + \theta_1^1 - w_{o,2} - C_5(\theta_2^1 + w_{o,1}) \\ \bar{\tau}_{23}^{B} + \theta_1^N - w_{o,2} - C_6(\theta_2^N + w_{o,1}) \\ \bar{\tau}_{13}^{T} + (\theta_1^1 - w_{o,2})C_7 - (\theta_2^1 + w_{o,1}) \\ \tau_{13}^{B} + (\theta_1^N - w_{o,2})C_8 - (\bar{\theta}_2^N + w_{o,1}) \end{Bmatrix} \tag{4.21}$$

where $C_5 = \dfrac{\bar{Q}_{45}^1}{\bar{Q}_{44}^1}$; $C_6 = \dfrac{\bar{Q}_{45}^N}{\bar{Q}_{44}^N}$; $C_7 = \dfrac{\bar{Q}_{45}^1}{\bar{Q}_{55}^1}$; $C_8 = \dfrac{\bar{Q}_{45}^N}{\bar{Q}_{55}^N}$; $H = \dfrac{h}{2}$

and $\bar{\tau}_{23}^{T} = \dfrac{\tau_{23}^{T}}{\bar{Q}_{44}^1}$; $\bar{\tau}_{23}^{B} = \dfrac{\tau_{23}^{B}}{\bar{Q}_{44}^N}$; $\bar{\tau}_{13}^{T} = \dfrac{\tau_{13}^{T}}{\bar{Q}_{55}^1}$; $\bar{\tau}_{13}^{B} = \dfrac{\tau_{13}^{B}}{\bar{Q}_{55}^N}$.

Hence, there are four equations for four unknowns, the coefficients a_1, a_2, b_1 and b_2 can be determined. However, since the rotations θ_1^k and θ_2^k (k = 1 for the top surface layer and k = N for the bottom surface layer) are unknown in the last expression, the interface shear continuity conditions must be used to solve for them. The continuity conditions at each interlaminar surface require that

$$\begin{aligned} \sigma_{23}^{k}(x, y, h_k) &= \sigma_{23}^{k-1}(x, y, h_k) \\ \sigma_{13}^{k}(x, y, h_k) &= \sigma_{13}^{k-1}(x, y, h_k) \end{aligned} \tag{4.22}$$

Writing these equations explicitly, one obtains

$$
\begin{bmatrix}
1 & 1 & 1 & 1 & \cdots & 0 & 0 & 0 & 0 & \cdots \\
0 & 0 & 0 & 0 & \cdots & 1 & 1 & 1 & 1 & \cdots \\
-\overline{C}^1_{44} & \overline{C}^2_{44} & 0 & 0 & \cdots & \overline{C}^1_{45} & -\overline{C}^2_{45} & 0 & 0 & \cdots \\
-\overline{C}^1_{45} & \overline{C}^2_{45} & 0 & 0 & \cdots & \overline{C}^1_{55} & -\overline{C}^2_{55} & 0 & 0 & \cdots \\
0 & -\overline{C}^2_{44} & \overline{C}^3_{44} & 0 & \cdots & 0 & \overline{C}^2_{45} & -\overline{C}^3_{45} & 0 & \cdots \\
0 & -\overline{C}^2_{45} & \overline{C}^3_{45} & 0 & \cdots & 0 & \overline{C}^2_{55} & -\overline{C}^3_{55} & 0 & \cdots \\
\cdot & \cdot & \cdot & \cdot & \cdots & \cdot & \cdot & \cdot & \cdot & \cdots \\
\cdot & \cdot & \cdot & \cdot & \cdots & \cdot & \cdot & \cdot & \cdot & \cdots \\
\cdot & \cdot & \cdot & \cdot & \cdots & \cdot & \cdot & \cdot & \cdot & \cdots
\end{bmatrix}
\begin{Bmatrix}
\theta^1_1 \\ \theta^2_1 \\ \cdot \\ \cdot \\ \cdot \\ \theta^1_2 \\ \theta^2_2 \\ \cdot \\ \cdot \\ \cdot
\end{Bmatrix}
=
\begin{Bmatrix}
N\theta^0_1 \\ N\theta^0_2 \\ D^2_1 \\ D^2_2 \\ D^3_1 \\ D^3_2 \\ \cdot \\ \cdot \\ \cdot
\end{Bmatrix}
\tag{4.23}
$$

where $D^k_1 = \overline{C}^k_{44}\overline{U}^k_{32} - \overline{C}^{k-1}_{44}\overline{U}^{k-1}_{32} + \overline{C}^k_{45}\overline{U}^k_{31} - \overline{C}^{k-1}_{45}\overline{U}^{k-1}_{31}$

$D^k_2 = \overline{C}^k_{45}\overline{U}^k_{32} - \overline{C}^{k-1}_{45}\overline{U}^{k-1}_{32} + \overline{C}^k_{55}\overline{U}^k_{31} - \overline{C}^{k-1}_{55}\overline{U}^{k-1}_{31}$

and $\overline{U}^k_{31} = w_{o,1} + a_1 h_k + a_2 h_k^2$

$\overline{U}^k_{32} = w_{o,2} + b_1 h_k + b_2 h_k^2.$

Since $\overline{U}^k_{31}$ and $\overline{U}^k_{32}$ depend on a's and b's, an iterative scheme must be used to obtain a set of satisfactory a_1, a_2, b_1, b_2 and θ^k_1, θ^k_2. The numerical experiments indicate that the convergence among equations (4.21) and (4.22) is very fast. From the examples which have been solved in this study, it is found that 3 to 6 iterations is enough to obtain 10^{-5} convergence tolerance.

Once coefficients a_1, a_2, b_1 and b_2 are solved, the coefficients c_1 and c_2 can be determined easily. Using equation (3.10), the normal stress component σ_3 from equation (4.18) can be written as

$$\sigma_3^k(x, y, z) = \overline{Q}_{33}^k[x(a_1 + 2a_2z) + y(b_1 + 2b_2z) + c_1z^2 + c_2z^3] \tag{4.24}$$

Applying the normal pressure boundary condition on both the top and bottom surfaces, it is seen that

$$\begin{aligned}
\sigma_3(x, y, \frac{+h}{2}) &= \overline{Q}^1[x(a_1 + 2a_2h) + y(b_1 + b_2h) + c_1\frac{h^2}{4} + c_2\frac{h^3}{8}] = P^T(x, y) \\
\sigma_3(x, y, \frac{-h}{2}) &= \overline{Q}^N[x(a_1 - 2a_2h) + y(b_1 - b_2h) + c_1\frac{h^2}{4} - c_2\frac{h^3}{8}] = P^B(x, y)
\end{aligned} \tag{4.25}$$

from which the coefficients c_1 and c_2 are given by

$$\begin{aligned}
c_1 &= \frac{2}{h^2}[(\frac{P^T}{\overline{Q}_{33}^1} + \frac{P^B}{\overline{Q}_{33}^N}) - 2(a_1x + b_1y)] \\
c_2 &= \frac{4}{h^3}[(\frac{P^T}{\overline{Q}_{33}^1} - \frac{P^B}{\overline{Q}_{33}^N}) - 2h(a_2x + b_2y)]
\end{aligned} \tag{4.26}$$

Hence equation (4.18) is solved.

The comparison between FSDT and current theory is made in Figure 4.4. It can be seen that the proposed theory can not just satisfy all the boundary conditions and continuity conditions, but also can yield more reasonable rotational displacements. Of course this is due to the contribution of transverse deformation throughout the plate thickness.

Comparing the stress-strain relations of FSDT with the stress-strain relations of the current theory, it is easy to make the following observations :

1. Straight lines normal to the plate mid surface are no longer straight. Each layer has its own rotations.
2. The length of a normal changes after deformation.

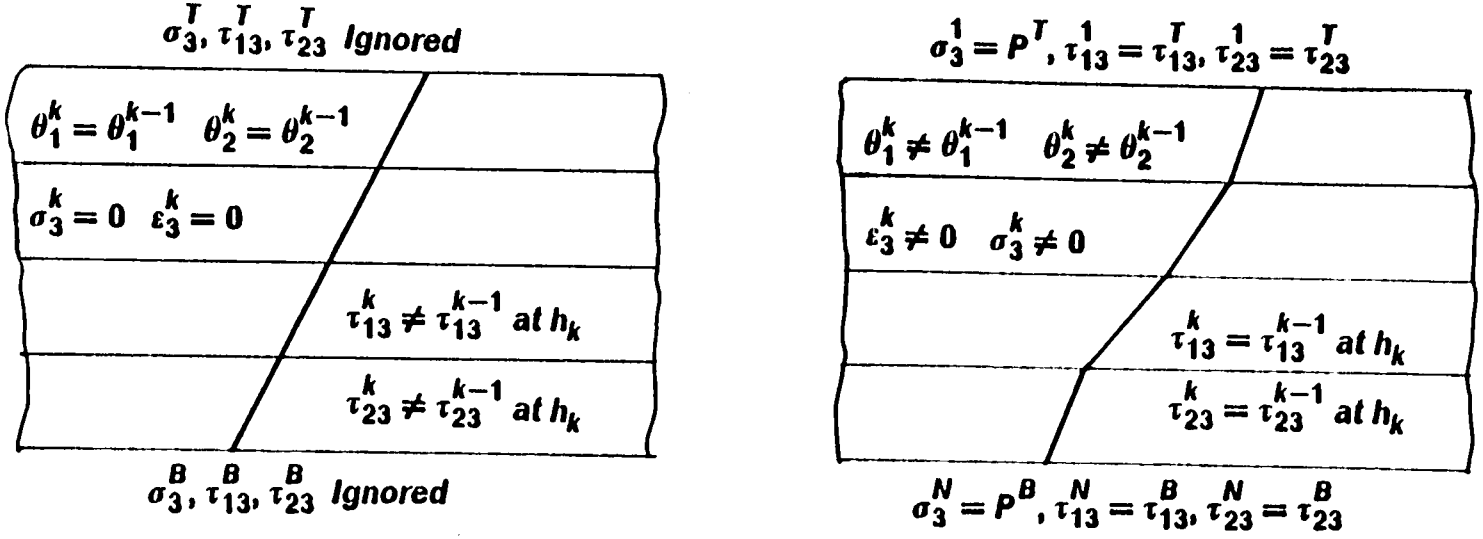

Figure 4.4 Comparisons between FSDT and current work

3. The normal stress may be small but not necessarily negligible.
4. For any non-zero plate surface pressure difference, the in-plane stresses are unsymmetrical with respect to the mid plane of the plate.
5. The shear stresses are continuous functions of z, and plate surface boundary conditions can be satisfied.

TRANSVERSE DEFORMATION THEORY OF SHELLS

5.1 INTRODUCTION

An uniform thickness plate is a solid continuum bounded by two parallel flat planes, while a shell is a solid continuum bounded by two separated curved surfaces by a small distance compared to the surface dimensions. A transversely loaded plate, after deformation, will never be flat. Because of this reason, geometric nonlinear analyses are not performed using plate theory unless its geometry change is very small compared to its dimension. Since one may like to describe the structure motion from an Updated Lagrangian viewpoint, all parameters(i.e. displacements, strains, stresses.....) are referred to the current configuration.

5.2 THE FIRST-ORDER CONTINUUM SHELL ELEMENT

5.2.1 DISPLACEMENT FIELD

Let x,y,z be the original coordinate system (a coordinate system at time t=0), x_1, x_2, x_3 the current coordinate system (a coordinate system always attached to the mid plane at current time t) and ξ, η, ζ the natural coordinate system(a mathematical coordinate system at the center of the mid plane of each element), as shown in Figure 5.1, it is easy to write the displacement field of the first order shear deformation theory for an arbitrarily oriented shell in the current coordinate system as follows :

$$u_1(x_1, x_2, x_3, t) = u_1^0(x_1, x_2, t) + x_3\theta_2(x_1, x_2, t) \tag{5.1}$$

$$u_2(x_1, x_2, x_3, t) = u_2^0(x_1, x_2, t) - x_3\theta_1(x_1, x_2, t)$$

$$u_3(x_1, x_2, x_3, t) = u_3^0(x_1, x_2, t)$$

where u_1^0, u_2^0, and u_3^0 represent the mid plane displacements, θ_1 and θ_2 represent the "averaged" rotations. By means of tensor transformation, the displacement components in the original coordinate system can be obtained as

$$\begin{Bmatrix} u \\ v \\ w \end{Bmatrix} = [V]^T \begin{Bmatrix} u_1 \\ u_2 \\ u_3 \end{Bmatrix} = \begin{bmatrix} V_{11} & V_{21} & V_{31} \\ V_{12} & V_{22} & V_{32} \\ V_{13} & V_{23} & V_{33} \end{bmatrix} \begin{Bmatrix} u_1^0 + x_3\theta_2 \\ u_2^0 - x_3\theta_1 \\ u_3^0 \end{Bmatrix} \tag{5.2}$$

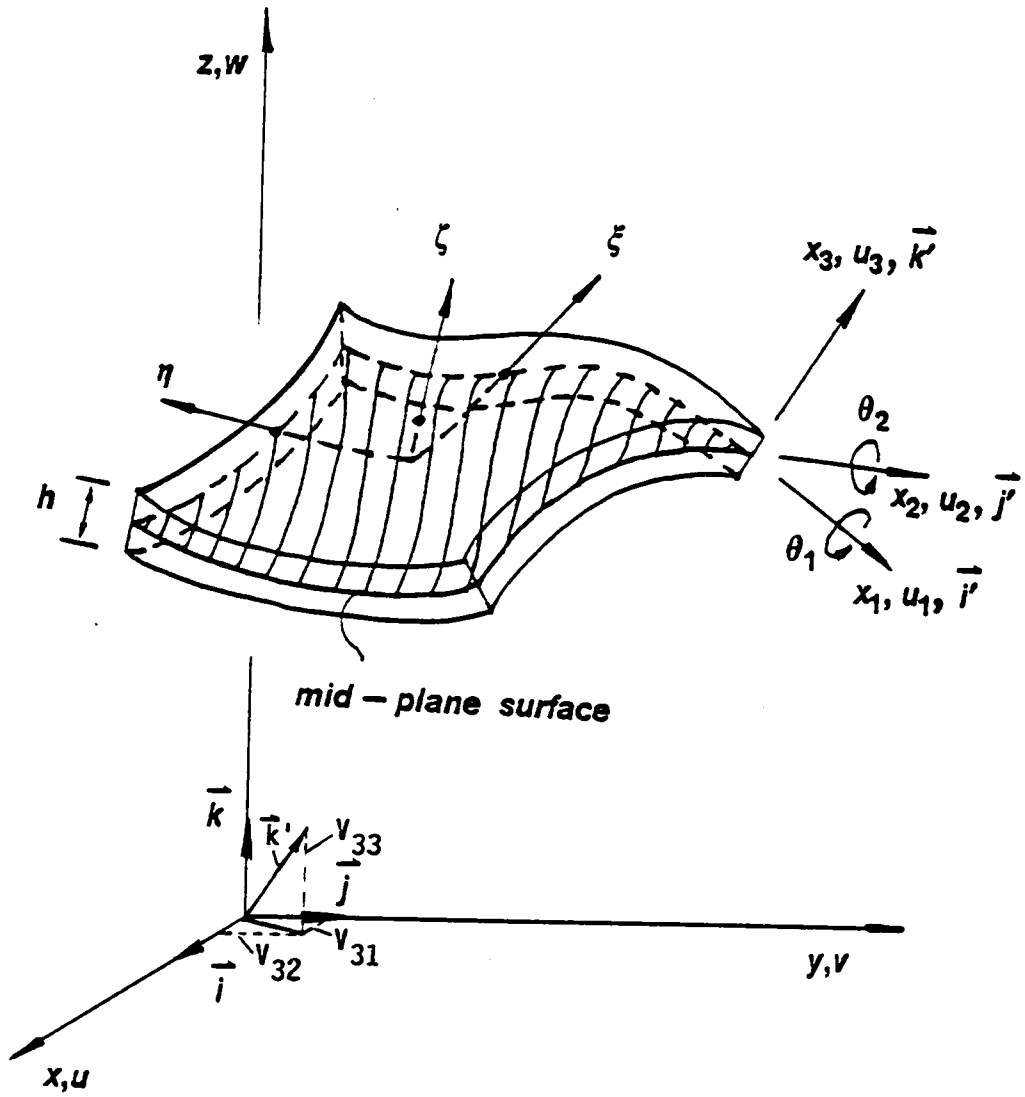

Figure 4.5 Notations used in continuum-based shell deformation

$$\begin{Bmatrix} u \\ v \\ w \end{Bmatrix} = \begin{Bmatrix} u^0 \\ v^0 \\ w^0 \end{Bmatrix} + x_3 \begin{Bmatrix} V_{11}\theta_2 - V_{21}\theta_1 \\ V_{12}\theta_2 - V_{22}\theta_1 \\ V_{13}\theta_2 - V_{23}\theta_1 \end{Bmatrix} \tag{5.3}$$

in which [V] denotes the transformation matrix between the current configuration (x_1, x_2, x_3) and the original configuration (x,y,z). Conversely,

$$\begin{Bmatrix} u_1 \\ u_2 \\ u_3 \end{Bmatrix} = [V] \begin{Bmatrix} u \\ v \\ w \end{Bmatrix} \tag{5.4}$$

The transformation between the gradients of displacements in the original coordinate system and the current coordinate system can be easily found [47]

$$\begin{bmatrix} u_{1,1} & u_{2,1} & u_{3,1} \\ u_{1,2} & u_{2,2} & u_{3,2} \\ u_{1,3} & u_{2,3} & u_{3,3} \end{bmatrix} = [V] \begin{bmatrix} u_{,x} & v_{,x} & w_{,x} \\ u_{,y} & v_{,y} & w_{,y} \\ u_{,z} & v_{,z} & w_{,z} \end{bmatrix} [V]^T \tag{5.5}$$

Let

$$\begin{aligned} u &= \sum_{k=1}^{n} \phi_k(\xi, \eta)\, u^k + x_3 \sum_{k=1}^{n} \phi_k(\xi, \eta)\, (\theta_2^k V_{11}^k - \theta_1^k V_{21}^k) \\ v &= \sum_{k=1}^{n} \phi_k(\xi, \eta)\, v^k + x_3 \sum_{k=1}^{n} \phi_k(\xi, \eta)\, (\theta_2^k V_{12}^k - \theta_1^k V_{22}^k) \\ w &= \sum_{k=1}^{n} \phi_k(\xi, \eta)\, w^k + x_3 \sum_{k=1}^{n} \phi_k(\xi, \eta)\, (\theta_2^k V_{13}^k - \theta_1^k V_{23}^k) \end{aligned} \tag{5.6}$$

where ϕ_k is the shape function of node k, and n is the total number of nodal points of an element(NPE). In this expression u^k, v^k, w^k are the nodal mid plane displacements in the original coordinate system, and θ_1^k, θ_2^k are the nodal averaged rotations in the current coordinate system, while $V_{1_j}^k$ and $V_{2_j}^k$ are the components of $\vec{V}_1$ and $\vec{V}_2$ at node "k".

The transformation between the original coordinates and the natural coordinates of the global displacements is defined by

$$\begin{bmatrix} u_{,x} & v_{,x} & w_{,x} \\ u_{,y} & v_{,y} & w_{,y} \\ u_{,z} & v_{,z} & w_{,z} \end{bmatrix} = [J]^{-1} \begin{bmatrix} u_{,\xi} & v_{,\xi} & w_{,\xi} \\ u_{,\eta} & v_{,\eta} & w_{,\eta} \\ u_{,\zeta} & v_{,\zeta} & w_{,\zeta} \end{bmatrix} \tag{5.7}$$

in which [J] is the Jacobi matrix,

$$[J] = \begin{bmatrix} x_{,\xi} & y_{,\xi} & z_{,\xi} \\ x_{,\eta} & y_{,\eta} & z_{,\eta} \\ x_{,\zeta} & y_{,\zeta} & z_{,\zeta} \end{bmatrix} \tag{5.8}$$

In order to determine the Jacobi matrix, the original coordinates (x,y,z) must be expressed in terms of the natural coordinates (ξ, ζ, η). This can be done by using the unit vector of x_3 coordinate. By definition, the unit vector of x_3 coordinate (see Figure 5.1) is

$$\vec{k'} = V_{31}\vec{i} + V_{32}\vec{j} + V_{33}\vec{k}$$

Hence, the location of each point inside the shell is

$$
\begin{aligned}
x = x_0 + x_3 V_{31} &= \sum_{k=1}^{n} \phi_k(\xi, \zeta) x_0^k + x_3 \sum_{k=1}^{n} \phi_k(\xi, \zeta) V_{31}^k \\
y = y_0 + x_3 V_{32} &= \sum_{k=1}^{n} \phi_k(\xi, \zeta) y_0^k + x_3 \sum_{k=1}^{n} \phi_k(\xi, \zeta) V_{32}^k \\
z = z_0 + x_3 V_{33} &= \sum_{k=1}^{n} \phi_k(\xi, \zeta) z_0^k + x_3 \sum_{k=1}^{n} \phi_k(\xi, \zeta) V_{33}^k
\end{aligned} \tag{5.9}
$$

Substituting equation (5.9) into equation (5.8) yields

$$
[J] = \sum_{k=1}^{n} \begin{bmatrix}
\frac{\partial \phi_k}{\partial \xi}(x_0^k + x_3 V_{31}^k) & \frac{\partial \phi_k}{\partial \xi}(y_0^k + x_3 V_{32}^k) & \frac{\partial \phi_k}{\partial \xi}(z_0^k + x_3 V_{33}^k) \\
\frac{\partial \phi_k}{\partial \eta}(x_0^k + x_3 V_{31}^k) & \frac{\partial \phi_k}{\partial \eta}(y_0^k + x_3 V_{32}^k) & \frac{\partial \phi_k}{\partial \eta}(z_0^k + x_3 V_{33}^k) \\
\frac{h}{2}\phi_k V_{31}^k & \frac{h}{2}\phi_k V_{32}^k & \frac{h}{2}\phi_k V_{33}^k
\end{bmatrix} \tag{5.10}
$$

in which the relation $x_3 = \zeta \frac{h}{2}$ is used. Here h denotes the thickness of the shell, and ζ ranges from -1 to 1 representing the natural coordinate in the x_3 -direction. It is found that this expression can be simplified by neglecting all the x_3 terms. The argument which allows doing so is that x_3 is far smaller than x_0^k, y_0^k and z_0^k. For any plate or shell the thickness is always far smaller than the other two dimensions. Thus x_3 terms are all dropped. After simplification, the notation $[J^*]$ is used to represent the inverse of the Jacobi matrix

$$
[J^*] = [J]^{-1}
$$

Similarly the first derivatives of the displacements in original coordinates with respect to the natural coordinate can be obtained. By taking the first derivative of u, v and w with respect to ξ, η and ζ, it is seen that

$$\begin{Bmatrix} u_{,\xi} \\ u_{,\eta} \\ u_{,\zeta} \\ v_{,\xi} \\ v_{,\eta} \\ v_{,\zeta} \\ w_{,\xi} \\ w_{,\eta} \\ w_{,\zeta} \end{Bmatrix} = \sum_{k=1}^{n} \begin{bmatrix} \phi_{k,\xi} & 0 & 0 & -x_3\phi_{k,\xi}V_{21}^k & x_3\phi_{k,\xi}V_{11}^k \\ \phi_{k,\eta} & 0 & 0 & -x_3\phi_{k,\eta}V_{21}^k & x_3\phi_{k,\eta}V_{11}^k \\ 0 & 0 & 0 & \frac{-h}{2}\phi_k V_{21}^k & \frac{h}{2}\phi_k V_{11}^k \\ 0 & \phi_{k,\xi} & 0 & -x_3\phi_{k,\xi}V_{22}^k & x_3\phi_{k,\xi}V_{12}^k \\ 0 & \phi_{k,\eta} & 0 & -x_3\phi_{k,\eta}V_{22}^k & x_3\phi_{k,\eta}V_{12}^k \\ 0 & 0 & 0 & \frac{-h}{2}\phi_k V_{22}^k & \frac{h}{2}\phi_k V_{12}^k \\ 0 & 0 & \phi_{k,\xi} & -x_3\phi_{k,\xi}V_{23}^k & x_3\phi_{k,\xi}V_{13}^k \\ 0 & 0 & \phi_{k,\eta} & -x_3\phi_{k,\eta}V_{23}^k & x_3\phi_{k,\eta}V_{13}^k \\ 0 & 0 & 0 & \frac{-h}{2}\phi_k V_{23}^k & \frac{h}{2}\phi_k V_{13}^k \end{bmatrix} \begin{Bmatrix} u^k \\ v^k \\ w^k \\ \theta_1^k \\ \theta_2^k \end{Bmatrix} \tag{5.11}$$

Substituting equation (5.10) into equation (5.7) and using last equation, the first derivatives of the displacements in current coordinates with respect to the current coordinates are,

$$\begin{Bmatrix} u_{1,1} \\ u_{1,2} \\ u_{1,3} \\ u_{2,1} \\ u_{2,2} \\ u_{2,3} \\ u_{3,1} \\ u_{3,2} \\ u_{3,3} \end{Bmatrix} = \sum_{j=1}^{n} \begin{bmatrix} q_{11}^j & q_{12}^j & q_{13}^j & (q_{16}^j x_3 + q_{14}^j) & (q_{17}^j x_3 + q_{15}^j) \\ q_{21}^j & q_{22}^j & q_{23}^j & (q_{26}^j x_3 + q_{24}^j) & (q_{27}^j x_3 + q_{25}^j) \\ q_{31}^j & q_{32}^j & q_{33}^j & (q_{36}^j x_3 + q_{34}^j) & (q_{37}^j x_3 + q_{35}^j) \\ q_{41}^j & q_{42}^j & q_{43}^j & (q_{46}^j x_3 + q_{44}^j) & (q_{47}^j x_3 + q_{45}^j) \\ q_{51}^j & q_{52}^j & q_{53}^j & (q_{56}^j x_3 + q_{54}^j) & (q_{57}^j x_3 + q_{55}^j) \\ q_{61}^j & q_{62}^j & q_{63}^j & (q_{66}^j x_3 + q_{64}^j) & (q_{67}^j x_3 + q_{65}^j) \\ q_{71}^j & q_{72}^j & q_{73}^j & (q_{76}^j x_3 + q_{74}^j) & (q_{77}^j x_3 + q_{75}^j) \\ q_{81}^j & q_{82}^j & q_{83}^j & (q_{86}^j x_3 + q_{84}^j) & (q_{87}^j x_3 + q_{85}^j) \\ q_{91}^j & q_{92}^j & q_{93}^j & (q_{96}^j x_3 + q_{94}^j) & (q_{97}^j x_3 + q_{95}^j) \end{bmatrix} \begin{Bmatrix} u^j \\ v^j \\ w^j \\ \theta_1^j \\ \theta_2^j \end{Bmatrix} \tag{5.12}$$

where

$$
\begin{aligned}
q_{i1} &= R_{i1}\phi_{k,\xi} + R_{i2}\phi_{k,\eta} \\
q_{i2} &= R_{i4}\phi_{k,\xi} + R_{i5}\phi_{k,\eta} \\
q_{i3} &= R_{i7}\phi_{k,\xi} + R_{i8}\phi_{k,\eta} \\
q_{i4} &= t^{k}_{i3}\phi_{k} \\
q_{i5} &= t^{k}_{i6}\phi_{k} \\
q_{i6} &= t^{k}_{i1}\phi_{k,\xi} + t^{k}_{i2}\phi_{k,\eta} \\
q_{i7} &= t^{k}_{i4}\phi_{k,\xi} + t^{k}_{i5}\phi_{k,\eta}
\end{aligned}
\tag{5.13}
$$

where i = 1,2,3,4,5,6,7,8,9 and

$$
\begin{Bmatrix} t^{k}_{i1} \\ t^{k}_{i2} \\ t^{k}_{i3} \end{Bmatrix} = -\begin{bmatrix} R_{i1} & R_{i4} & R_{i7} \\ R_{i2} & R_{i5} & R_{i8} \\ \frac{h}{2}R_{i3} & \frac{h}{2}R_{i6} & \frac{h}{2}R_{i9} \end{bmatrix} \begin{Bmatrix} V^{k}_{21} \\ V^{k}_{22} \\ V^{k}_{23} \end{Bmatrix} \tag{5.14}
$$

$$
\begin{Bmatrix} t^{k}_{i4} \\ t^{k}_{i5} \\ t^{k}_{i6} \end{Bmatrix} = \begin{bmatrix} R_{i1} & R_{i4} & R_{i7} \\ R_{i2} & R_{i5} & R_{i8} \\ \frac{h}{2}R_{i3} & \frac{h}{2}R_{i6} & \frac{h}{2}R_{i9} \end{bmatrix} \begin{Bmatrix} V^{k}_{21} \\ V^{k}_{22} \\ V^{k}_{23} \end{Bmatrix}
$$

and R_{ij} are the elements of the product matrix of the matrix defined in equation (5.5) to the matrix defined in equation (5.7).

5.2.2 STRAIN COMPONENTS

The strain components are obtained directly from equation (5.12), namely

$$\{\varepsilon\} = \begin{Bmatrix} u_{1,1} \\ u_{2,2} \\ u_{2,3}+u_{3,2} \\ u_{1,3}+u_{3,1} \\ u_{1,2}+u_{2,1} \end{Bmatrix} = \sum_{k=1}^{n} \begin{bmatrix} p_{11}^{j} & p_{12}^{j} & p_{13}^{j} & (p_{16}^{j}x_3+p_{14}^{j}) & (p_{17}^{j}x_3+p_{15}^{j}) \\ p_{21}^{j} & p_{22}^{j} & p_{23}^{j} & (p_{26}^{j}x_3+p_{24}^{j}) & (p_{27}^{j}x_3+p_{25}^{j}) \\ p_{31}^{j} & p_{32}^{j} & p_{33}^{j} & (p_{36}^{j}x_3+p_{34}^{j}) & (p_{37}^{j}x_3+p_{35}^{j}) \\ p_{41}^{j} & p_{42}^{j} & p_{43}^{j} & (p_{46}^{j}x_3+p_{44}^{j}) & (p_{47}^{j}x_3+p_{45}^{j}) \\ p_{51}^{j} & p_{52}^{j} & p_{53}^{j} & (p_{56}^{j}x_3+p_{54}^{j}) & (p_{57}^{j}x_3+p_{55}^{j}) \end{bmatrix} \begin{Bmatrix} u^j \\ v^j \\ w^j \\ \theta_1^j \\ \theta_2^j \end{Bmatrix} \quad (5.15)$$

or in a short form

$$\{\varepsilon\} = \sum_{j=1}^{n} ([\bar{P}_1^j] + x_3[\bar{P}_2^j])\{u^j\} = \sum_{j=1}^{n} [B_L^j]\{u^j\} \quad (5.16)$$

The strain-displacement matrix is

$$[B_L^j] = [\bar{P}_1^j] + x_3[\bar{P}_2^j] \quad (5.17)$$

Comparing equation (5.15) with equation (4.9), it is found that

$$[\bar{P}_1^j] = \begin{bmatrix} p_{11}^{j} & p_{12}^{j} & p_{13}^{j} & 0 & 0 \\ p_{21}^{j} & p_{22}^{j} & p_{23}^{j} & 0 & 0 \\ p_{31}^{j} & p_{32}^{j} & p_{33}^{j} & p_{34}^{j} & 0 \\ p_{41}^{j} & p_{42}^{j} & p_{43}^{j} & 0 & p_{45}^{j} \\ p_{51}^{j} & p_{52}^{j} & p_{53}^{j} & 0 & 0 \end{bmatrix} \quad [\bar{P}_2^j] = \begin{bmatrix} 0 & 0 & 0 & 0 & p_{17}^{j} \\ 0 & 0 & 0 & p_{26}^{j} & 0 \\ 0 & 0 & 0 & 0 & 0 \\ 0 & 0 & 0 & 0 & 0 \\ 0 & 0 & 0 & p_{56}^{j} & p_{57}^{j} \end{bmatrix} \quad (5.18)$$

Thus, the Updated Lagrangian strain-displacement matrix is defined by equation (5.17) and (5.18).

5.3 ELEMENT MATRICES AND FORCE VECTORS

5.3.1 LINEAR STIFFNESS MATRIX

Once the strain-displacement matrix is determined, the linear stiffness matrix can be constructed easily. According to equation (2.15), the linear stiffness matrix is

$$[K_L] = \int_v [B_L]^T [\bar{Q}][B_L] dV$$

Substituting the linear strain-displacement matrix (equation (5.17)) into last equation yields

$$[K_L] = \int_v [\bar{P}_1]^T [\bar{Q}][\bar{P}_1] dV + \int_v ([\bar{P}_1]^T [\bar{Q}][\bar{P}_2] + [\bar{P}_2]^T [\bar{Q}][\bar{P}_1]) x_3 dx_1 dx_2 dx_3 + \int_v [\bar{P}_2]^T [\bar{Q}][\bar{P}_2] x_3^2 dx_1 dx_2 dx_3 \quad (5.19)$$

Performing the analytical integration in x_3 direction explicitly, and using the notations defined in equation (4.12), the linear stiffness matrix can be obtained easily from following expression

$$[K_L] = \int_A [\bar{P}_1]^T[A][\bar{P}_1]dx_1dx_2 + \int_A ([\bar{P}_1]^T[B][\bar{P}_2] + [\bar{P}_2]^T[B][\bar{P}_1])dx_1dx_2 + \int_A [\bar{P}_2]^T[D][\bar{P}_2]dx_1dx_2 \tag{5.20}$$

Where [A], [B] and [D] are the usual laminate stiffnesses. A complete listing of the elements of $[K_L]$ are given in Appendix A.

5.3.2 THROUGH-THE-THICKNESS INTEGRATION

For the reason it will become obvious in the next two sections, three integration quantities are defined below. These quantities can be called "resultants ", because they represent thickness-weighted stress summations.

The force resultants are the integrations of the stress components through the shell thickness,i.e.

$$\{E\} = \begin{Bmatrix} E_1 \\ E_2 \\ E_4 \\ E_5 \\ E_6 \end{Bmatrix} = \int_{-h/2}^{h/2} \begin{Bmatrix} \sigma_1 \\ \sigma_2 \\ \sigma_4 \\ \sigma_5 \\ \sigma_6 \end{Bmatrix} dx_3 = \sum_{k=1}^{N} \int_{h_{k-1}}^{h_k} \begin{Bmatrix} \sigma_1 \\ \sigma_2 \\ \sigma_4 \\ \sigma_5 \\ \sigma_6 \end{Bmatrix}_k dx_3$$

where the single-subscript notation $\sigma_1 = \sigma_{11}$, $\sigma_2 = \sigma_{22}$, $\sigma_4 = \sigma_{23}$, $\sigma_5 = \sigma_{13}$, and $\sigma_6 = \sigma_{12}$. is used. Recalling the stress-strain relations (3.11) and (3.12) and the strain-displacement relation (5.17), the last equation can be written as

$$\{E\} = \sum_{k=1}^{N}\int_{h_{k-1}}^{h_k} [\bar{Q}^k]\{\varepsilon\}_k \, dx_3 = \sum_{k=1}^{N}\int_{h_{k-1}}^{h_k} [\bar{Q}^k]\sum_{j=1}^{n}([\bar{P}_1^j]_k + x_3[\bar{P}_2^j]_k)\{u^j\}_k \, dx_3$$
$$= \sum_{k=1}^{N}\sum_{j=1}^{n}(\{P_1^j\}_k t_k + \{P_2^j\} t_k \bar{z}_k) \tag{5.21}$$

where vectors $\{p_1^j\}_k = [\bar{Q}^k][\bar{P}_1^j]\{u^j\}_k$ and $\{p_2^j\}_k = [\bar{Q}^k][\bar{P}_2^j]\{u^j\}_k$ are defined in Appendix B. Note that N is the total number of layers (NLY), and n is the number of nodes per elements(NPE).

Similarly, the moment resultant {F} and the inertia resultant {G} can be defined as follows :

$$\{F\} = \begin{Bmatrix} F_1 \\ F_2 \\ F_4 \\ F_5 \\ F_6 \end{Bmatrix} = \int_{-h/2}^{h/2} \begin{Bmatrix} \sigma_1 \\ \sigma_2 \\ \sigma_4 \\ \sigma_5 \\ \sigma_6 \end{Bmatrix} x_3 \, dx_3 = \sum_{k=1}^{N}\int_{h_{k-1}}^{h_k} [\bar{Q}^k]\sum_{j=1}^{n}([\bar{P}_1^j]_k + x_3[\bar{P}_2^j]_k)\{u^j\}_k \, x_3 \, dx_3$$

$$\{F\} = \sum_{k=1}^{N}\sum_{j=1}^{n}(\{P_1^j\}_k t_k \bar{z}_k + \{P_2^j\}_k (t_k \bar{z}_k^2 + \frac{t_k^2}{12})) \tag{5.22}$$

$$\{G\} = \begin{Bmatrix} G_1 \\ G_2 \\ G_4 \\ G_5 \\ G_6 \end{Bmatrix} = \int_{-h/2}^{h/2} \begin{Bmatrix} \sigma_1 \\ \sigma_2 \\ \sigma_4 \\ \sigma_5 \\ \sigma_6 \end{Bmatrix} x_3^2 \, dx_3 = \sum_{k=1}^{N} \int_{h_{k-1}}^{h_k} [\bar{Q}^k] \sum_{j=1}^{n} ([\bar{P}_1^j]_k + x_3[\bar{P}_2^j]_k) \{u^j\}_k \, x_3^2 \, dx_3$$

$$\{G\} = \sum_{k=1}^{N} \sum_{j=1}^{n} (\{P_1^j\}_k (t_k \bar{z}_k^2 + \frac{t_k}{12}) + \{P_2^j\}_k t_k \bar{z}_k (\bar{z}^2 + \frac{t_k^2}{4})) \tag{5.23}$$

This completes the analytical integration formulations through the shell thickness.

5.3.3 NONLINEAR STIFFNESS MATRIX

Writing equation (5.12) in a short form, one obtains

$$\{u_{m,n}\} = \sum_{j=1}^{n} ([\bar{q}_1^j] + x_3[\bar{q}_2^j])\{u^j\} \tag{5.24}$$

where $u_{m,n}$ represents the first derivatives of the displacement "m" with respect to the current coordinate "n". The symbol "j" on the r.h.s represents the j-th nodal point of the element. Thus according to equation (2.16), the nonlinear stiffness matrix becomes

$$[K_{NL}] = \int_V [B_{NL}]^T [\tau][B_{NL}] dV = \int_V ([\bar{q}_1] + x_3[\bar{q}_2])^T [\tau]([\bar{q}_1] + x_3[\bar{q}_2]) dV \tag{5.25}$$

where the stress matrix $[\tau]$ and matrices $[\bar{q}_1]$ and $[\bar{q}_2]$ are defined below

$$[\tau] = \begin{bmatrix} \tau_1 & 0 & 0 & \tau_6 & 0 & 0 & \tau_5 & 0 & 0 \\ 0 & \tau_1 & 0 & 0 & \tau_6 & 0 & 0 & \tau_5 & 0 \\ 0 & 0 & \tau_1 & 0 & 0 & \tau_6 & 0 & 0 & \tau_5 \\ \tau_6 & 0 & 0 & \tau_2 & 0 & 0 & \tau_4 & 0 & 0 \\ 0 & \tau_6 & 0 & 0 & \tau_2 & 0 & 0 & \tau_4 & 0 \\ 0 & 0 & \tau_6 & 0 & 0 & \tau_2 & 0 & 0 & \tau_4 \\ \tau_5 & 0 & 0 & \tau_4 & 0 & 0 & \tau_3 & 0 & 0 \\ 0 & \tau_5 & 0 & 0 & \tau_4 & 0 & 0 & \tau_3 & 0 \\ 0 & 0 & \tau_5 & 0 & 0 & \tau_4 & 0 & 0 & \tau_3 \end{bmatrix} \tag{5.26}$$

$$[\bar{q}_1] = \begin{bmatrix} q'_{11} & q'_{12} & q'_{13} & 0 & 0 \\ q'_{21} & q'_{22} & q'_{23} & 0 & 0 \\ q'_{31} & q'_{32} & q'_{33} & 0 & q'_{35} \\ q'_{41} & q'_{42} & q'_{43} & 0 & 0 \\ q'_{51} & q'_{52} & q'_{53} & 0 & 0 \\ q'_{61} & q'_{62} & q'_{63} & q'_{64} & 0 \\ q'_{71} & q'_{72} & q'_{73} & 0 & 0 \\ q'_{81} & q'_{82} & q'_{83} & 0 & 0 \\ q'_{91} & q'_{92} & q'_{93} & 0 & 0 \end{bmatrix} \qquad [\bar{q}_2] = \begin{bmatrix} 0 & 0 & 0 & 0 & q'_{17} \\ 0 & 0 & 0 & 0 & q'_{27} \\ 0 & 0 & 0 & 0 & 0 \\ 0 & 0 & 0 & q'_{46} & 0 \\ 0 & 0 & 0 & q'_{56} & 0 \\ 0 & 0 & 0 & 0 & 0 \\ 0 & 0 & 0 & 0 & 0 \\ 0 & 0 & 0 & 0 & 0 \\ 0 & 0 & 0 & 0 & 0 \end{bmatrix} \tag{5.27}$$

Substituting the resultants obtained in equations (5.21), (5.22) and (5.23) into the last equation, the nonlinear stiffness matrix becomes

$$[K_{NL}] = \int_A [\bar{q}_1]^T[E][\bar{q}_2]dx_1dx_2 + \int_A ([\bar{q}_2]^T[F][\bar{q}_1] + [\bar{q}_1]^T[F][\bar{q}_2])dx_1dx_2 + \int_A [\bar{q}_2]^T[G][\bar{q}_2]dx_1dx_2 \tag{5.28}$$

where [E],[F] and [G] are the 9x9 matrices and A denotes the area of the midsurface of the element. Again the integration of last equation must be carried out numerically over the shell surface. A complete listing of the elements of $[K_{NL}]$ is given in Appendix C.

5.3.4 UNBALANCED FORCE

The unbalanced force is the right hand side of equation (2.13), where {R} is the vector of externally applied forces, and {U} is the vector of internal, stress-induced, reaction forces. From this equation it is seen that this force is a time dependent and stress dependent quantity. Substituting the linear strain-displacement matrix $[B_L]$ from equation (5.17) and the stress matrix $[\tau]$ from equation (5.26) into equation (2.17), the vector {U} becomes

$$\{U\} = \int_v [B_L]^t\{\tau\}dV = \int_v ([\bar{P}_1^j]^T + x_3[\bar{P}_2^j]^T)\{\tau\}dV \tag{5.29}$$

Again using the resultants {E} and {F} defined in equation (5.21) and (5.22), the vector {U} can be found easily.

5.3.5 CONSISTENT MASS MATRIX

There are two types of mass matrices that are used in the finite element dynamic analysis. One is the diagonalized lumped-mass matrix. The other is the consistent mass matrix. The lumped-mass matrix reduces the numerical operation significantly. However in spite of the fact that a systematical procedure has been set up to lump the element mass to nodal point, in coarse mesh analysis the lumped-mass matrix may still yield inaccurate results [55]. This is due to the fact that the formulations among the stiffness matrix, the nodal point load and the mass matrix are inconsistent. Because of this reason, the consistent mass matrix is used in this work. From equation (5.4) it is seen that

$$\begin{Bmatrix} u_1^0 \\ u_2^0 \\ u_3^0 \end{Bmatrix} = [V] \begin{Bmatrix} u_0 \\ v_0 \\ w_0 \end{Bmatrix} \tag{5.30}$$

Substituting u_1^0, u_2^0, u_3^0 obtained from this equation into equation (5.1), it is found that

$$\begin{aligned} u_1 &= V_{11}u_0 + V_{12}v_0 + V_{13}w_0 + x_3\theta_2 \\ u_2 &= V_{21}u_0 + V_{22}v_0 + V_{23}w_0 - x_3\theta_1 \\ u_3 &= V_{31}u_0 + V_{32}v_0 + V_{33}w_0 \end{aligned} \tag{5.31}$$

In terms of the finite element interpolation, equation (5.31) takes the form

$$
\begin{aligned}
u_1 &= \sum_{i=1}^{n} (\phi_i V_{11}^i u_0^i + \phi_i V_{12}^i v_0^i + \phi_i V_{13}^i w_0^i + x_3 \phi_i \theta_2^i) \\
u_2 &= \sum_{i=1}^{n} (\phi_i V_{21}^i u_0^i + \phi_i V_{22}^i v_0^i + \phi_i V_{23}^i w_0^i - x_3 \phi_i \theta_1^i) \\
u_3 &= \sum_{i=1}^{n} (\phi_i V_{31}^i u_0^i + \phi_i V_{32}^i v_0^i + \phi_i V_{33}^i w_0^i)
\end{aligned} \tag{5.32}
$$

or in short,

$$
\{u\} = \sum_{i=1}^{n} ([H_1^i] + x_3 [H_2^i]) \{u_i\} \tag{5.33}
$$

Substituting [H] into equation (2.15), the consistent mass matrix can be obtained as

$$
\begin{aligned}
[M] &= \int_v \rho_o [H^i]^T [H^i] \, dv \\
&= \int_v \rho_o ([H_1^i]^T + x_3 [H_2^i]^T) ([H_1^i] + x_3 [H_2^i]) \, dv \\
&= \int_v \rho_o [H_1^i]^T [H_1^i] dv + \int_v \rho_o x_3 ([H_2^i]^T [H_1^i] + [H_1^i]^T [H_2^i]) \, dv + \int_v \rho_o x_3^2 [H_1^i]^T [H_1^i] dv
\end{aligned} \tag{5.34}
$$

where

$$
[H_1^i] = \begin{bmatrix}
\phi_i V_{11}^i & \phi_i V_{12}^i & \phi_i V_{13}^i & 0 & 0 \\
\phi_i V_{21}^i & \phi_i V_{22}^i & \phi_i V_{23}^i & 0 & 0 \\
\phi_i V_{31}^i & \phi_i V_{32}^i & \phi_i V_{33}^i & 0 & 0
\end{bmatrix} \tag{5.35}
$$

and

$$[H_2^i] = \begin{bmatrix} 0 & 0 & 0 & 0 & \phi_i \\ 0 & 0 & 0 & -\phi_i & 0 \\ 0 & 0 & 0 & 0 & 0 \end{bmatrix} \tag{5.36}$$

Defining the mass inertias

$$(I_1, I_2, I_3) = \int \rho_0 (1, x_3, x_3^2) dx_3 \tag{5.37}$$

equation (5.34) can be expressed as

$$[M] = I_1 \int_A [H_1^i]^T [H_1^i] dA + I_2 \int_A ([H_2^i]^T [H_1^i] + [H_1^i]^T [H_2^i]) dA + I_3 \int_A [H_2^i]^T [H_2^i] dA \tag{5.38}$$

A complete listing of the mass matrix is given in Appendix D. This mass matrix is called consistent mass matrix "because the same interpolation functions are employed in the calculation of the load vectors and the mass matrix as in the evaluation of the stiffness matrix" [55].

5.3.5 EQUATIONS OF MOTION

Substituting the mass matrix [M], the linear stiffness matrix $[K_L]$,the nonlinear stiffness matrix $[K_{NL}]$ and the unbalanced force vector {U} into equation (2.13), the equations of motion become

$$[{}_tM] \{{}^{t+\Delta t}\ddot{u}\} + ([{}_tK_L] + [{}_tK_{NL}])\{\delta u\} = \{{}^{t+\Delta t}R\} - \{{}^{t+\Delta t}U\} \tag{5.39}$$

Several methods can be used to solve for the ordinary differential equation (5.39) in time. In this work the Newmark direct integration method and the Modified Newton Raphson iteration are used.

5.4. THE STRESS RECOVERY TECHNIQUE

5.4.1 DISPLACEMENTS AND STRESSES

The displacement field is assumed to be of the form,

$$\begin{aligned} u_1(x_1, x_2, x_3) &= u_1^0(x_1, x_2) + x_3\theta_2(x_1, x_2) \\ u_2(x_1, x_2, x_3) &= u_2^0(x_1, x_2) - x_3\theta_1(x_1, x_2) \\ u_3(x_1, x_2, x_3) &= u_3^0(x_1, x_2) + x_1(a_1x_3 + a_2x_3^2) + x_2(b_1x_3 + b_2x_3^2) + \frac{c_1}{3}x_3^3 + \frac{c_2}{4}x_3^4 \end{aligned} \tag{5.40}$$

Computing the strains associated with the displacement field (5.40) and substituting into the lamina stress-strain relations, one obtains

$$\begin{Bmatrix} \sigma_{11} \\ \sigma_{22} \\ \sigma_{33} \\ \sigma_{23} \\ \sigma_{13} \\ \sigma_{12} \end{Bmatrix}_k = \sum_{j=1}^{n} \begin{bmatrix} \overline{Q}_{11} & \overline{Q}_{12} & \overline{Q}_{13} & 0 & 0 & \overline{Q}_{16} \\ \overline{Q}_{12} & \overline{Q}_{22} & \overline{Q}_{23} & 0 & 0 & \overline{Q}_{26} \\ \overline{Q}_{13} & \overline{Q}_{23} & \overline{Q}_{33} & 0 & 0 & \overline{Q}_{36} \\ 0 & 0 & 0 & \alpha^2\overline{Q}_{44} & \beta^2\overline{Q}_{45} & 0 \\ 0 & 0 & 0 & \beta^2\overline{Q}_{45} & \gamma^2\overline{Q}_{55} & 0 \\ \overline{Q}_{16} & \overline{Q}_{26} & \overline{Q}_{36} & 0 & 0 & \overline{Q}_{66} \end{bmatrix}_k \begin{Bmatrix} u^j_{1,1} + x_3\theta^j_{2,1} \\ u^j_{2,2} - x_3\theta^j_{1,2} \\ f_j(x_1, x_2, x_3) \\ -\theta^j_1 + u^j_{3,2} + b^j_1x_3 + b^j_2x_3^2 \\ \theta^j_2 + u^j_{3,2} + a^j_1x_3 + a^j_2x_3^2 \\ u^j_{1,2} + x_3\theta^j_{2,2} + u^j_{2,1} - x_3\theta^j_{1,1} \end{Bmatrix}_k \tag{5.41}$$

where $f_j(x_1, x_2, x_3) = x_1(a_1^j + 2a_2^j x_3) + x_2(b_1^j + 2b_2^j x_3) + c_1^j x_3^2 + c_2^j x_3^3$, $n = NPE$ and α^2, β^2 and γ^2 are the shear correction factors.

5.4.2 SURFACE TRACTION AND INTERFACE CONTINUITY CONDITIONS

Denoting θ_1^k and θ_2^k the "recovered or refined" rotations of k-th layer, the shear stresses of each layer are

$$\begin{aligned}\sigma_{23}^k &= \overline{Q}_{44}^k[-\theta_1^k + u_{3,2} + b_1 x_3 + b_2 x_3^2] + \overline{Q}_{45}^k[\theta_2^k + u_{3,1} + a_1 x_3 + a_2 x_3^2] \\ \sigma_{13}^k &= \overline{Q}_{45}^k[-\theta_1^k + u_{3,2} + b_1 x_3 + b_2 x_3^2] + \overline{Q}_{55}^k[\theta_2^k + u_{3,1} + a_1 x_3 + a_2 x_3^2]\end{aligned} \tag{5.42}$$

where the subscript "j" for each nodal point is omitted for simplicity. Applying the plate surface traction boundary conditions, we have

$$\begin{aligned}\sigma_{23}^1(x_1, x_2, +\frac{h}{2}) &= \tau_{23}^T(x_1, x_2) \\ \sigma_{13}^1(x_1, x_2, +\frac{h}{2}) &= \tau_{13}^T(x_1, x_2) \\ \sigma_{23}^N(x_1, x_2, -\frac{h}{2}) &= \tau_{23}^B(x_1, x_2) \\ \sigma_{13}^N(x_1, x_2, -\frac{h}{2}) &= \tau_{13}^B(x_1, x_2)\end{aligned} \tag{5.43}$$

in which τ^T and τ^B represent the shear stresses at plate top surface and bottom surface, respectively. The continuity conditions at each interlaminar surface require that

$$\begin{aligned}\sigma_{23}^k(x_1, x_2, h_k) &= \sigma_{23}^{k-1}(x_1, x_2, h_k) \\ \sigma_{13}^k(x_1, x_2, h_k) &= \sigma_{13}^{k-1}(x_1, x_2, h_k)\end{aligned} \tag{5.44}$$

Equations (5.43) and (5.44) can be used to determine a_1, a_2, b_1 and b_2. Using the condition of equation (3.10), the normal stress component σ_3 from equation (5.41) can be written as

$$\sigma_3^k(x_1, x_2, x_3) = \overline{Q}^k[x_1(a_1 + 2a_2x_3) + x_2(b_1 + 2b_2x_3) + c_1x_3^2 + c_2x_3^3] \tag{5.45}$$

Applying the normal pressure boundary condition on both the top surface and bottom surface, it is seen that

$$\begin{aligned}
\sigma_3(x, y, \frac{+h}{2}) &= \overline{Q}^1[x_1(a_1 + 2a_2h) + x_2(b_1 + b_2h) + c_1\frac{h^2}{4} + c_2\frac{h^3}{8}] = P^T(x_1, x_2) \\
\sigma_3(x, y, \frac{-h}{2}) &= \overline{Q}^N[x_1(a_1 - 2a_2h) + x_2(b_1 - b_2h) + c_1\frac{h^2}{4} - c_2\frac{h^3}{8}] = P^B(x_1, x_2)
\end{aligned} \tag{5.46}$$

Equations (5.46) provide the conditions to determine c_1 and c_2 as

$$\begin{aligned}
c_1 &= \frac{2}{h^2}[(\frac{P^T}{\overline{Q}_{33}^1} + \frac{P^B}{\overline{Q}_{33}^N}) - 2(a_1x_1 + b_1x_2)] \\
c_2 &= \frac{4}{h^3}[(\frac{P^T}{\overline{Q}_{33}^1} - \frac{P^B}{\overline{Q}_{33}^N}) - 2h(a_2x_1 + b_2x_2)]
\end{aligned} \tag{5.47}$$

Clearly, equations (5.43) and (5.44) are coupled to equation (5.47). Therefore, an iterative method is needed to compute a_1, a_2, b_1, b_2, c_1 and c_2.

5.5 SOLUTION PROCEDURES

Two numerical techniques needed for the solution of the nonlinear finite element equations are briefly mentioned in this section. The dynamic equations of motion are

first reduced to algebraic equations using the Newmark direct time integration method. Then the resulting nonlinear algebraic equations are solved using the Newton-Raphson iterative method. These methods are summarized below.

5.5.1 THE NEWMARK DIRECT INTEGRATION METHOD

In the Newmark method, the displacements and the velocities are approximated by

$$^{t+\Delta t}\{\Delta u\} = {}^{t}\{\Delta u\} + {}^{t}\{\Delta \dot{u}\}\Delta t + [(\frac{1}{2} - \alpha) + {}^{t}\{\Delta \ddot{u}\} + \alpha\, {}^{t+\Delta t}\{\Delta \ddot{u}\}](\Delta t)^2 \tag{5.48}$$

$$^{t+\Delta t}\{\Delta \dot{u}\} = {}^{t}\{\Delta \dot{u}\} + [(1 - \delta)\,{}^{t}\{\Delta \ddot{u}\} + \delta\, {}^{t+\Delta t}\{\Delta \ddot{u}\}](\Delta t) \tag{5.49}$$

in which $\delta = \frac{1}{2}$ and $\alpha = \frac{1}{4}$ correspond to the constant-average-acceleration method which also called the trapezoidal rule. This method provides unconditional stability and has the self-start capability. Substituting these two relations into equation (5.39) and rearranging it, one obtains (see [1,56])

$$[\tilde{K}]\,{}^{t+\Delta t}\{\Delta u\} = {}^{t+\Delta t}\{\tilde{R}\} - {}^{t+\Delta t}\{U\} \tag{5.50a}$$

where

$$\begin{aligned} [\tilde{K}] &= \frac{4}{\Delta t^2}[M] + [K_L] + [K_{NL}] \\ {}^{t+\Delta t}\{\tilde{R}\} &= {}^{t+\Delta t}\{R\} + [M](\frac{4}{\Delta t^2}\,{}^{t}\{\Delta u\} + \frac{4}{\Delta t}\,{}^{t}\{\Delta \dot{u}\} + {}^{t}\{\Delta \ddot{u}\}) \end{aligned} \tag{5.50b}$$

Once $^{t+\Delta t}\{\Delta u\}$ is solved from equation (5.50), the acceleration increments $^{t+\Delta t}\{\Delta \ddot{u}\}$ at time $t + \Delta t$ can be determined from equation (5.48). Then substituting $^{t+\Delta t}\{\Delta u\}$ and $^{t+\Delta t}\{\Delta u\}$ into equation (5.49), the velocity increment $^{t+\Delta t}\{\Delta u\}$ at time $t + \Delta t$ can be

solved from equation (5.49). Repeating these steps iteratively, consecutive configurations can be determined. At time = 0, the vector ${}^{\circ}\{\Delta u\}$ is computed from equation (5.39), and ${}^{\circ}\{\Delta u\}$ and ${}^{\circ}\{\Delta \dot{u}\}$ are known from the initial conditions.

5.5.2 THE MODIFIED NEWTON RAPHSON METHOD

Equation (5.50) can not be solved by a single step because the nonlinear stiffness matrix and the unbalanced force are stress dependent quantities. At each time step the nonlinear stiffness matrix and the unbalance force are unknown quantities. Thus an iteration scheme must be used to solve equation (5.50). The most frequently used iteration schemes for the nonlinear finite element equations is the Newton-Raphson iteration method [55]. The incremental iteration form of equation (5.50) is given by

$$ {}^{\tau}[\tilde{K}]^{t+\Delta t}\{\Delta u\}^{(i)} = {}^{t+\Delta t}\{\tilde{R}\}^{(i-1)} - {}^{t+\Delta t}\{U\}^{(i-1)} \tag{5.51} $$

which is known as the modified Newton-Raphson method. Without any a-priori knowledge of the system behavior, it may be most efficient to update the tangential stiffness matrix at the beginning of each time step [55]. However convergence is not guaranteed by this method [55,79,47].

NUMERICAL RESULTS

6.1 INTRODUCTION

To evaluate the new-higher order transverse deformation theory developed in this work, several example problems are solved and the results are presented in this chapter. Each of the example problem either contains an analytical solution or a parallel ABAQUS finite element analysis result for comparison. For those problems for which no solutions are available may be used as reference for future studies.

As emphasized at beginning of the work, the goal of this work is to obtain an accurate stress field for both plate and arbitrarily oriented shell laminated composite structures. Thus attention is paid to the accuracy and completeness of stress results, particularly the transverse normal and shear stresses. Shear stress continuity conditions across the layer interfaces and the satisfaction of the nonzero traction boundary conditions are illustrated.

6.2 PROBLEM 1: CANTILEVER PLATE

One of the major goals of this work is to obtain reasonable distribution of shear stress through the plate/shell thickness. Another major goal of this work is to prove and to obtain the transverse normal stress. To demonstrate the achievements of these two goals, several example problems are presented here.

A. Isotropic cantilever plate with concentrated load at free end

The geometry, material property and loading condition of an isotropic cantilever plate are shown in the figure below.

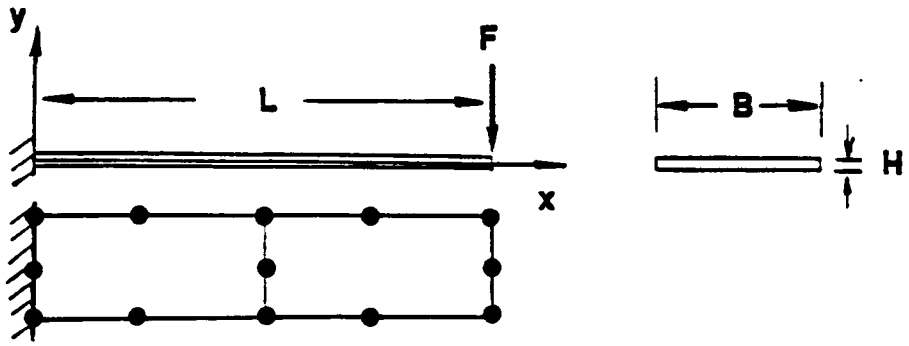

L=4″ H=0.1″ B=1.0″ E=1.0x10⁷ psi ν =0.0 F=-30.0lb

The analytical solution from [61], and the results of the first-order shear deformation theory (FSDT) and current theory are plotted in Figure 6.1. From this plot it is clear that current solution yields compatible analytical shear stress, which is a great improvement over the FSDT solution. The excellent agreement between current work and analytical solution (see Table 6.1) verifies the formulation of the linear stiffness matrix derived in this work.

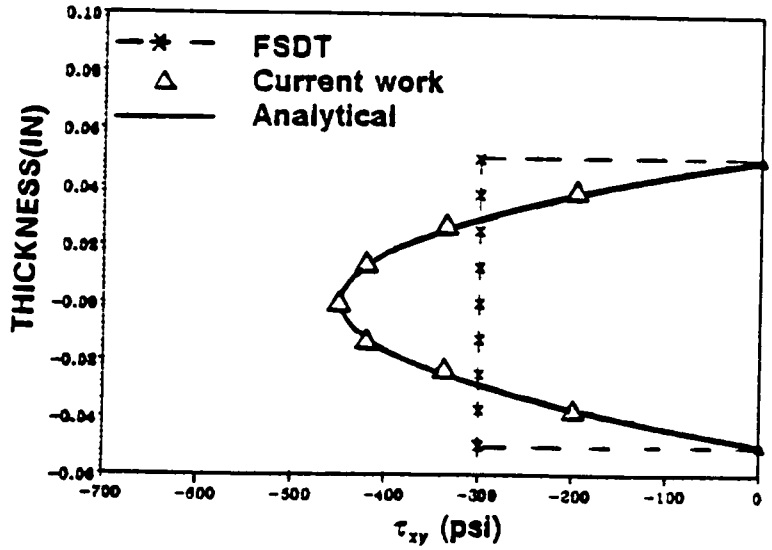

Figure 6.1 Shear stress distribution

Table 6.1 Stresses of a Cantilever Plate

x	y	σ_x (psi)		τ_{xy} (psi)	
		Exact	FEM	Exact	FEM
0.0	0.050	72000.00	72001.75	0.00	0.00
	0.025	36000.00	36000.87	-337.50	-337.51
	0.000	0.00	0.00	-450.00	-450.01
	-0.025	-36000.00	-36000.87	-337.50	-337.51
	-0.050	-72000.00	-72001.75	0.00	0.00
2.0	0.050	36000.00	36000.39	0.00	0.00
	0.025	18000.00	18000.19	-337.50	-337.50
	0.000	0.00	0.00	-450.00	-450.01
	-0.025	-18000.00	-18000.19	-337.50	-337.50
	-0.050	-36000.00	-36000.39	0.00	0.00

B. cantilever plate with uniform load

The geometry, loading and boundary conditions and finite element meshes of a cantilever plate with uniform load are shown in Figure 6.2, where plate mesh is used for current work analysis and ABAQUS mesh is used for ABAQUS [60] analysis. Two different material plates are investigated, namely isotropic plate and laminated composite plate.

(i) isotropic plate

The Young's modulus is assumed 1.0E7 psi and the Poisson's ratio is assumed 0.3 for this plate. The stresses of current plate theory are compared with the ABAQUS plane stress element analysis in Table 6.2. A good agreement between current work results and ABAQUS results is observed.

(ii) laminated composite plate

The same problem is analyzed for a four layer cross-ply [0/90/90/0] composite plate. The material properties of each layer used in this analysis are :

$$E_1 = 1.0x10^7 \text{ psi}, \quad E_2 = E_3 = 2.0x10^6 \text{ psi}, \quad \nu_{12} = \nu_{13} = \nu_{23} = 0.3$$

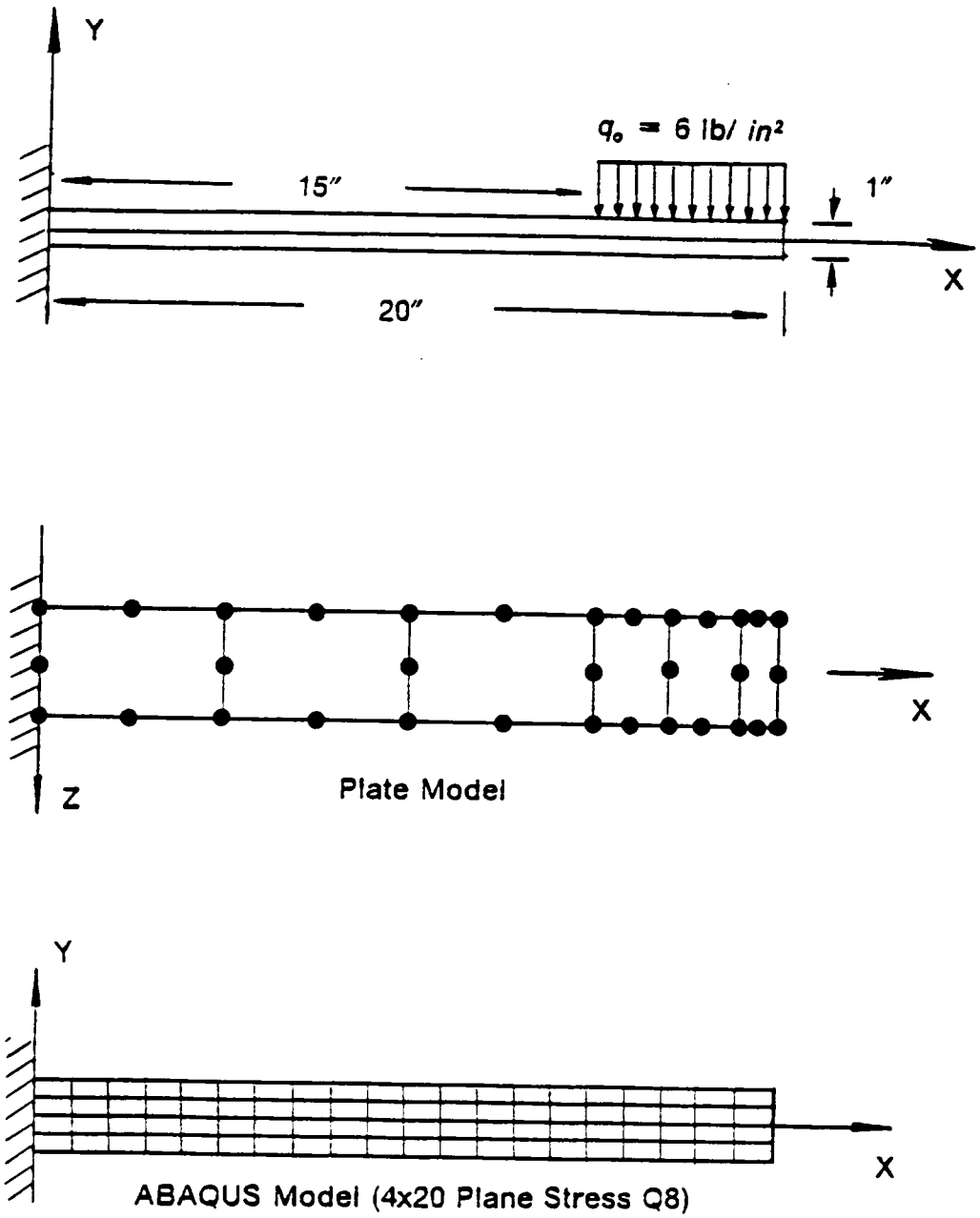

Figure 6.2 Cantilever plate with uniform load

Table 6.2 Stresses of an isotropic plate due uniformly distributed transverse load

x	y	σ_x(psi)		σ_y(psi)		τ_{xy}(psi)	
		FEM	ABAQUS	FEM	ABAQUS	FEM	ABAQUS
10.0	0.50	1350.0	1350.0	0.00	0.0034	0.00	-1.87
	0.25	675.0	675.0	0.00	0.0008	-33.75	-35.60
	0.00	0.0	0.0	0.00	-0.0006	-45.00	-46.90
	-0.25	-675.0	-675.0	0.00	0.0001	-33.75	-35.60
	-0.50	-1350.0	-1350.0	0.00	-0.0001	0.00	-1.87
15.0	0.50	411.2	448.0	-6.00	-3.07	0.00	-1.87
	0.25	205.2	225.0	-5.06	-2.58	-33.75	-35.40
	0.00	-0.6	0.0	-3.00	-1.50	-45.00	-46.60
	-0.25	-206.5	-225.0	-0.94	-0.42	-33.75	-35.90
	-0.50	-412.5	-448.0	0.00	0.07	0.00	-2.34
17.0	0.50	147.4	158.0	-6.00	-6.18	0.00	-1.87
	0.25	72.8	80.2	-5.06	-5.18	-33.75	-35.40
	0.00	-1.3	0.0	-3.00	-3.01	-45.00	-46.60
	-0.25	-75.4	-80.2	-0.94	-0.85	-33.75	-35.90
	-0.50	-150.0	-158.0	0.00	0.12	0.00	-2.34

NOTE:

1. FEM is current work with free end vertical deflection = -0.07747 in.
2. ABAQUS free end vertical deflection = -0.07831 in.

Table 6.3 Stresses of a laminated composite plate due to uniformly distributed transverse load

x	y		σ_x(psi)		σ_y(psi)		τ_{xy}(psi)	
			FEM	ABAQUS	FEM	ABAQUS	FEM	ABAQUS
10.	0	0.50	1462.7	1500.0	0.00	-0.134	0.00	-1.92
		0.375	1097.1	1125.0	0.00	-0.138	-19.92	-20.8
		0.25	731.4	450.0	0.00	-0.055	-34.15	-38.8
	90	0.25	139.2	450.0	0.00	-0.055	-34.15	-38.8
		0.00	0.00	0.0	0.00	0.000	-38.71	-40.4
		-0.25	-139.2	-450.0	0.00	-0.058	-34.15	-38.8
	0	-0.25	-731.4	-450.0	0.00	-0.058	-34.15	-38.8
		-0.375	-1097.1	-1125.0	0.00	0.143	-19.92	-20.8
		-0.50	-1462.7	-1500.0	0.00	0.137	0.00	-1.93
17.	0	0.50	146.1	169.0	-6.00	-6.30	0.00	-1.25
		0.375	109.1	132.0	-5.74	-5.64	-11.95	-12.50
		0.25	72.3	57.4	-5.06	-4.94	-20.49	-23.30
	90	0.25	16.7	57.4	-5.06	-4.94	-20.49	-23.30
		0.00	-0.9	-0.6	-3.00	-2.98	-23.22	-24.3
		-0.25	-18.6	-8.9	-0.94	-0.965	-20.49	-23.30
	0	-0.25	-74.6	-8.9	-0.94	-0.965	-20.49	-23.30
		-0.375	-111.4	-134.0	-0.26	-0.365	-11.95	-12.50
		-0.50	-148.5	-170.0	0.00	1.31	0.00	-1.25

NOTE:
1. FEM is current work with free end vertical deflection = -0.08814 in.
2. ABAQUS free end vertical deflection = -0.08740 in.

The stresses of current plate theory are compared with the ABAQUS plane stress results in Table 6.3. The transverse shear stress and the transverse normal stress at x = 17″ are plotted in Figure 6.3 for comparison. From Table 6.3, it is seen that there is a better stress agreement at x = 10″ than those at x = 17″. In Figure 6.3, it is shown that current work fits the boundary conditions much better than the ABAQUS result and demonstrates a more smooth stress distribution which may indicate the superiority of current work.

It is important to realize that in above demonstrated examples, two completely different finite elements have been used for comparison, namely plate element for current work versus plane stress element for ABAQUS. The good agreement between these two elements clearly verifies the existence of the transverse normal stress and the reasonable shear stress generation capabilities of current work. Besides, the coarse plate model versus the fine plane stress model proves the computational efficiency of current work.

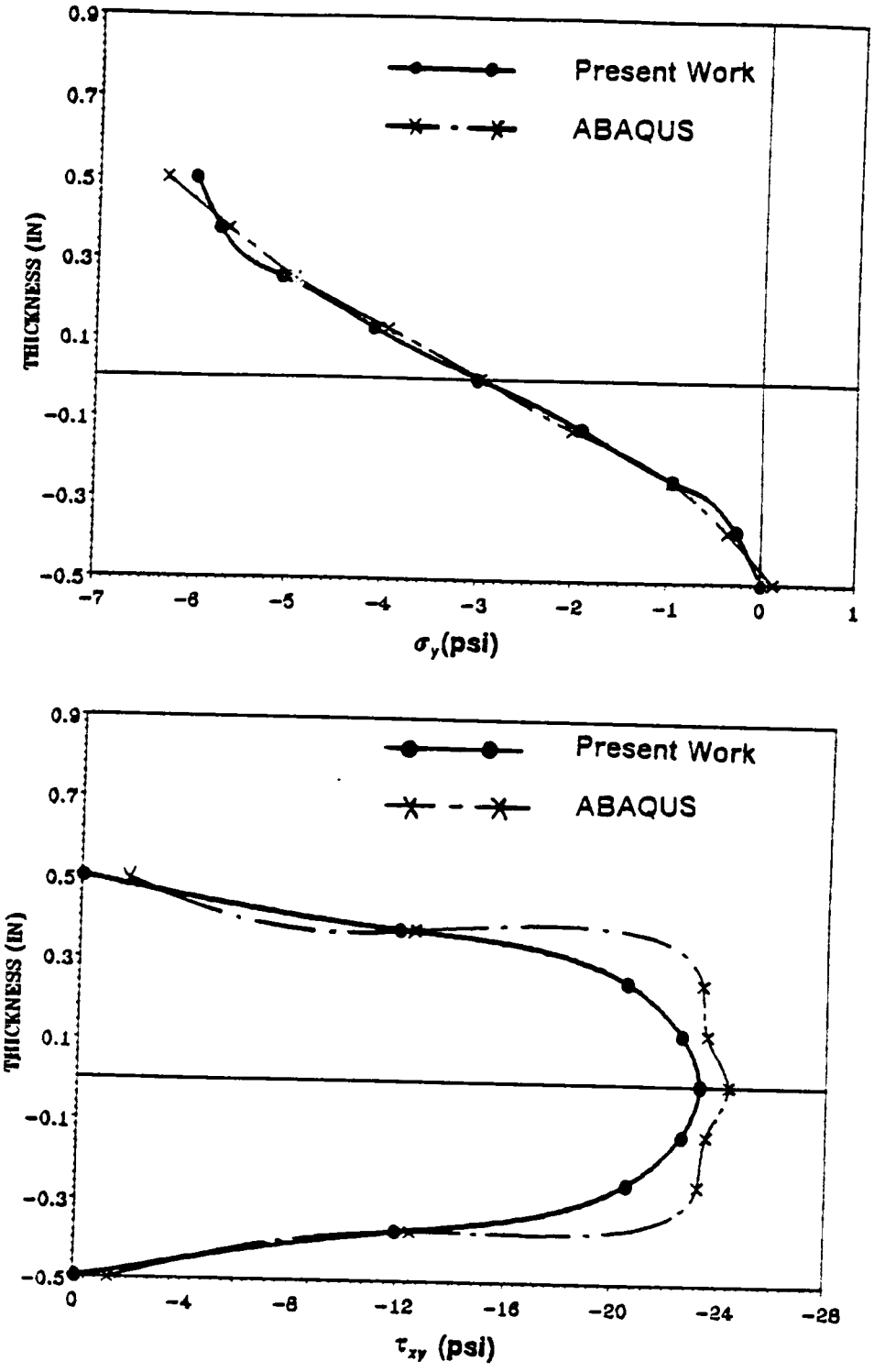

Figure 6.3 Stresses of a uniformly loaded composite plate at location under the loading(x=17″)

6.3 PROBLEM 2: LARGE BENDING DEFLECTION

The most common large deformation test problem is a cantilever beam subjected to cylindrical bending. The reason to choose this problem as a large deformation test problem is because the availability of the analytical solution for an isotropic beam. The geometry, loading condition and finite element mesh used are shown below :

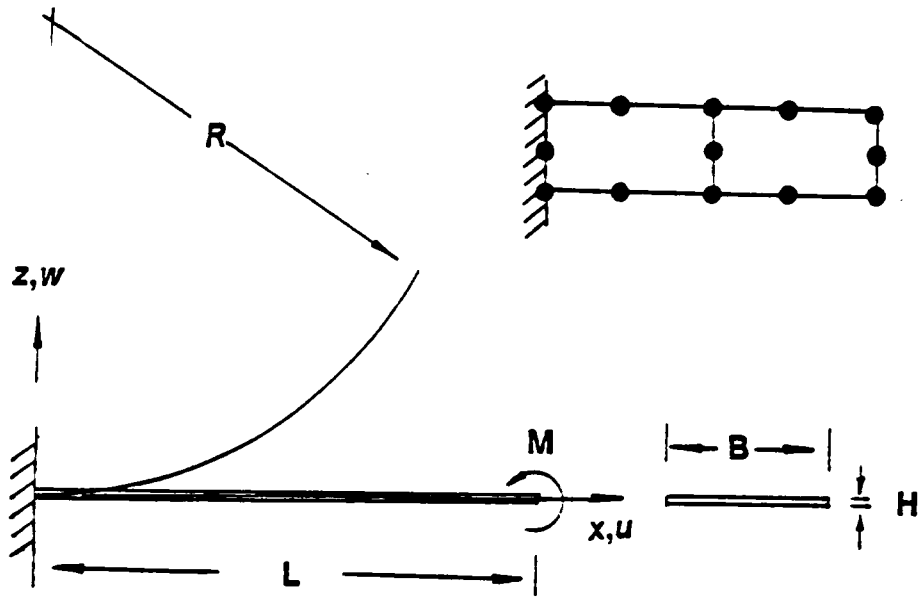

L=4" H=0.1" B=1.0" M_y=-30.0 in-lb

An isotropic beam and a three layer [0/90/0] laminated composite beams are investigated.

A. isotropic beam

For this beam, the Young's modulus is assumed to be E = 1.0E7 psi and the Poisson's ratio is assumed to be ν = 0.0 to simulate a pure bending state. Analytical solution of this problem are :

$$\sigma_x = \frac{M_y C}{I} \qquad \text{Radius} = \frac{EI}{M_y}$$

B. symmetrical three layer [0/90/0] composite beam

Material properties used for this beam are :

E_1 = 7.5E6 psi, $E_2 = E_3$ = 2.0E6 psi,

G_{12} = 1.25E6 psi, $G_{12} = G_{13} = G_{23}$,

$\nu_{23} = \nu_{12} = \nu_{13}$ = 0.25

The results of the isotropic beam are presented in Table 6.4. The excellent agreement between current work solution and the analytical solution verifies the nonlinear matrix derivation of this work. In this example, since there is no shear loading, the shear stresses are zero. The number of iterations taken for convergence of the first order shear deformation theory and the current theory of this example provides a strong evidence that reasonable shear stress distribution will accelerate the numerical iteration procedures. The reason is because unrealistic shear stresses can not generate correct stress resultants. For this reason, current work show strong superior convergent speed. Radius of both isotropic beam and orthotropic beam are plotted in

Figure 6.5, where a smooth curve of radius distribution shows a reasonably good result has been obtained for the laminated composite beam. The major bending radius and the minor bending radius of the composite beam are listed in Table 6.5 for future comparison.

Table 6.4 Cylindrical bending

Load	*Iteration*(1)		Radius(in)		σ_{11}(psi)			$\sigma_{13}^{(2)}$(psi)		$\sigma_{12}^{(2)}$(psi)	
	FSDT	*FEM*(4)	Exact	*FEM*(3)	Exact	FSDT	*FEM*(4)	FSDT	*FEM*(4)	FSDT	*FEM*(4)
0.2M	2	2	138.8	139.9	3600	3600	3600	0.0	0.0	0.0	0.0
0.4M	7	3	69.4	69.3	7200	7199	7200	86.3	0.0	-0.3	-0.2
0.6M	7	4	46.3	46.2	10800	10799	10800	259.3	0.0	-1.9	-1.3
0.8M	7	4	34.7	34.6	14400	14398	14400	518.4	0.0	-5.8	-3.9
1.0M	8	4	27.7	27.6	18000	17997	18000	862.1	0.0	-12.8	-8.6

Note :

(1) Number of iterations (i) is determined according to the following convergence criterion

$$\left| \frac{\{^{t+\Delta t}R\} - \{^{t+\Delta t}U^{i}\}}{\{^{t+\Delta t}R\}} \right| \leq Tol = (3.0\text{x}10^{-3} - 0.5\text{x}10^{-3}i)$$

(2) The exact values of σ_{13} and σ_{12} are zero.

(3) The radius for FSDT is the same for current work.

(4) *FEM*(4) represents current work.

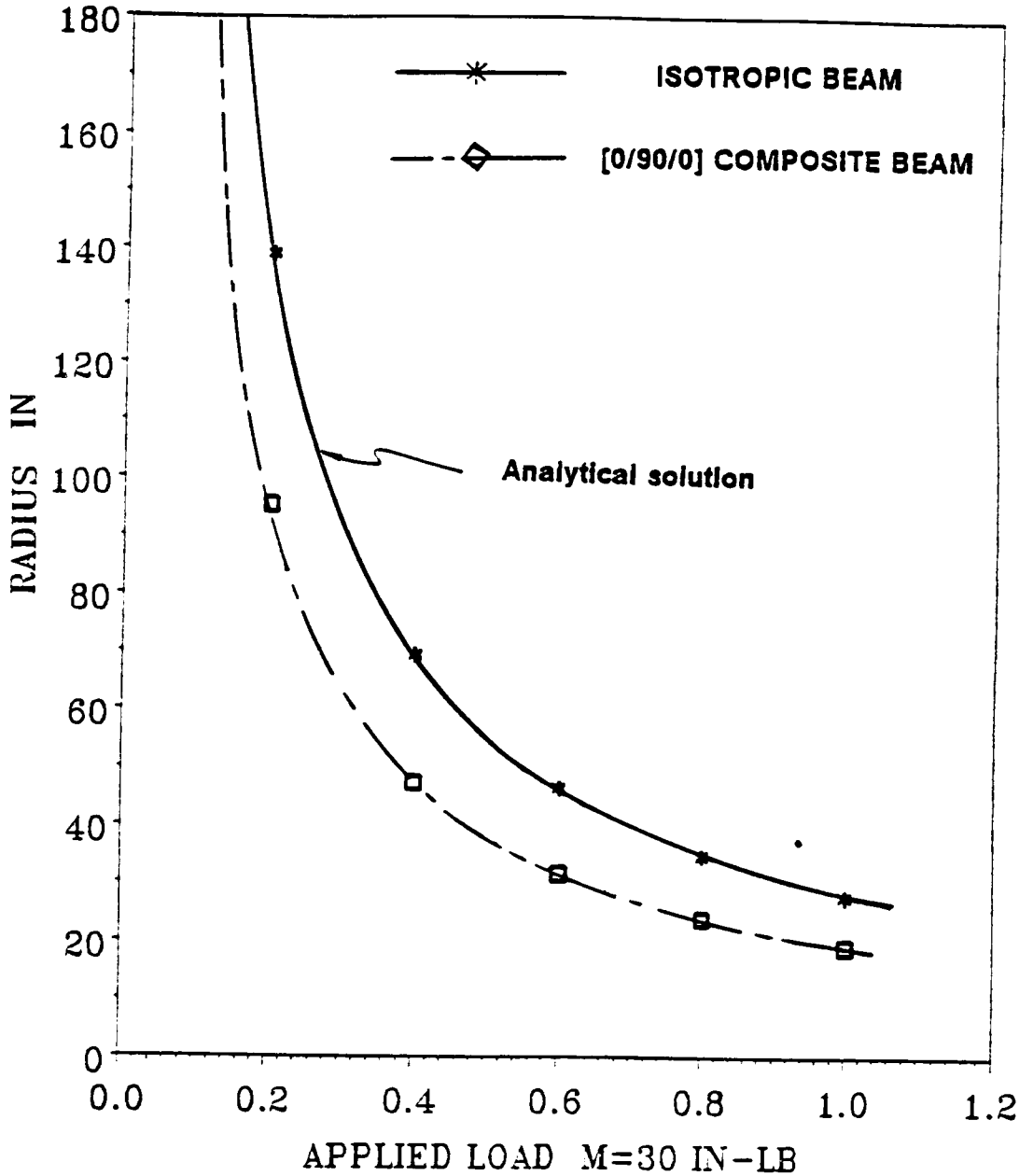

Figure 6.5 Radii of cylindrical bending of a cantilevel beam

Table 6.5 Radii of cylindrical bending of a composite beam

Load M=30in-lb	Major Radius(in)	Minor Radius(in)			
		1"	2"	3"	4"
0.2M	95.2	805.8	402.9	476.5	583.0
0.4M	47.2	403.3	201.6	238.0	290.0
0.6M	31.6	269.9	134.9	158.7	191.8
0.8M	23.8	203.8	101.9	119.2	142.3

NOTE :

1. Major radius is the radius along the beam.
2. Minor radius is the radius across the beam.

6.4 PROBLEM 3 : FOLDED STRUCTURE

The purpose of this example is to illustrate the capability of the present program to model folded structures, which requires transformation of element matrices and activates the rotational degree of freedom (about the z-axis). In this example, a "L" shaped structure (see figure below) is chosen as a test problem because the availability of its analytical solution. The geometry, loading, material properties and mesh used are shown in following figure.

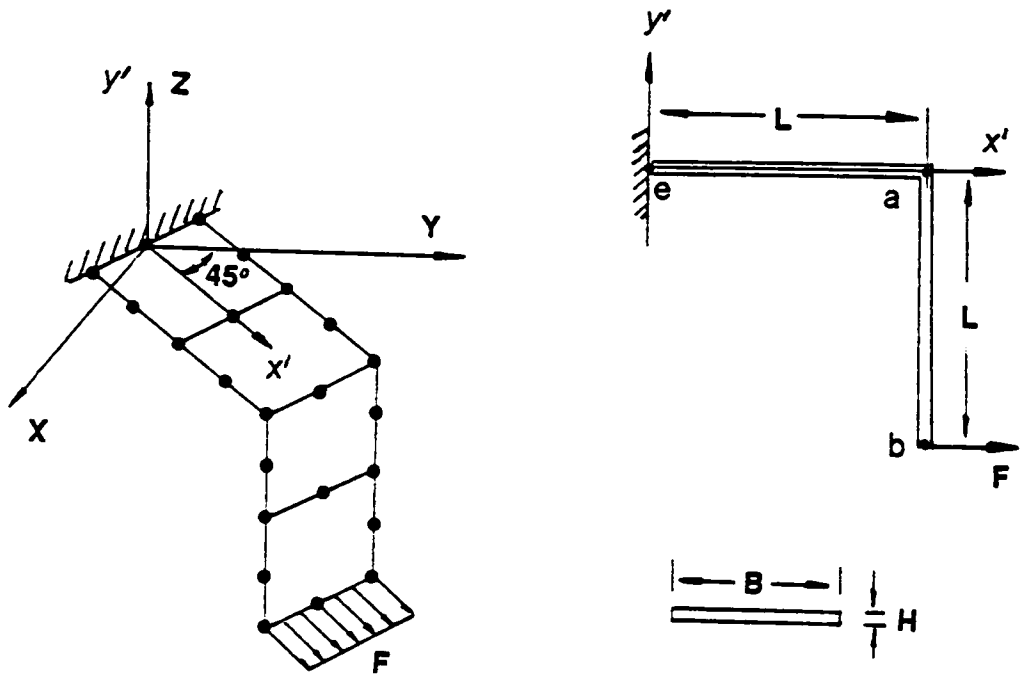

L = 4″ H = 0.1″ B = 1.0″ E = 1.0x10⁷ psi, ν = 0.0 F = 6.0lb

The analytical solution of this problem is given in [61] :

A.Displacements:

$$\delta^a_{y'} = \frac{ML^2}{2EI} \qquad \delta^a_{y'} = \delta^b_{y'} \qquad \delta^b_{x'} = \theta L + \frac{FL^3}{3EI}$$

B. Stresses $\sigma_1 = \frac{MX_3}{EI} \pm \frac{F}{A}$ $\sigma_{13} = \frac{F}{2I}\left(\frac{h^2}{4} - x_3^2\right)$

The displacements and the stresses obtained using the present element are given in Tables 6.6 and 6.7, respectively. The analytical solutions are not included due to their simplicity. The good agreement between current work and the analytical solution verifies the transformed stiffness matrix derived in current work.

Table 6.6 Displacements

Node	u(in)	v(in)	w(in)	θ_x(rad)	θ_y(rad)	θ_z (rad)
a	0.0	0.0	0.1152	0.04073	-0.04073	0.0
b	0.2172	0.2172	0.1152	0.06109	-0.06109	0.0

Table 6.7 Stresses

Node	x_3	σ_{11} (psi)	τ_{13} (psi)
e	0.05	-7170.19	0.0
	0.025	-3570.05	0.0
	0.0	30.00	0.0
	-0.025	3630.05	0.0
	-0.05	7230.10	0.0
a	0.05	-7185.04	0.0
	0.025	-3585.02	16.88
	0.0	15.00	22.50
	-0.025	3615.02	16.88
	-0.05	7215.04	0.0
b	0.05	0.0	0.0
	0.025	0.0	33.75
	0.0	0.0	45.00
	-0.025	0.0	33.75
	-0.05	0.0	0.0

Note : Node "a" yields the average solutions.

6.5 PROBLEM 4: COMPOSITE PLATE

This example deals with a three-layer cross-ply (0/90/0) square laminate with all four edges simply supported and subjected to sinusoidally distributed transverse load (see figure below). This problem has a 3-D elasticity solution [57]. Due to symmetricity, only quarter of the laminate is modeled by eight-node quadratic elements.

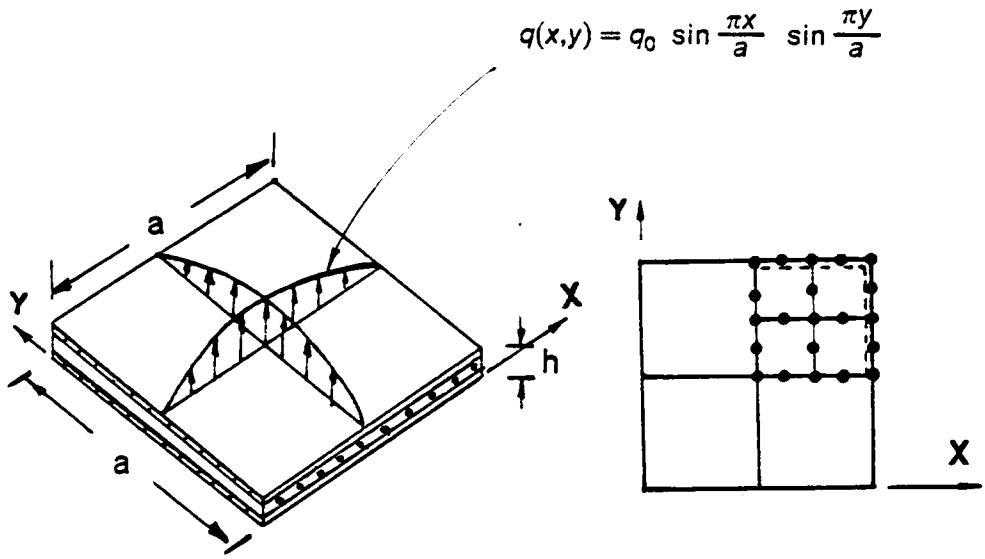

The ply thickness are $h_1 = h_3 = h/4$, $h_2 = h/2$.

The lamina properties are $\frac{E_1}{E_2} = 25$, $\frac{G_{12}}{E_2} = 0.5$, $\frac{G_{23}}{E_2} = 0.2$, $\nu_{12} = \nu_{13} = \nu_{23} = 0.25$.

The nondimensional stress and displacement quantities are defined as

$$\bar{w} = \frac{w(a/2, a/2)E_2 h^3 x100}{q_0 a^4}, \qquad \bar{\sigma}_1 = (\frac{h}{a})^2 \sigma_1(A,A,\frac{\pm h}{2})$$

$$\bar{\sigma}_2 = (\frac{h}{a})^2 \sigma_2(A,A,\frac{\pm h}{4}), \qquad \bar{\sigma}_{12} = (\frac{h}{a})^2 \sigma_{12}(B,B,\frac{\pm h}{2}) \text{ in ply 1 \& 3}$$

$$\bar{\sigma}_{13} = (\frac{h}{a})\sigma_{13}(B,A) \text{ in ply 2}, \qquad \bar{\sigma}_{23} = (\frac{h}{a})\sigma_{23}(A,B) \text{ in ply 2.}$$

where A and B are the Gauss-Point coordinates (w.r.t the center of the plate) given below:

	2x2Q mesh	4x4Q mesh
A	0.05283a	0.02642a
B	0.44720a	0.47360a

The three-dimensional elasticity solution, and results of the first-order shear deformation theory and current work are compared at Gauss points for different plate thicknesses in Table 6.8. As expected, there is no improvement in the accuracy of the displacement solution. The reason for this is that the higher order terms of the normal displacement are not being used in the kinematics conditions and stiffness matrix formulation for the global displacement solution. However, remarkable improvement can be observed in the stress components. The transverse shear stresses ($\overline{\sigma}_{13}$, $\overline{\sigma}_{23}$) show higher degree of improvements than the in-plane shear stress ($\overline{\sigma}_{12}$).

Similar comparisons are made in Table 6.9 at different nodal points. Note that the in-plane stress ($\hat{\sigma}_1$) is unsymmetrical for thick plates as predicted by 3-D elasticity solution. Such unsymmetricity is not predicted by the first-order shear deformation theory. The nondimensional displacement ($\hat{U}$) and the nondimensional transverse shear stresses ($\hat{\sigma}_{13}$, $\hat{\sigma}_{23}$) are plotted through the plate thickness in Figures 6.6, 6.7 and 6.8. As expected, the rotational degrees of freedom of current work are layer dependent quantities. The continuous distribution and relative accuracy of the transverse shear stress verifies the improvements of the current work.

Table 6.8 Result comparisons at Gauss points

a/h	Method	$\overline{w}$	$\overline{\sigma}_1$	$\overline{\sigma}_2$	$\overline{\sigma}_{12}$	$\overline{\sigma}_{13}$	$\overline{\sigma}_{23}$
10	3D	7.434	0.599	0.403	0.0276	0.301	0.196
	FEM4	6.262	0.5586	0.3710	0.0250	0.3196	0.1660
	FSDT4	6.262	0.495	0.359	0.0240	0.414	0.128
	FEM2	6.152	0.5245	0.3605	0.0239	0.3126	0.1626
	FSDT2	6.152	0.4842	0.3509	0.0234	0.404	0.1255
20	3D	5.173	0.543	0.308	0.0230	0.328	0.156
	FEM4	4.911	0.5402	0.2961	0.0222	0.3353	0.1397
	FSDT4	4.911	0.524	0.294	0.0219	0.434	0.108
	FEM2	4.901	0.5224	0.2890	0.0215	0.3275	0.1368
	FSDT2	4.901	0.5112	0.2870	0.0214	0.424	0.1057
100	3D	4.385	0.539	0.271	0.0214	0.339	0.139
	FEM4	4.336	0.5351	0.2686	0.0212	0.3411	0.1296
	FSDT4	4.336	0.535	0.269	0.0212	0.442	0.1002
	FEM2	4.319	0.5217	0.2621	0.0206	0.334	0.1131
	FSDT2	4.319	0.5214	0.2621	0.0206	0.435	0.1020

Where

1. 3D : 3D-Elasticity Solution [57]
2. FEM4 : Present work with 4X4Q mesh
3. FEM2 : Present work with 2X2Q mesh
4. FSDT4 : First Order Theory with 4X4Q mesh [1]
5. FSDT2 : First Order Theory with 2X2Q mesh [1]

Table 6.9 Result comparisons at nodal points

a/h	$\hat{\sigma}_1(\frac{a}{2},\frac{b}{2},\frac{\pm h}{2})$		$\hat{\tau}_{13}(0,\frac{b}{2},0)$		$\hat{\tau}_{23}(\frac{a}{2},0,0)$		$\hat{\tau}_{12}(0,0,\frac{\pm h}{2})$	
	3D	FEM	3D	FEM	3D	FEM	3D	FEM
2	1.436	1.374	.164	.251	0.259	0.258	-.0859	-.0578
	-.938	-1.296	.309	.251	0.260	0.258	.0702	.0578
4	.801	.728	.256	.291	.2172	.1823	-.0511	-.0406
	-.755	-.708	.282	.291	.2172	.1823	.0505	.0406
10	±.590	±.565	.357	.330	.1228	.1068	∓.0289	∓.0259
20	±.552	±.545	.385	.339	.0938	.0886	∓.0234	∓.0225
50	±.541	±.539	.393	.3419	.0842	.0831	∓.0216	∓.0214
100	±.539	±.538	.395	.3422	.0828	.0826	∓.0213	∓.0213

Where

1. $(\hat{\sigma}_1, \hat{\sigma}_2, \hat{\tau}_{12}) = \frac{(\sigma_1, \sigma_2, \tau_{12})}{\sigma S^2}$, $(\hat{\tau}_{13}, \hat{\tau}_{23}) = \frac{(\tau_{13}, \tau_{23})}{\sigma S}$, $S = \frac{a}{h}$
2. 3D : 3D-Elasticity Solution [57]
3. FEM : Present work with 4X4Q mesh

Figure 6.6 NONDIMENSIONAL STRESS OF A 4 EDGES SIMPLY SUPPORTED SQUARE LAMINATED(0/90/0) PLATE (A/H=4) UNDER SINUSOIDAL LOAD

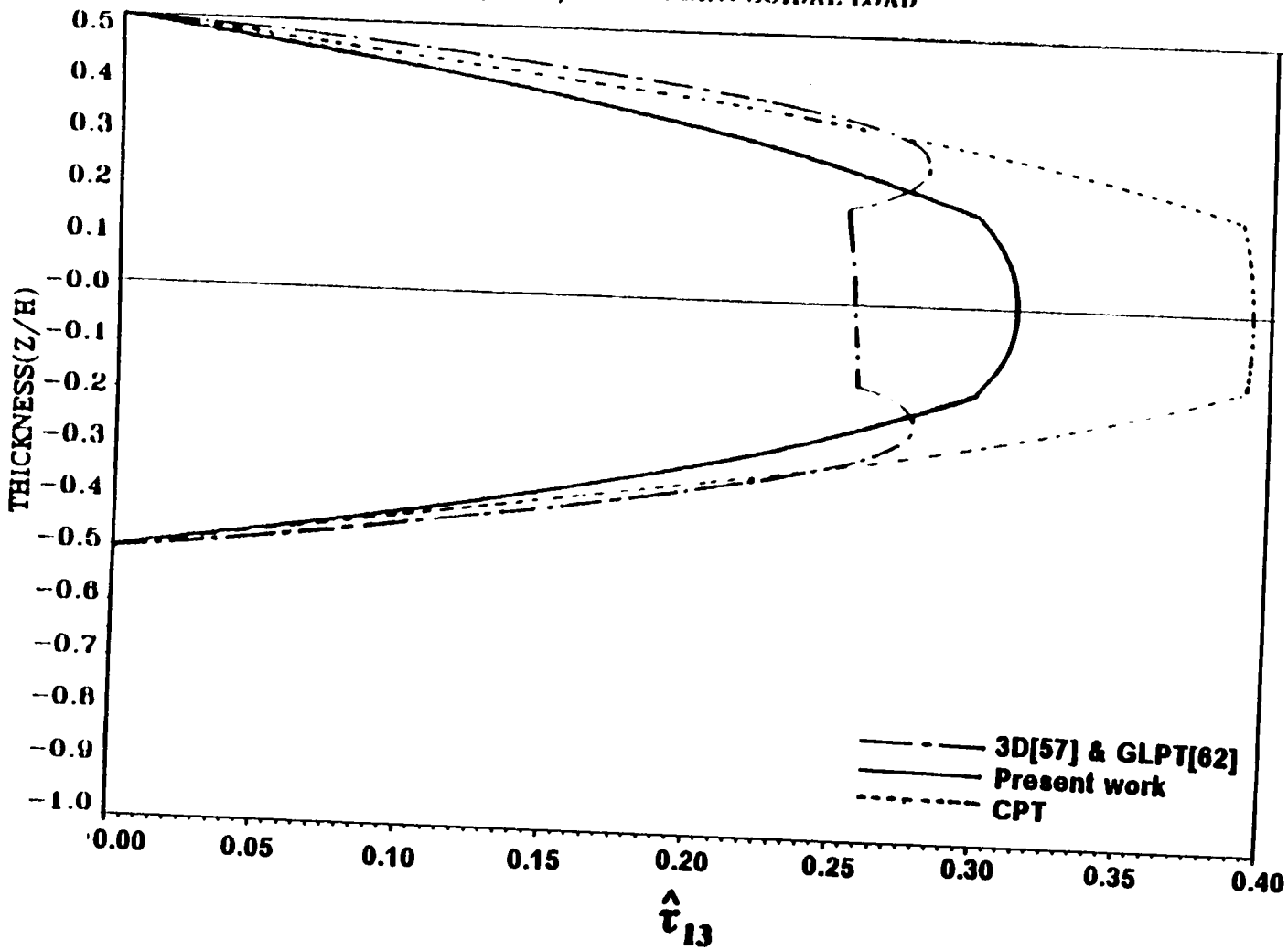

Figure 6.7 NONDIMENSIONAL U OF A 4 EDGES SIMPLY SUPPORTED SQUARE LAMINATED(0/90/0) PLATE (A/H=4) UNDER SINUSOIDAL LOAD

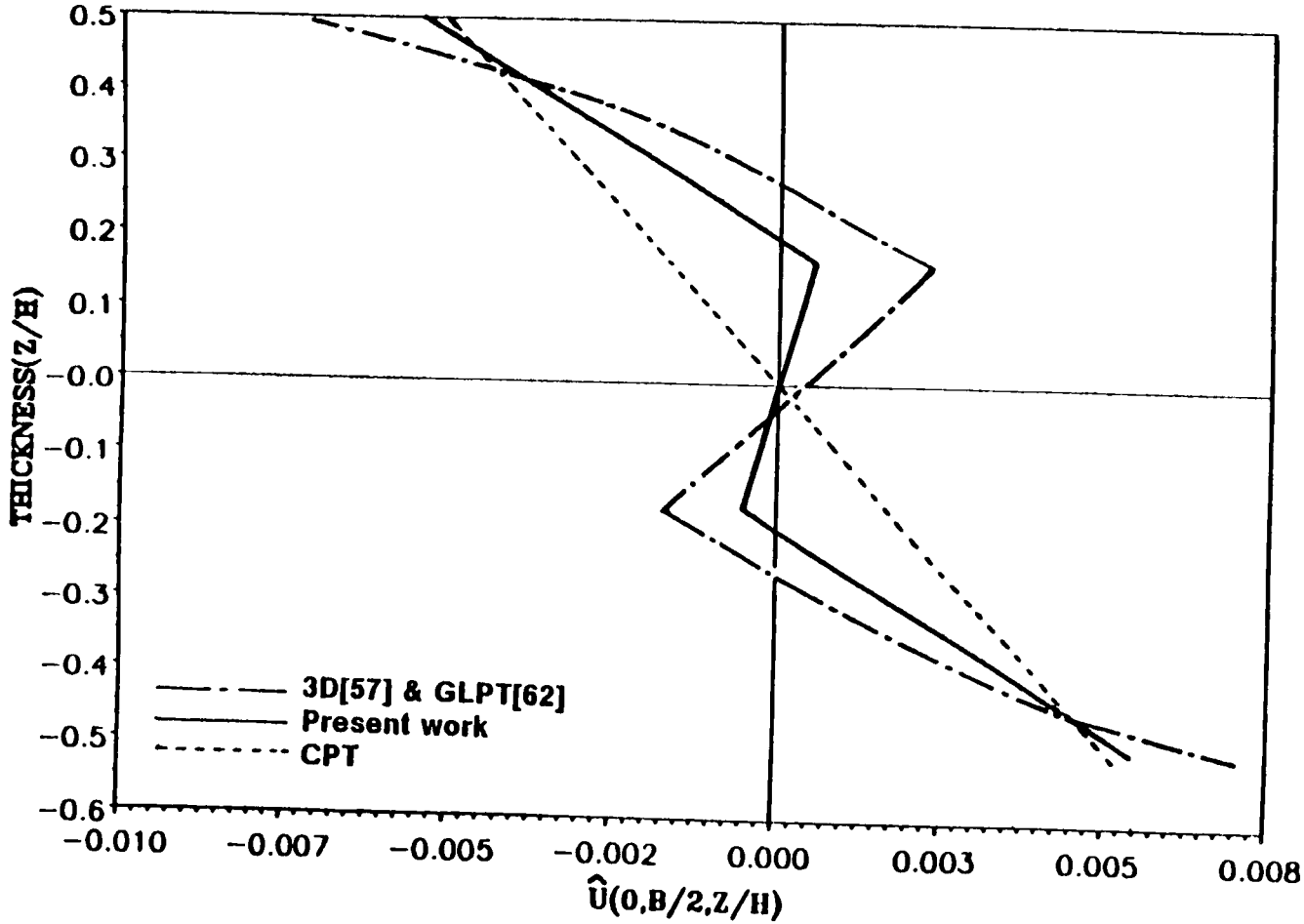

Figure 6.8 NONDIMENSIONAL STRESS OF A 4 EDGES SIMPLY SUPPORTED SQUARE LAMINATED(0/90/0) PLATE (A/H=4) UNDER SINUSOIDAL LOAD

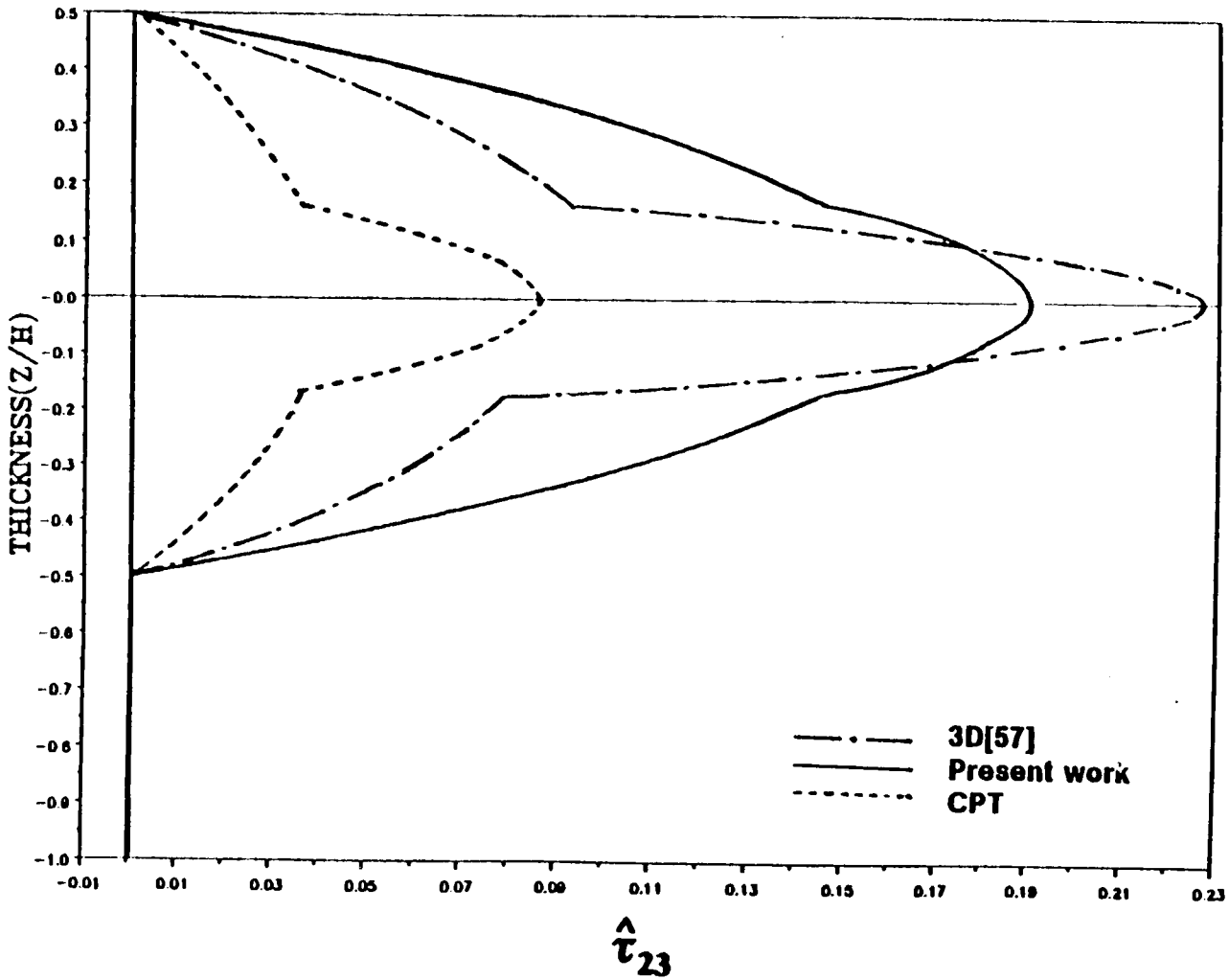

6.6 *PROBLEM 5 : PLATE WITH SURFACE TRACTION*

Plate with nonzero surface traction are not frequently found in the literature. In this example, a cantilever plate with continuously distributed constant surface traction and partially distributed constant surface traction are investigated.

A. isotropic plate with fully distributed constant surface traction

The geometry, loading condition and material properties of an isotropic plate is shown in the figure below.

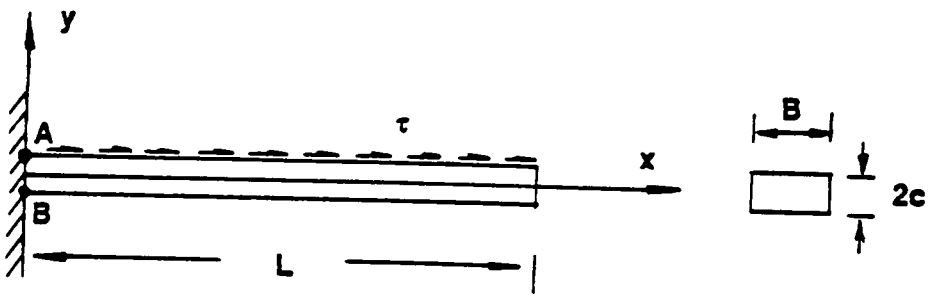

$E = 3.0 \times 10^6$ psi, $\nu = 0.0$, $L = 20''$, $B = 1.0''$, $2c = 1.0''$, $\tau = 6$ psi

The finite element mesh used in this problem is the same as in Problem 1. The exact solution of the problem from Ref. [63] is listed below :

(i) at point A: $\sigma_x = \frac{-\tau L}{c}$; $\tau_{xy} = 0$

(ii) at point B: $\sigma_x = \frac{2\tau L}{c}$; $\tau_{xy} = \tau$

Stress comparisons are listed in Table 6.10. The excellent agreement of analytical solution and current work solution validates the stress recovery technique developed in this work.

Table 6.10 Stresses of an isotropic plate with full surface traction

Location	σ_x (psi)		τ_{xy} (psi)	
	Exact	FEM	Exact	FEM
Point A	480.0	480.01	6.0	6.0
Point B	-240.0	-240.01	0.0	0.0

B. isotropic plate with partially distributed constant surface traction

The geometry, loading condition and material properties of this plate are shown in the figure below.

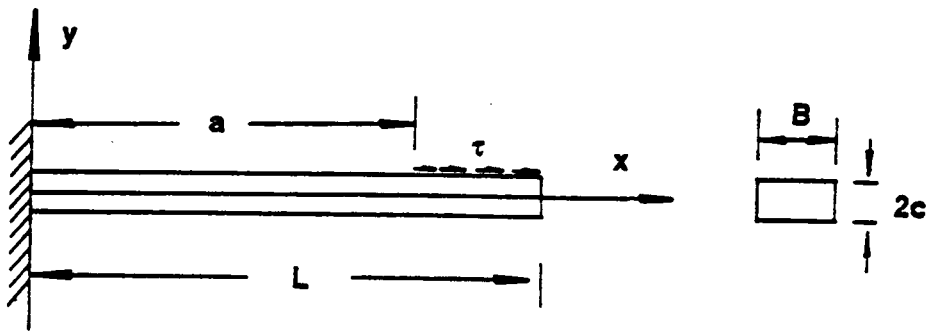

$E = 3.0x10^6$ psi, $\nu = 0.0$, L = 20″, B = 1.0″, 2c = 1.0″, $\tau = 6$ psi, a = 15″

Stresses computed in the current work are compared with those from ABAQUS program in Table 6.11. In general, this table shows good agreement between these two results.

Table 6.11 Stresses of nonzero surface traction plate

x (in)	y (in)	σ_x(psi)		τ_{xy}(psi)	
		FEM	ABAQUS	FEM	ABAQUS
10.0	0.5	120.0	120.0	0.0	-0.00106
	0.25	75.0	75.0	0.0	0.00024
	0.0	30.0	30.0	0.0	-0.00001
	-0.25	-15.0	-15.0	0.0	0.00049
	-0.5	-60.0	-60.0	0.0	-0.00030
15.0	0.5	120.0	123.0	3.0	2.91
	0.25	75.0	73.8	1.13	0.465
	0.0	30.0	29.1	0.0	-0.843
	-0.25	-15.0	-14.8	-0.38	-1.03
	-0.5	-60.0	-59.0	0.0	-0.092
17.0	0.5	72.0	72.0	6.0	5.79
	0.25	45.0	45.0	2.5	0.946
	0.0	30.0	18.0	0.0	-1.69
	-0.25	-9.0	-9.0	-0.75	-2.04
	-0.5	-36.0	-36.0	0.0	-0.171

NOTE:

1.FEM is present work with free end vertical deflect. = -0.003525 in.
2.ABAQUS free end vertical deflect. = -0.0035259 in.
3.Both FEM and ABAQUS yield σ_y = 0.0 through out the whole plate.

C. composite plate with partially distributed constant surface traction

The geometry, loading and finite element meshes used in this composite plate are the same as in case B. The lamination scheme used is [0/90/0] with following material properties of a layer :

E_1 = 25.0E6 psi, $E_2 = E_3$ = 1.0E6 psi,

$G_{12} = G_{13}$ = 0.5E6 psi, G_{23} = 0.2E6 psi, $\nu_{12} = \nu_{13} = \nu_{23}$ = 0.25

The ply thicknesses are assumed to be $h_1 = h_3 = 0.25in$, $h_2 = 0.5in$.

Stresses from the present work are compared with those from ABAQUS in Table 6.12. In general, a good agreement between these two results is noted, except at the lamina interfaces, where the in-plane stress of current work is discontinuous (as it should be) and that of ABAQUS is continuous. This is because ABAQUS computes average stresses [60] at lamina interfaces even for in-plane stresses (which are discontinuous at interfaces).

The transverse shear stresses of Table 6.11 and Table 6.12 are plotted in Figure 6.9, where current work results fit the boundary condition better and form more smooth stress curve than the ABAQUS results. The discrepancy between the current results and ABAQUS results is most likely due to the fact that the mesh used in ABAQUS is not fine enough to generate accurate results, which further proves the computational efficiency of current work.

Table 6.12 Stresses of nonzero surface traction composite plate

x (in)	y (in)	σ_x(psi)		τ_{xy}(psi)	
		FEM	ABAQUS	FEM	ABAQUS
10.0	0.5	160.77	160.00	0.0	0.00544
	0.375	135.00	134.00	0.0	0.00007
	0.25	109.23	56.60	0.0	-0.00286
	0.25	4.32	56.60	0.0	-0.00286
	0.0	2.30	2.31	0.0	0.00016
	-0.25	0.29	3.41	0.0	-0.00059
	-0.25	6.82	3.41	0.0	-0.00059
	-0.375	-18.63	-19.00	0.0	-0.00004
	-0.5	-44.58	-44.00	0.0	0.00113
17.0	0.5	97.94	96.10	6.00	5.72
	0.375	82.11	80.60	3.50	2.43
	0.25	66.28	33.9	1.40	-0.794
	0.25	2.57	33.9	1.40	-0.794
	0.0	1.38	1.37	0.22	-0.905
	-0.25	0.18	1.99	-0.31	-1.06
	-0.25	4.57	1.99	-0.31	-1.06
	-0.375	-10.46	-11.4	-0.36	-0.678
	-0.5	-25.48	-26.6	0.0	-0.203

NOTE:
1.FEM is present work with free end vertical deflect. = -0.0015993 in.
2.ABAQUS free end vertical deflect. = -0.0016091in.

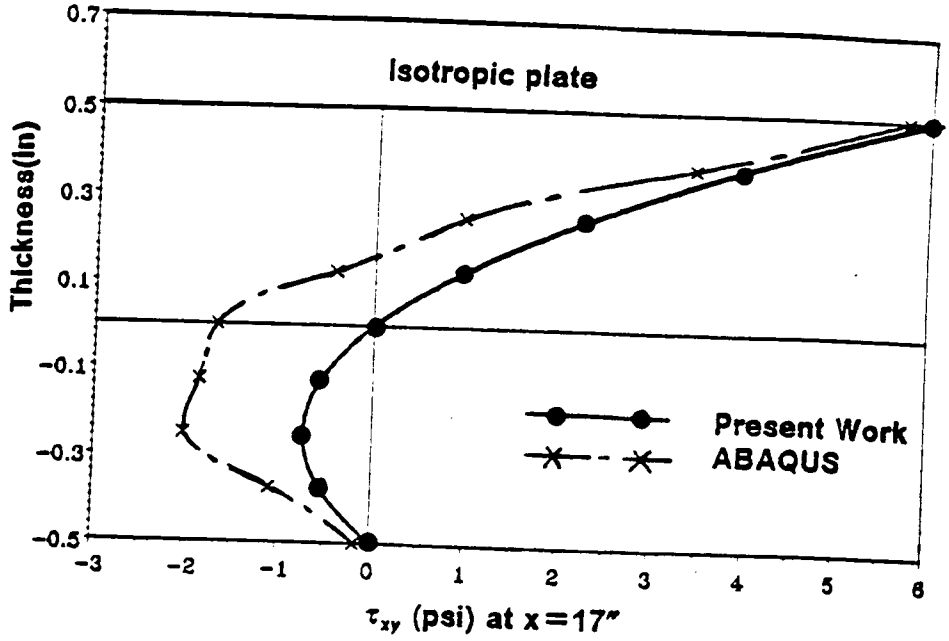

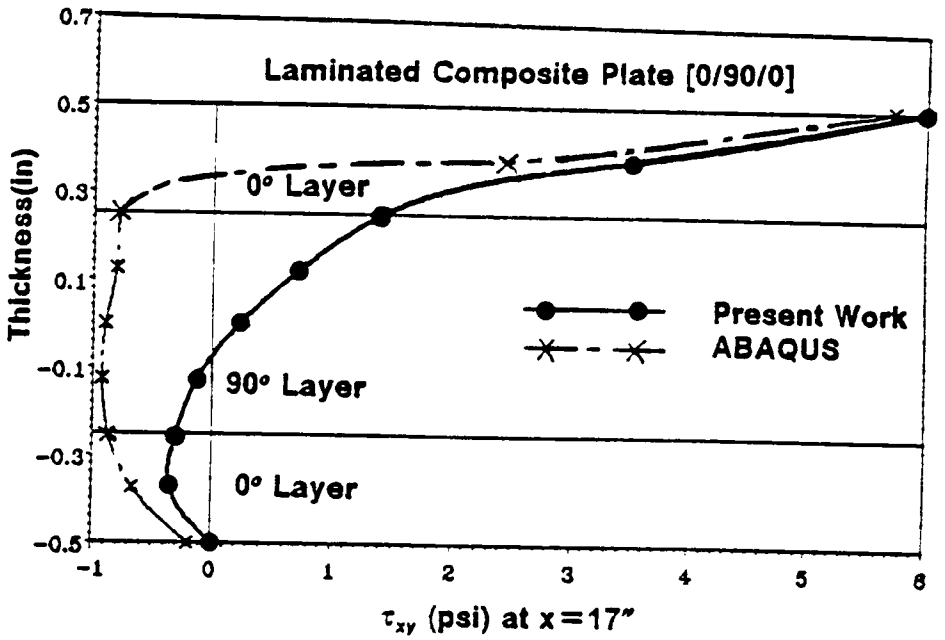

Figure 6.9 **Shear stress due to partial constant surface traction**

6.7 PROBLEM 6 : CYLINDRICAL SHELL ROOF SUBJECTED TO SELF-WEIGHT

An open circular cylindrical shell panel, supported at its two ends by rigid diaphragms (i.e. walls) and has its longitudinal edges free, is subjected to gravitational load due to its own weight. This problem has been investigated extensively by many researchers [64,65,66,67,68,69] and constitutes a standard test problem for the verification of shell elements. The geometry, loading and finite element meshes used in this work are shown below:

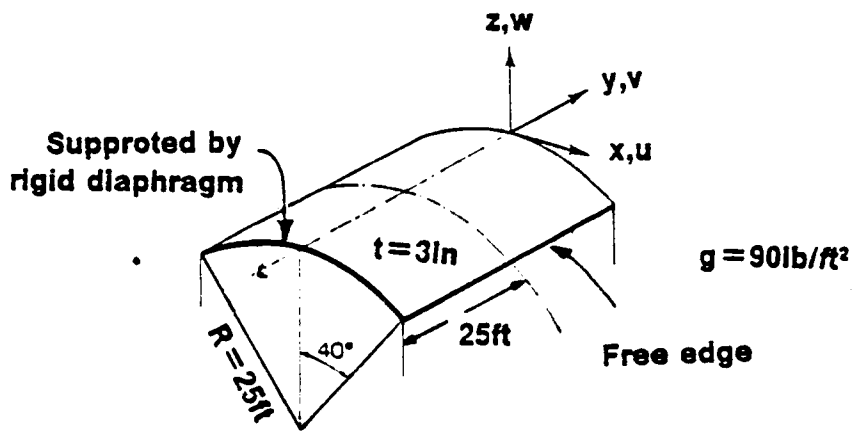

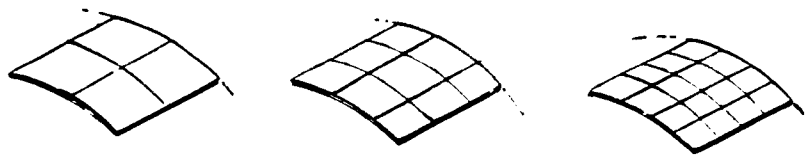

2x2Q8 3x3Q8 4x4Q8

Meshes used

Two different material shell roofs are investigated.

A. isotropic shell roof

The material properties of this shell roof are taken to be E = 3.0E6 psi and ν = 0.0, which are the same values used in Ref. [68]. The 3x3Q8 mesh (3x3 mesh of quadratic eight-node element) results of current work are compared with the exact solution [68] in Table 6.13, which shows very good agreement. The results of different mesh sizes of current work are plotted in Figure 6.10 for comparison with the analytical solution due to Gibson's series [68]. The agreement of the present solution with the exact solution for different mesh sizes verifies the shell element stiffness matrix formulation.

Table 6.13 Deflections of an isotropic shell roof

Angle	W(ft) at mid-span		V(ft) at diaphragm	
(degree)	Exact	FEM	Exact	FEM
0	0.043745	0.045912	0.000248	0.000174
6.67	0.028776	0.030570	0.000712	0.000567
13.33	-0.013887	-0.013380	0.001820	0.001823
20.0	-0.077860	-0.078810	0.002719	0.002744
26.67	-0.153944	-0.156190	0.002004	0.002057
33.33	-0.232743	-0.234480	-0.002268	-0.002131
40.0	-0.308609	-0.307203	-0.012611	-0.012654

NOTE :

1. EXACT is the exact solution obtained from Gibson's series for fifty terms[68].
2. FEM is present work with 2x2 integration as recommended by Zienkiewicz[65].

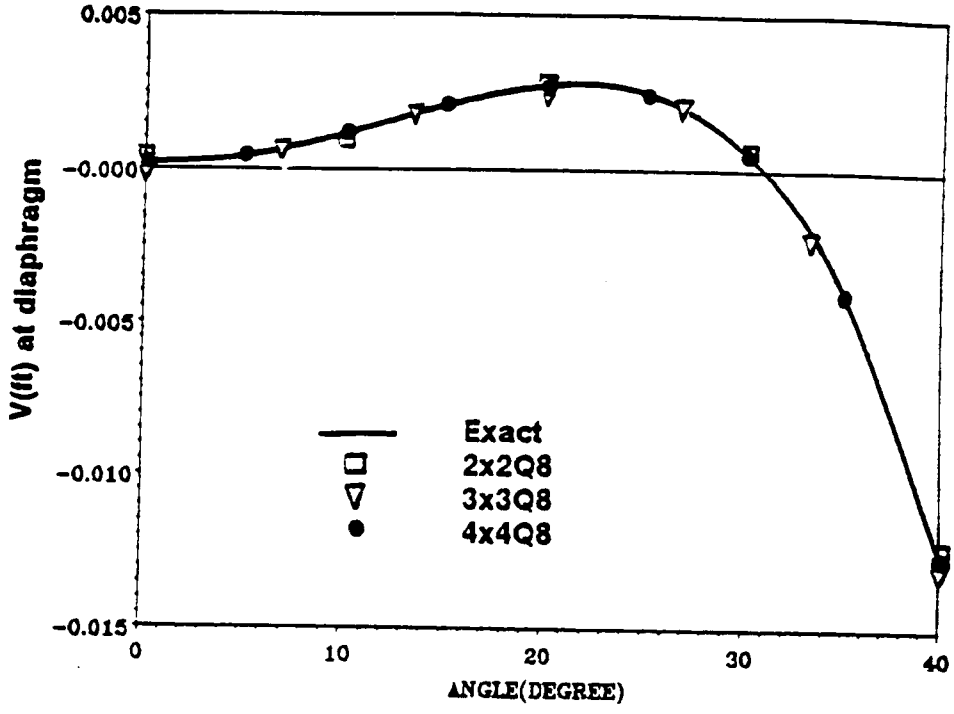

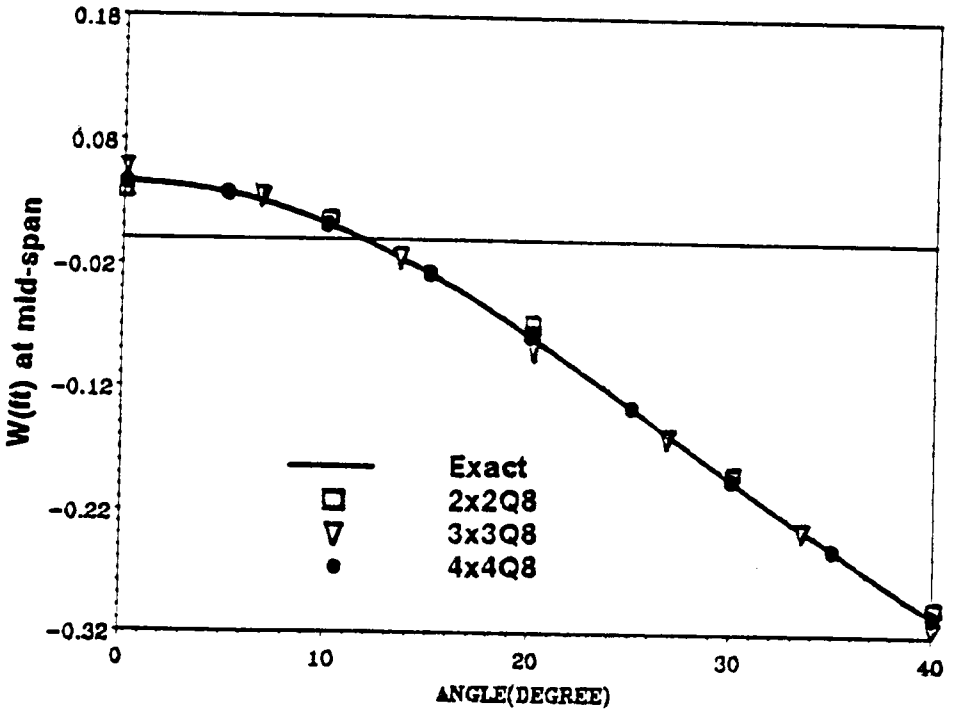

Figure 6.10 Deflections of an isotropic cylindrical shell roof

B. laminated composite shell roof

The geometry and boundary conditions are the same as in case A. The lamina properties used are :

$E_1 = 25.0x10^5$ psf, $E_2 = E_3 = 1.0x10^5$ psf

$G_{12} = G_{13} = 0.5x10^5$ psf, $G_{23} = 0.2x10^5$ psf

$\nu_{12} = \nu_{13} = \nu_{23} = 0.25$

Lamina thickness is $t = 0.05ft$.

Loading due to gravity is g = 9.0 lb/ft^2.

The stacking sequence is [0/0/0/45/-45/90/90/90/-45/45/0/0/0].

The displacement of the 4x4Q8 results of current work are listed in Table 6.14 for future comparison. To examine the effect of mesh, three different meshes are used and the results are plotted in Figure 6.11.

Table 6.14 Deflections of a composite shell roof

Angle (degree)	W(ft) at mid-span	V(ft) at diaphragm
0.0	-0.0364529	0.0036092
5.0	-0.0382482	0.0035227
10.0	-0.0435197	0.0032598
15.0	-0.0517973	0.0027117
20.0	-0.0623128	0.0017436
25.0	-0.0741705	0.0001425
30.0	-0.0865092	-0.002416
35.0	-0.0986092	-0.006234
40.0	-0.1100042	-0.0121372

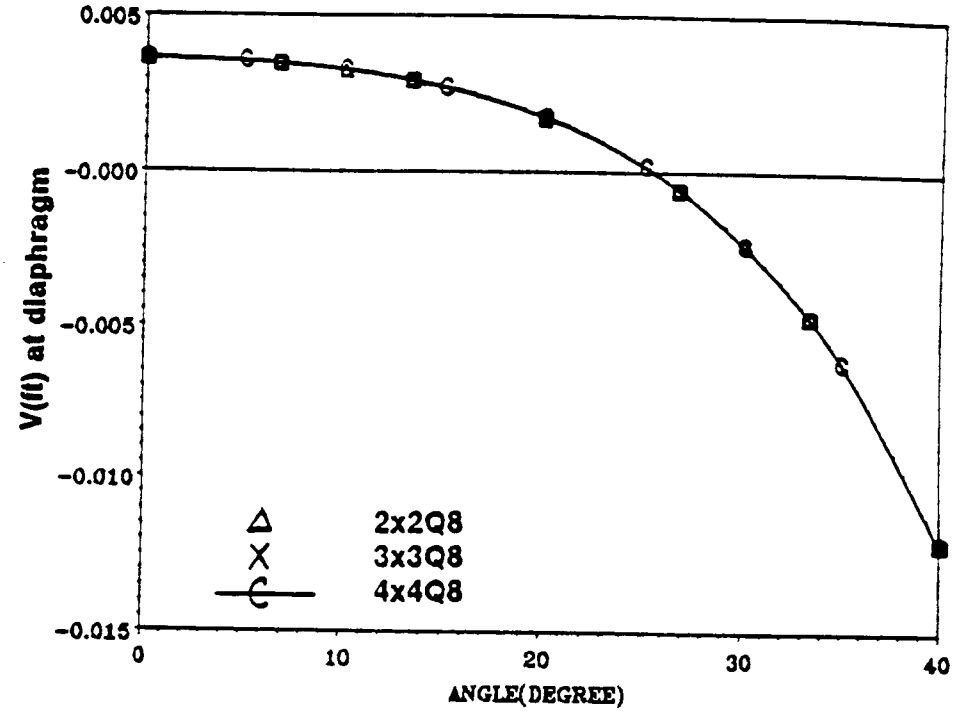

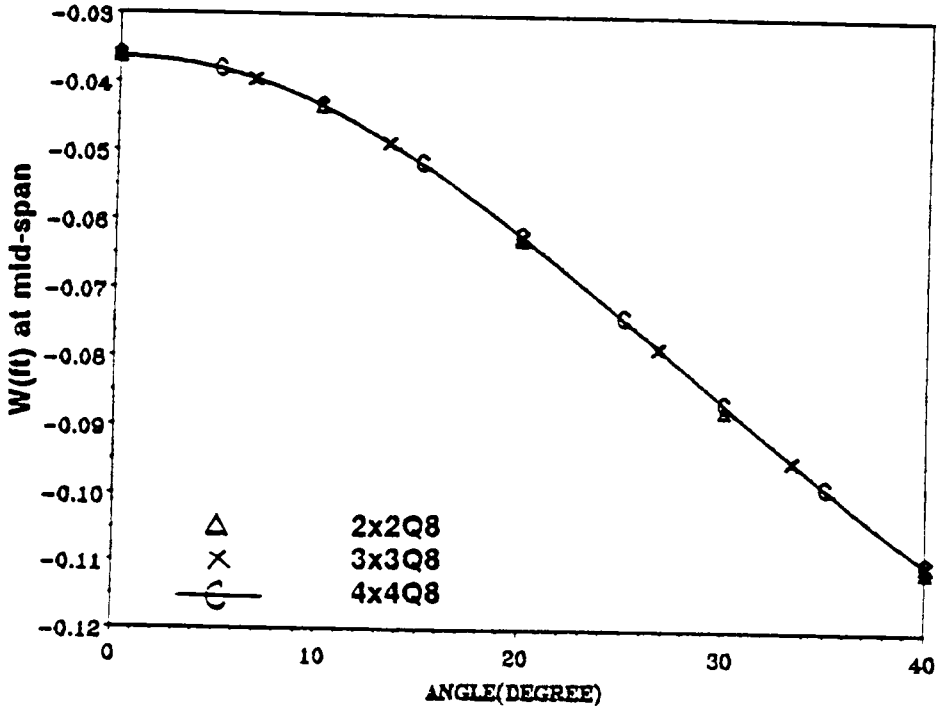

Figure 6.11 Deflections of a laminated composite shell roof

6.8 PROBLEM 7 : THICK CYLINDER UNDER PRESSURE

The conventional way of analyzing a pressurized vessel is to use a 3D solid element to determine the radius stress (i.e. transverse normal stress in shell element). This approach requires larger amounts of computer memory and computational time. This approach would become very combersome when the vessel is made of laminated composite materials. In this example, the 2D continuum-based shell element is used to test the accuracy of the solution. The radial and circumferential stresses from the 2D elasticity solutions are given by

$$\sigma_r = \frac{p_i b^2}{a^2 - b^2}\left(1 - \frac{a^2}{r^2}\right) - \frac{p_o a^2}{a^2 - b^2}\left(1 - \frac{b^2}{r^2}\right) \quad \text{..... } Eqn.1$$

$$\sigma_\theta = \frac{p_i b^2}{a^2 - b^2}\left(1 + \frac{a^2}{r^2}\right) - \frac{p_o a^2}{a^2 - b^2}\left(1 + \frac{b^2}{r^2}\right) \quad \text{..... } Eqn.2$$

The geometry, loading and material properties of this problem are presented in the figure below.

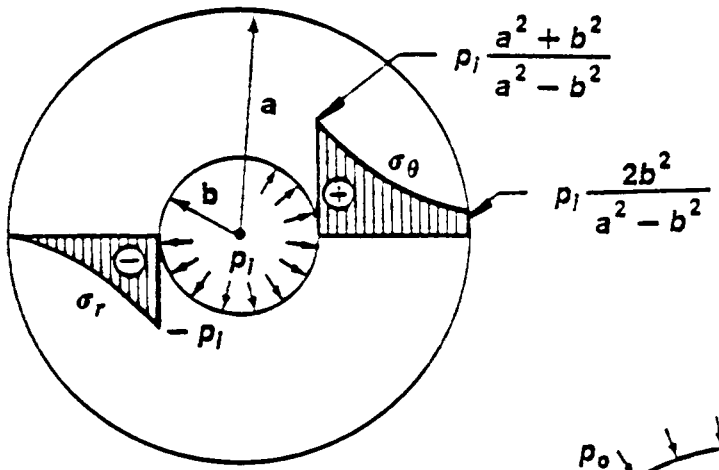

Stresses due to internal pressure

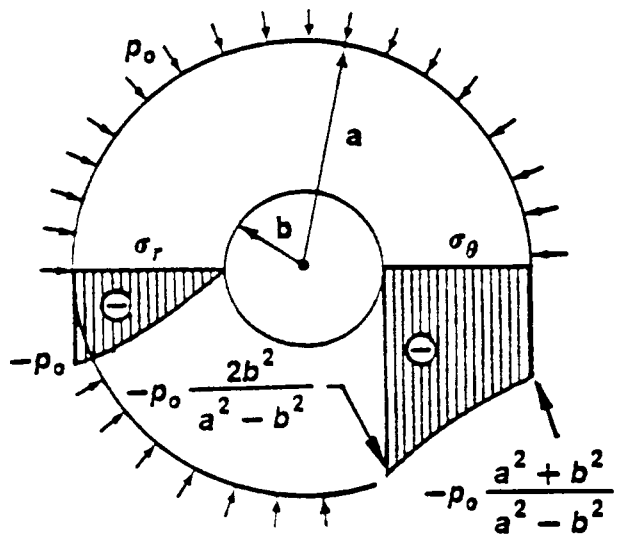

Stresses due to external pressure

a = 22.5 in, b = 17.5 in, E = 1.0×10^7 $\nu = 0.3$

Three different cases of pressurizations have been considered here.

(i) internal pressure P_i = 5.0 psi

The stresses due to internal pressure are listed in Table 6.15 and plotted in Figure 6.12 for comparison.

(ii) external pressure P_o = 2.0 psi

The stresses due to external pressure are listed in Table 6.16 and plotted in Figure 6.13 for comparison.

(ii) internal pressure P_i = 5 psi and external pressure P_o = 2.0 psi

The stresses due to internal pressure and external pressure are listed in Table 6.17 and plotted in Figure 6.14 for comparison.

From Tables 6.15, 6.16 and 6.17 and Figures 6.12, 6.13 and 6.14, it is found that the transverse normal stresses (σ_r) predicted by current work are in good agreement with the analytical solutions. However, the transverse shear stresses (σ_θ) present about 10% to 50% discrepancy from the analytical solutions. The possible reason for this discrepancy is that in 2D shell element approach the surface pressure is loaded in the mid-surface instead of the actual pressurized surface(s) which would enlarge the hoop stress in case of internal pressure loading and would reduce the hoop stress in case of external pressure loading. Based upon this explanation, it is understood that the FEM hoop stresses of Table 6.15 and Figure 6.12 are all greater than the analytical values. In this case, pressure is applied on the mid-surface instead of the inner surface of the cylinder which gives a larger membrane force resulting in a larger hoop

stress discrepancy. This discrepancy is expected to be small in a thin curve shell analysis.

In spite of the said hoop stress discrepancy, the results for the transverse normal stress (σ_r) through the wall-thickness of a pressurized curve thick-wall vessel by a single shell element are very good. Usually, this can only be achieved by a multi-layer solid element simulation.

Table 6.15 Stresses due to internal pressure

r	σ_θ (psi)		σ_r (psi)	
(in)	FEM	Eqn.2	FEM	Eqn.1
22.5	20.01	15.315	0.0	0.0
21.875	20.10	15.756	-0.21	-0.444
21.250	20.34	16.240	-0.78	-0.927
20.625	20.68	16.768	-1.58	-1.455
20.000	21.08	17.346	-2.50	-2.034
19.375	21.47	17.981	-3.42	-2.669
18.750	21.81	18.681	-4.22	-3.369
18.125	22.06	19.455	-4.79	-4.142
17.500	22.15	20.313	-5.0	-5.0

NOTE : FEM is present work with 2x2Q8 mesh.

Table 6.16 Stresses due to external pressure

r	σ_θ (psi)		σ_r (psi)	
(in)	FEM	Eqn.2	FEM	Eqn.1
22.5	-7.14	-8.125	-2.000	-2.000
21.875	-7.18	-8.303	-1.91	-1.823
21.250	-7.28	-8.496	-1.69	-1.629
20.625	-7.42	-8.707	-1.37	-1.418
20.000	-7.57	-8.938	-1.00	-1.187
19.375	-7.73	-9.193	-0.63	-0.932
18.750	-7.87	-9.473	-0.31	-0.653
18.125	-7.96	-9.782	-0.09	-0.343
17.500	-8.05	-10.125	0.0	0.0

NOTE : FEM is present work with 2x2Q8 mesh.

Table 6.17 Stresses due to inner pressure and external pressure

r	σ_ϑ (psi)		σ_r (psi)	
(in)	FEM	Eqn.2	FEM	Eqn.1
22.5	12.86	7.188	-2.0	-2.0
21.875	12.92	7.454	-2.13	-2.266
21.250	13.06	7.744	-2.47	-2.556
20.625	13.27	8.061	-2.95	-2.873
20.000	13.50	8.408	-3.50	-3.220
19.375	13.74	8.789	-4.05	-3.601
18.750	13.95	9.209	-4.53	-4.021
18.125	14.09	9.673	-4.87	-4.485
17.500	14.15	10.1887	-5.0	-5.0

NOTE : FEM is present work with 2x2Q8 mesh.

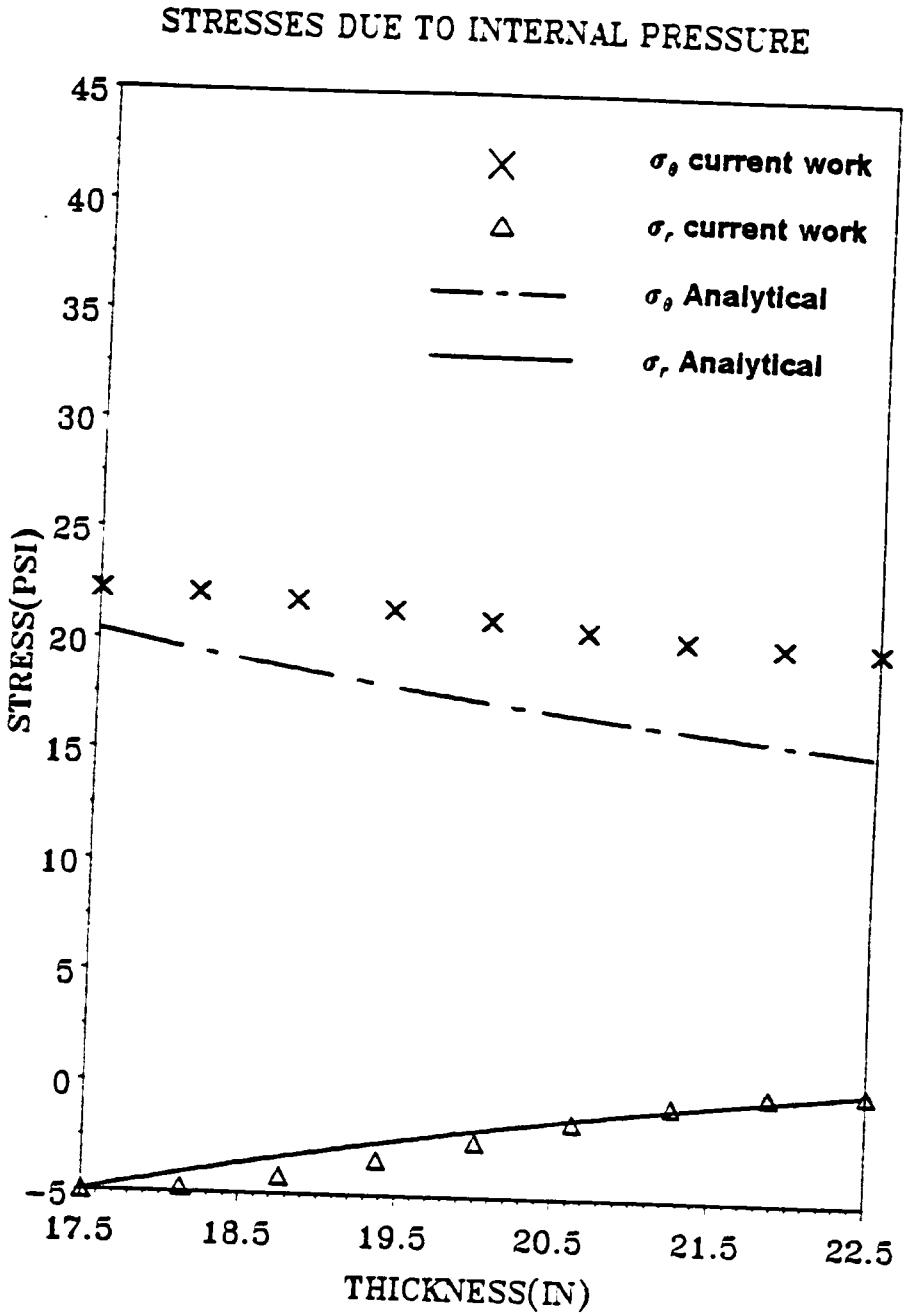

Figure 6.12 Stresses due to inner pressure

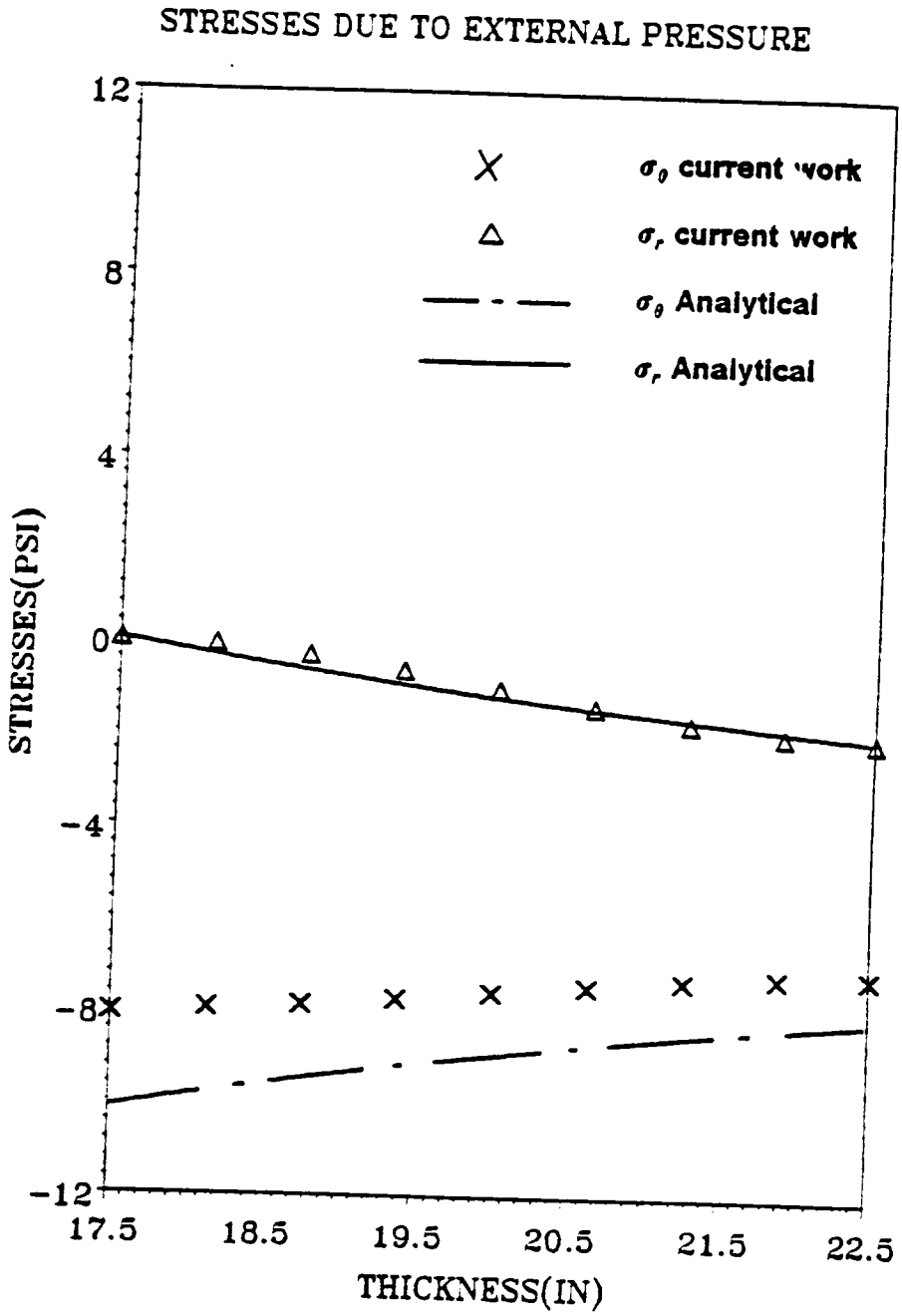

Figure 6.13 Stresses due to external pressure

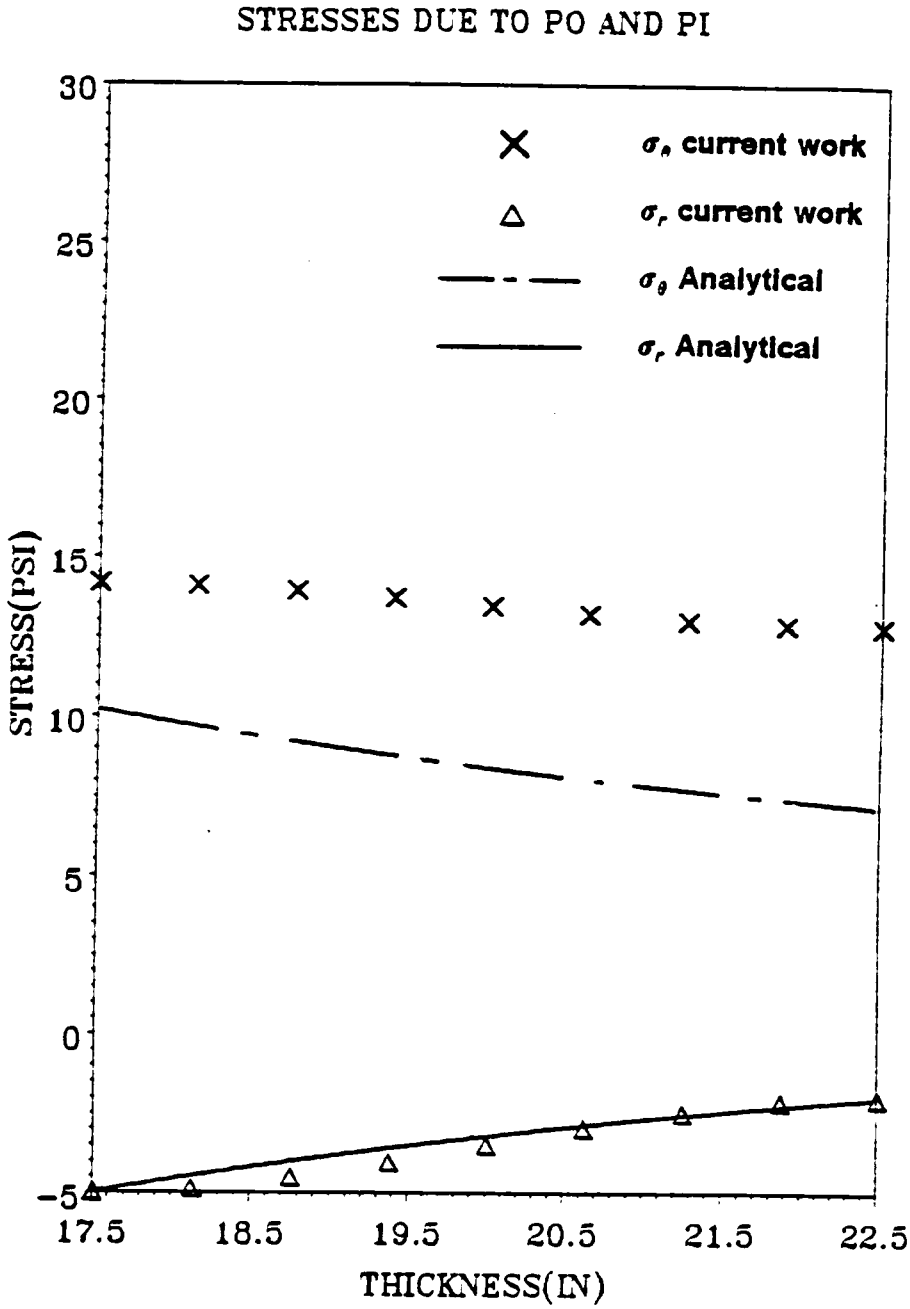

Figure 6.14 Stresses due to inner pressure and external pressure

6.9 PROBLEM 8 : NONLINEAR BENDING OF AN ISOTROPIC PLATE

Nonlinear bending of a clamped isotropic square plate subjected to top surface uniform pressure is investigated to verify the the nonlinear capability of current work. The geometry, loading, material properties, finite element mesh and nondimensional vertical deflection at the center of the plate are shown in Figure 6.15. The displacement of current work are smaller than the analytical solution. This is due to the numerical displacement-hardening error introduced by the modified Newton Raphson method [79].

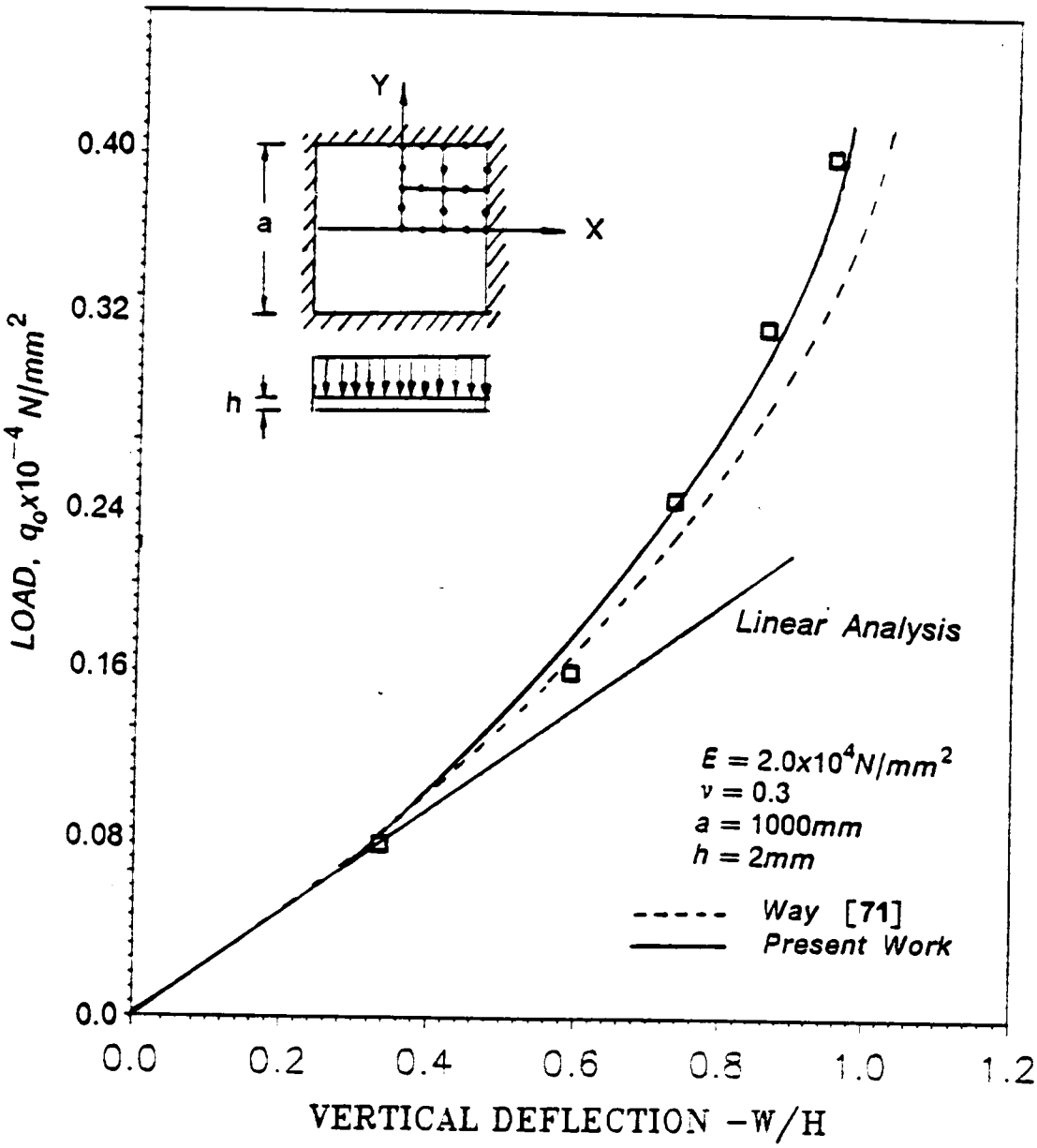

Figure 6.15 Bending of a clamped isotropic square plate under uniform normal pressure

6.10 PROBLEM 9 : NATURAL FREQUENCIES OF SPHERICAL SHELL

The analytical solution for the nondimensionalized fundamental frequencies of a cross-ply laminated Sander's type spherical shell are available in Ref. [71,1], in which, a simply supported spherical shell panel is analyzed. The geometry and material properties are shown in the figure below :

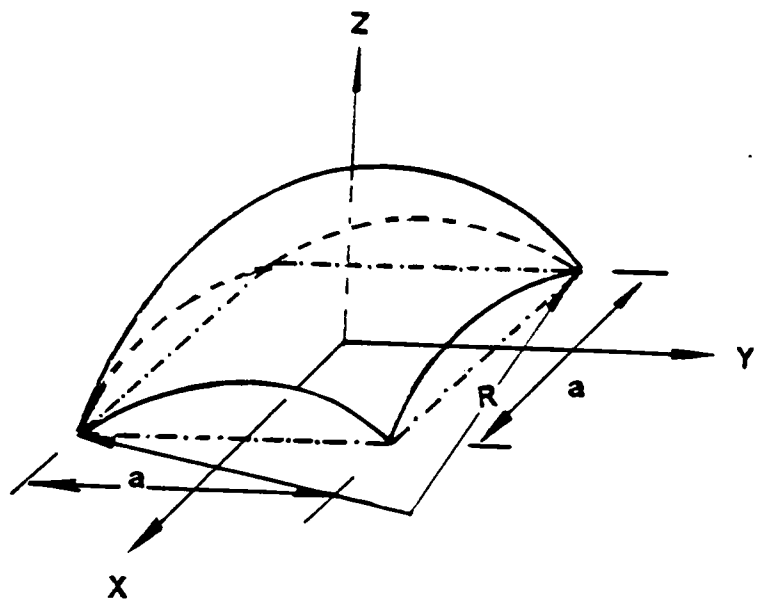

$E_1 = 25.0x10^6$ psi, $E_2 = E_3 = 1.0x10^6$ psi, $G_{12} = G_{13} = 0.5x10^6$ psi,

$G_{23} = 0.2x10^6$ psi, $\nu_{12} = \nu_{13} = \nu_{23} = 0.25$

The nondimensional fundamental natural frequencies of the current work(FEM) are compared with those of the first-order shear deformation theory (FSDT) and higher order deformation theory (HSDT) in Table 6.18 for a wide range of radius-to-panel length ratio. The good correlation of FEM result to the FSDT result verifies the mass matrix developed in current work.

Table 6.18 Nondimensional fundamental frequency of spherical shells

R/a	Method	0/90/0/	0/90/90/0
10	FEM	13.007	13.067
	FSDT	12.215	12.280
	HSDT	11.860	11.840
20	FEM	12.384	12.447
	FSDT	12.176	12.240
	HSDT	11.81	11.79
50	FEM	12.203	12.268
	FSDT	12.165	12.229
	HSDT	11.79	11.78
100	FEM	12.177	12.267
	FSDT	12.163	12.228
	HSDT	11.79	11.78
PLATE	FEM	12.169	12.233
	FSDT	12.162	12.226
	HSDT	11.790	11.780

NOTE: FEM is present work with 2x2Q8 mesh for quarter structure.

6.11 PROBLEM 10 : COMPOSITE CYLINDRICAL SHELL

The geometry, loading and finite element mesh of a clamped cylindrical shell subjected to internal pressure is shown below:

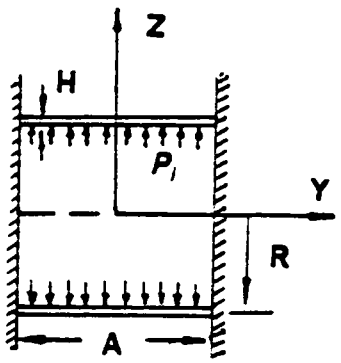

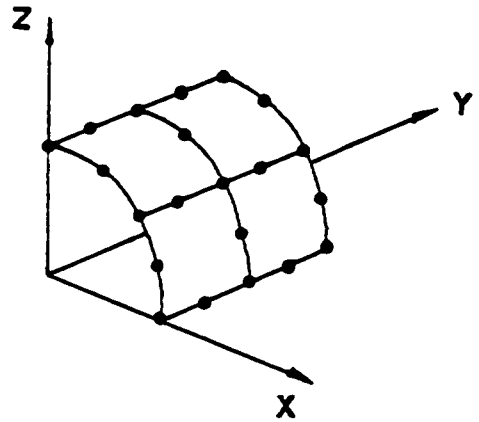

R = 20 in., A = 20 in., H = 1 in., P_i = 2.0403664 psi

The lamina properties are :

$E_1 = 7.5x10^6$psi, $E_2 = 2x10^6$psi,

$G_{12} = 1.25x10^6$psi, $G_{12} = G_{13} = G_{23}$, $\nu_{12} = \nu_{13} = 0.25$

This model is used for both static and transient analysis. In Table 6.19, the center deflections for orthotropic and two-layer (0/90) cross-ply shells are compared with known solutions.

Table 6.19 Comparison of the Center Deflection (inch)

Lamination Scheme	Present Work 2x2Q8	Ref.[1] 2x2Q9	Ref.[72]	Analytical[73]
0°	0.0003706	0.0003727	0.0003666	0.000367
0°/90°	0.0001841	0.0001803	—	—

The center deflections of the same cylindrical shell subjected to an internal impulse pressure of 5000 psi are shown in Figure.6.16, where results for both cross-ply and antisymmetrical angle-ply composite shells are plotted. For the [0/90] cross-ply shell, current work yields a slightly larger center deflection than that of Ref. [74]. However, this discrepancy is within an acceptable range. This verifies the dynamic analysis capability of current work.

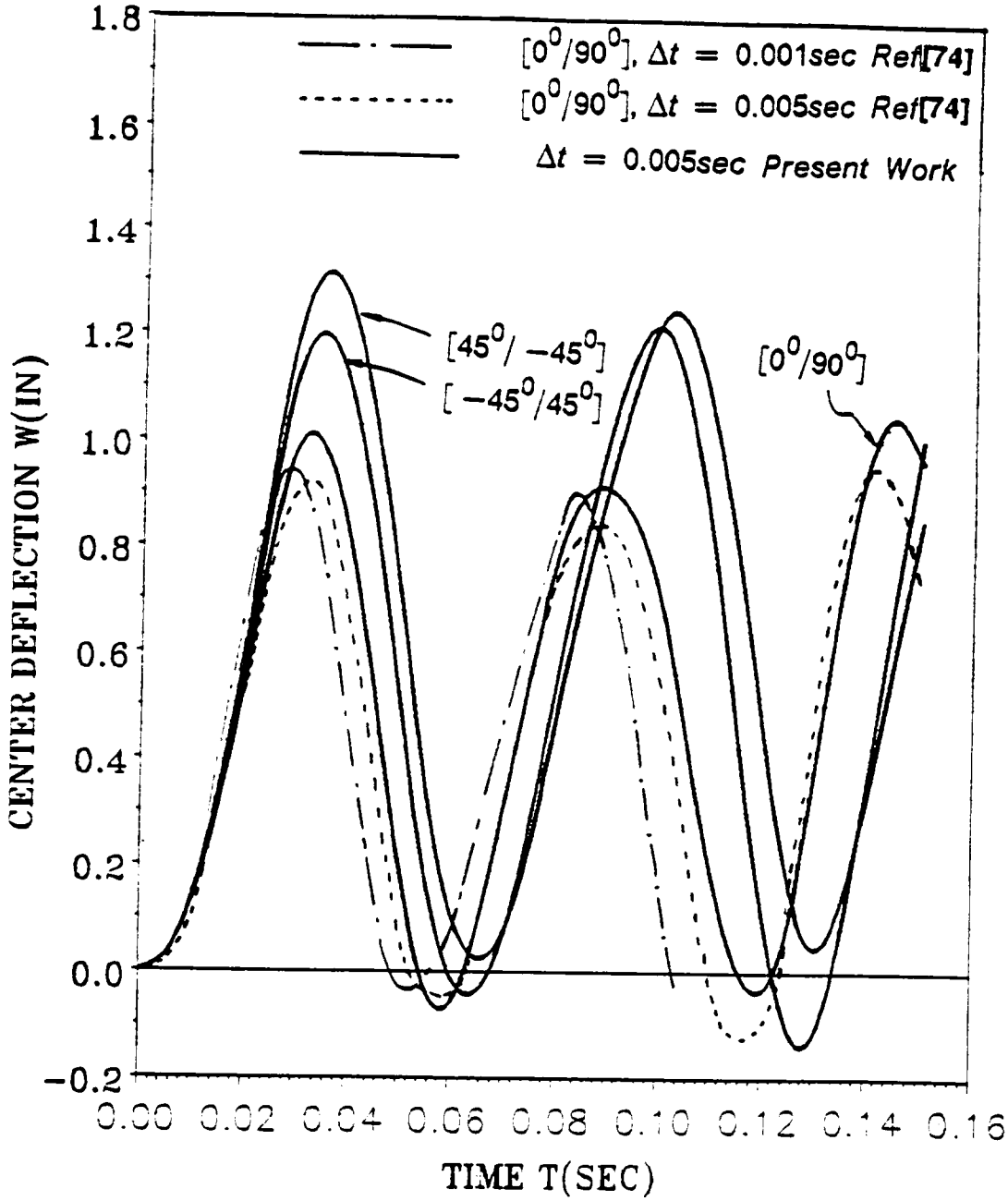

Figure 6.16 Transient responses of a two-layer clamped cylindrical shell under internal impulse pressure

CONCLUSIONS AND RECOMMENDATIONS

7.1 SUMMARY AND CONCLUSIONS

In summary, following important goals have been achieved in this work :

(i) A continuum-based shell element is developed with Updated Lagrangian formulation.

(ii) Nonzero surface boundary conditions and interlaminar shear stress continuity conditions are satisfied.

(iii) The analytical integrations through shell thickness are explicitly formulated.

(iv) Transverse normal stress is included thus completing the stress field computation.

(v) Computational efficiency is increased by the stress enhancement technique.

The transverse shear stresses are also accurately obtained in such a way that the interlaminar shear stress continuity conditions are fully satisfied and peak values of the transverse shear stresses can be located in an inexpensive manner. These rep-

resent very important achievements in the analysis of laminated composite shell structures.

The purpose of structural analysis is more than just to understand its mechanical responses, but also to make an accurate failure/fatigue evaluation such that design changes can be made to ensure the required mechanical functions are performed safely. Since the most commonly used failure criteria are stress-based criteria, it is important to determine the stress field accurately.

However, as stated in the literature review and demonstrated in Chapters 4,5 and 6 of this work, the classical plate theory, first order shear deformation plate theory and some other higher order shear deformation theories either ignore the normal stress or yield often inaccurate transverse shear stresses and fail to satisfy the nonzero surface traction boundary conditions. All the above mentioned theories could not provide an accurate description of the complete stress field.

The newly assumed displacement field and stress recovery technique developed in this work are able to provide a simple and effective tool for a complete and accurate stress field evaluation, which may represent an important contribution to shell finite element development.

7.2 RECOMMENDATIONS

As clearly stated in section 4.3, the whole solution strategy of this work is a refined displacement and stress recovery procedure based on the first-order shear deformation finite element. The transverse deformation parameters a_1, a_2, b_1, b_2, c_1 and c_2 are ignored from the kinematics conditions (equation 4.9 and 5.15) and are recovered during the post-computation (equation 4.18 and equation 5.41), after the averaged displacement components have been computed. Therefore no improvement is accomplished over the existing first-order theory displacements and natural frequencies, but stresses are improved cosiderably. As an extension of this work, one may try to apply this technique to the higher order shear deformation theory proposed by Reddy [5,6] or put the transverse deformation parameters a_1, a_2, b_1, b_2, c_1 and c_2 into the kinematics conditions (equation 4.9 and 5.15) and solve for them directly. Of course, the latter requires much more computational effort.

In addition, one may perform the first-ply and post-first-ply failure analysis using the more accurate stress field obtained by the present work. Comparing with the same failure analysis performed with FSDT stress field, early failure is expected for any surface pressurized or contacted shell structure such as a multi-layer automobile tire or high speed flying missiles made by laminated composite materials. In these cases, pressurization and surface tractions are significant loads, thus transverse normal stress and nonzero transverse shear stress exist in both cases. If this is true, the first-ply failure analysis based upon the FSDT stress field can not provide a conservative design criterion to any laminated composite structure.

APPENDIX A

SHELL LINEAR STIFFNESS

$$k_{11} = A_{11}P_{1111} + A_{22}P_{2121} + A_{44}P_{3131} + A_{55}P_{4141} + A_{66}P_{5151}$$
$$+ A_{12}(P_{2111} + P_{1121}) + A_{16}(P_{5111} + P_{1151}) + A_{26}(P_{5121} + P_{2151}) + A_{45}(P_{4131} + P_{3141})$$

$$k_{12} = A_{11}P_{1112} + A_{22}P_{2122} + A_{44}P_{3132} + A_{55}P_{4142} + A_{66}P_{5152}$$
$$+ A_{12}(P_{2112} + P_{1122}) + A_{16}(P_{5112} + P_{1152}) + A_{26}(P_{5122} + P_{2152}) + A_{45}(P_{4132} + P_{3142})$$

$$k_{13} = A_{11}P_{1113} + A_{22}P_{2123} + A_{44}P_{3133} + A_{55}P_{4143} + A_{66}P_{5153}$$
$$+ A_{12}(P_{2113} + P_{1123}) + A_{16}(P_{5113} + P_{1153}) + A_{26}(P_{5123} + P_{2153}) + A_{45}(P_{4133} + P_{3143})$$

$$k_{14} = A_{44}P_{3134} + A_{45}P_{4131}$$
$$+ B_{12}P_{1126} + B_{22}P_{2126} + B_{16}P_{1156} + B_{26}(P_{2156} + P_{5126}) + B_{66}P_{5156}$$

$$k_{15} = A_{45}P_{3145} + A_{55}P_{4145}$$
$$+ B_{11}P_{1117} + B_{12}P_{2117} + B_{26}P_{2157} + B_{16}(P_{5117} + P_{1157}) + B_{66}P_{5157}$$

$$k_{22} = A_{11}P_{1212} + A_{22}P_{2222} + A_{44}P_{3232} + A_{55}P_{4242} + A_{66}P_{5252}$$
$$+ A_{12}(P_{2212} + P_{1222}) + A_{16}(P_{5212} + P_{1252}) + A_{26}(P_{5222} + P_{2252}) + A_{45}(P_{4232} + P_{3242})$$

$$k_{23} = A_{11}P_{1213} + A_{22}P_{2223} + A_{44}P_{3233} + A_{55}P_{4243} + A_{66}P_{5253}$$
$$+ A_{12}(P_{2213} + P_{1223}) + A_{16}(P_{5213} + P_{1253}) + A_{26}(P_{5223} + P_{2253}) + A_{45}(P_{4233} + P_{3243})$$

$$k_{24} = A_{44}P_{3234} + A_{45}P_{4231}$$
$$+ B_{12}P_{1226} + B_{22}P_{2226} + B_{16}P_{1256} + B_{26}(P_{2256} + P_{5226}) + B_{66}P_{5256}$$

$$k_{25} = A_{45}P_{3245} + A_{55}P_{4245}$$
$$+ B_{11}P_{1217} + B_{12}P_{2217} + B_{26}P_{2257} + B_{16}(P_{5217} + P_{1257}) + B_{66}P_{5257}$$

$$k_{33} = A_{11}P_{1313} + A_{22}P_{2323} + A_{44}P_{3333} + A_{55}P_{4343} + A_{66}P_{5353}$$
$$+ A_{12}(P_{2313} + P_{1323}) + A_{16}(P_{5313} + P_{1353}) + A_{26}(P_{5323} + P_{2353}) + A_{45}(P_{4333} + P_{3343})$$

$$k_{34} = A_{44}P_{3334} + A_{45}P_{4331}$$

$$+ B_{12}P_{1326} + B_{22}P_{2326} + B_{16}P_{1356} + B_{26}(P_{2356} + P_{5326}) + B_{66}P_{5358}$$

$$k_{35} = A_{45}P_{3345} + A_{55}P_{4345}$$

$$+ B_{11}P_{1317} + B_{12}P_{2317} + B_{26}P_{2357} + B_{16}(P_{5317} + P_{1357}) + B_{66}P_{5357}$$

$$k_{44} = A_{44}P_{3434} + D_{22}P_{2626} + D_{26}(P_{2656} + P_{5626}) + D_{66}P_{5656}$$

$$k_{45} = A_{45}P_{3445} + D_{12}P_{2617} + D_{16}P_{2656} + D_{26}P_{2657} + D_{66}P_{5657}$$

$$k_{55} = A_{55}P_{4545} + D_{11}P_{1717} + D_{16}(P_{5717} + P_{1757}) + D_{66}P_{5757}$$

Where the symbol P_{klmn} represents the integration of P^l to P^l over the element surface,i.e.

$$P_{klmn} = \int_A P^l_{kl} P^l_{mn} \, dx_1 dx_2$$

APPENDIX B

P VECTORS

$$\{P_1^j\}_k = \begin{bmatrix} \overline{Q}_{11}^k & \overline{Q}_{12}^k & 0 & 0 & \overline{Q}_{16}^k \\ \overline{Q}_{12}^k & \overline{Q}_{22}^k & 0 & 0 & \overline{Q}_{26}^k \\ 0 & 0 & \overline{Q}_{44}^k & \overline{Q}_{45}^k & 0 \\ 0 & 0 & \overline{Q}_{45}^k & \overline{Q}_{55}^k & 0 \\ \overline{Q}_{16}^k & \overline{Q}_{26}^k & 0 & 0 & \overline{Q}_{66}^k \end{bmatrix}_k \begin{bmatrix} P_{11}^j & P_{12}^j & P_{13}^j & 0 & 0 \\ P_{21}^j & P_{22}^j & P_{23}^j & 0 & 0 \\ P_{31}^j & P_{32}^j & P_{33}^j & P_{34}^j & 0 \\ P_{41}^j & P_{42}^j & P_{43}^j & 0 & P_{45}^j \\ P_{51}^j & P_{52}^j & P_{53}^j & 0 & 0 \end{bmatrix}_k \begin{Bmatrix} u^j \\ v^j \\ w^j \\ \theta_1^j \\ \theta_2^j \end{Bmatrix}_k$$

$$\{P_2^j\}_k = \begin{Bmatrix} (\overline{Q}_{12}^k P_{26} + \overline{Q}_{16}^k P_{56})\theta_1^j + (\overline{Q}_{11}^k P_{17} + \overline{Q}_{16}^k P_{57})\theta_2^j \\ (\overline{Q}_{22}^k P_{26} + \overline{Q}_{26}^k P_{56})\theta_1^j + (\overline{Q}_{12}^k P_{17} + \overline{Q}_{26}^k P_{57})\theta_2^j \\ 0 \\ 0 \\ (\overline{Q}_{26}^k P_{26} + \overline{Q}_{66}^k P_{56})\theta_1^j + (\overline{Q}_{16}^k P_{17} + \overline{Q}_{66}^k P_{57})\theta_2^j \end{Bmatrix}$$

APPENDIX C

SHELL NONLINEAR STIFFNESS

$$k_{11} = E_1(Q_{1111} + Q_{4141} + Q_{7171}) + E_2(Q_{2121} + Q_{5151} + Q_{8181}) + E_3(Q_{3121} + Q_{2131} + Q_{6151} + Q_{6151})$$
$$+ E_5(Q_{2111} + Q_{1121} + Q_{5141} + Q_{4151} + Q_{8171} + Q_{7181}) + E_4(Q_{3111} + Q_{1131} + Q_{6141} + Q_{4161})$$

$$k_{12} = E_1(Q_{1112} + Q_{4142} + Q_{7172}) + E_2(Q_{2122} + Q_{5152} + Q_{8182}) + E_3(Q_{3122} + Q_{2132} + Q_{6152} + Q_{6152})$$
$$+ E_5(Q_{2112} + Q_{1122} + Q_{5142} + Q_{4152} + Q_{8172} + Q_{7182}) + E_4(Q_{3112} + Q_{1132} + Q_{6142} + Q_{4162})$$

$$k_{13} = E_1(Q_{1113} + Q_{4143} + Q_{7173}) + E_2(Q_{2123} + Q_{5153} + Q_{8183}) + E_3(Q_{3123} + Q_{2133} + Q_{6153} + Q_{6153})$$
$$+ E_5(Q_{2113} + Q_{1123} + Q_{5143} + Q_{4153} + Q_{8173} + Q_{7183}) + E_4(Q_{3113} + Q_{1133} + Q_{6143} + Q_{4183})$$

$$k_{22} = E_1(Q_{1212} + Q_{4242} + Q_{7272}) + E_2(Q_{2222} + Q_{5252} + Q_{8282}) + E_3(Q_{3222} + Q_{2232} + Q_{6252} + Q_{6252})$$
$$+ E_5(Q_{2212} + Q_{1222} + Q_{5242} + Q_{4252} + Q_{8272} + Q_{7282}) + E_4(Q_{3212} + Q_{1232} + Q_{8242} + Q_{4262})$$

$$k_{23} = E_1(Q_{1213} + Q_{4243} + Q_{7273}) + E_2(Q_{2223} + Q_{5253} + Q_{8283}) + E_3(Q_{3223} + Q_{2233} + Q_{6253} + Q_{6253})$$
$$+ E_5(Q_{2213} + Q_{1223} + Q_{5243} + Q_{4253} + Q_{8273} + Q_{7283}) + E_4(Q_{3213} + Q_{1233} + Q_{6243} + Q_{4263})$$

$$k_{33} = E_1(Q_{1313} + Q_{4343} + Q_{7373}) + E_2(Q_{2323} + Q_{5353} + Q_{8383}) + E_3(Q_{3323} + Q_{2333} + Q_{6353} + Q_{6353})$$
$$+ E_5(Q_{2313} + Q_{1323} + Q_{5343} + Q_{4353} + Q_{8373} + Q_{7383}) + E_4(Q_{3313} + Q_{1333} + Q_{6343} + Q_{4363})$$

$$k_{14} = F_1Q_{4146} + F_1Q_{5156} + F_5(Q_{5146} + Q_{4156}) + E_3Q_{5164} + E_4Q_{4164} + F_3Q_{6156} + F_4Q_{6146}$$

$$k_{24} = F_1Q_{4246} + F_1Q_{5256} + F_5(Q_{5246} + Q_{4258}) + E_3Q_{5264} + E_4Q_{4264} + F_3Q_{6256} + F_4Q_{6246}$$

$$k_{34} = F_1Q_{4346} + F_2Q_{5356} + F_5(Q_{5348} + Q_{4356}) + E_3Q_{5364} + E_4Q_{4364} + F_3Q_{6356} + F_4Q_{6346}$$

$$k_{15} = F_1Q_{1117} + F_2Q_{2127} + F_5(Q_{1127} + Q_{2117}) + E_3Q_{2135} + E_4Q_{1135} + F_3Q_{3127} + F_4Q_{3117}$$

$$k_{25} = F_1Q_{1217} + F_2Q_{2227} + F_5(Q_{1227} + Q_{2217}) + E_3Q_{2235} + E_4Q_{1235} + F_3Q_{3227} + F_4Q_{3217}$$

$$k_{35} = F_1Q_{1317} + F_2Q_{2327} + F_5(Q_{1327} + Q_{2317}) + E_3Q_{2335} + E_4Q_{1335} + F_3Q_{3327} + F_4Q_{3317}$$

$$k_{44} = G_1Q_{4646} + G_2Q_{5656} + G_5(Q_{5646} + Q_{4656}) + F_3(Q_{5664} + Q_{4656}) + F_4(Q_{4664} + Q_{6446})$$

$$k_{45} = G_2Q_{2627} + G_5(Q_{2617} + Q_{5647})$$

$$k_{55} = G_1Q_{1717} + G_2Q_{2727} + G_5(Q_{2717} + Q_{1727}) + F_3(Q_{2735} + Q_{3527}) + F_4(Q_{1735} + Q_{3517})$$

Where the symbol Q_{klmn} represents the integration of q^i to q^j over the element surface,i.e.

$$Q_{klmn} = \int_A q^i_{kl}\, q^j_{mn}\, dx_1 dx_2$$

APPENDIX D

SHELL CONSISTENT MASS MATRIX

$$m_{11} = I_1 \int \phi_i \phi_j (v'_{11} v^i_{11} + v'_{21} v^i_{21} + v'_{31} v^i_{31})\, dx_1 dx_2$$

$$m_{12} = I_1 \int \phi_i \phi_j (v'_{11} v^i_{12} + v'_{21} v^i_{22} + v'_{31} v^i_{32})\, dx_1 dx_2$$

$$m_{13} = I_1 \int \phi_i \phi_j (v'_{11} v^i_{13} + v'_{21} v^i_{23} + v'_{31} v^i_{33})\, dx_1 dx_2$$

$$m_{21} = I_1 \int \phi_i \phi_j (v'_{12} v^i_{11} + v'_{22} v^i_{21} + v'_{32} v^i_{31})\, dx_1 dx_2$$

$$m_{22} = I_1 \int \phi_i \phi_j (v'_{12} v^i_{12} + v'_{22} v^i_{22} + v'_{32} v^i_{32})\, dx_1 dx_2$$

$$m_{23} = I_1 \int \phi_i \phi_j (v'_{12} v^i_{13} + v'_{22} v^i_{23} + v'_{32} v^i_{33})\, dx_1 dx_2$$

$$m_{31} = I_1 \int \phi_i \phi_j (v'_{13} v^i_{11} + v'_{23} v^i_{21} + v'_{33} v^i_{31})\, dx_1 dx_2$$

$$m_{32} = I_1 \int \phi_i \phi_j (v'_{13} v^i_{12} + v'_{23} v^i_{22} + v'_{33} v^i_{32})\, dx_1 dx_2$$

$$m_{33} = I_1 \int \phi_i \phi_j (v'_{13} v^i_{13} + v'_{23} v^i_{23} + v'_{33} v^i_{33})\, dx_1 dx_2$$

$$m_{14} = -I_2 \int \phi_i \phi_j v^i_{21}\, dx_1 dx_2$$

$$m_{15} = I_2 \int \phi_i \phi_j v^i_{11}\, dx_1 dx_2$$

$$m_{24} = -I_2 \int \phi_i \phi_j v^i_{22}\, dx_1 dx_2$$

$$m_{25} = I_2 \int \phi_i \phi_j v^i_{12}\, dx_1 dx_2$$

$$m_{34} = -I_2 \int \phi_i \phi_j v^i_{23}\, dx_1 dx_2$$

$$m_{35} = I_2 \int \phi_i \phi_j v^i_{13}\, dx_1 dx_2$$

$$m_{41} = -I_2 \int \phi_i \phi_j v^i_{21}\, dx_1 dx_2$$

$$m_{51} = I_2 \int \phi_i \phi_j v^i_{11}\, dx_1 dx_2$$

$$m_{42} = -I_2 \int \phi_i \phi_j v^i_{22}\, dx_1 dx_2$$

$$m_{52} = I_2 \int \phi_i \phi_j v^i_{12}\, dx_1 dx_2$$

$$m_{43} = -I_2 \int \phi_i \phi_j v^i_{23}\, dx_1 dx_2$$

$$m_{53} = I_2 \int \phi_i \phi_j v^i_{13}\, dx_1 dx_2$$

$$m_{44} = I_3 \int \phi_i \phi_j \, dx_1 dx_2$$

$$m_{45} = 0$$

$$m_{55} = I_3 \int \phi_i \phi_j \, dx_1 dx_2$$

Where ϕ_i is the shape fuction of node i.

REFERENCES

1. Reddy, J.N., Energy and Variational Methods in Applied Mechanics, John Wiley, N.Y., 1984.

2. Pipes, B.R. and Pagano, N.J., "Interlaminar stresses in composite laminates under uniform axial extension," J. Comp. Materials, pp.538-548, Oct. 1970.

3. Pipes, B.R. and Daniel, I.M., "Moire analysis of the interlaminar shear edge effect in laminated composites," J. Comp. Materials, pp. 255-259, April 1971.

4. Wang, S.S. and Choi, I., "Boundary-layer effects in composite laminates: part I-free-edge stress singularities," J. Appl. Mech., Vol. 49, p. 49, Sept. 1982.

5. Reddy, J.N., "A refined nonlinear theory of plates with transverse shear deformation," J. Solids Struct., Vol. 20, pp. 881-896, 1984.

6. Reddy, J.N., "A simple higher order theory for laminated composite plates," J. Appl. Mech., Vol. 51, pp. 745-752, 1985.

7. Reddy, J.N., "A generalization of two-dimensional theory of laminated composite plates," Commun. Appl. Numer. Methods, Vol. 3, pp. 173-180, 1987.

8. Reddy, J.N., Barbero, E.J. and Teply, J.L., "A generalized laminate theory for the analysis of composite laminates," Report No. VPI-E-88.17, 1988.

9. Naghdi, P.M., "A survey of recent progress in the theory of elastic shells," Appl. Mech. Rev., Vol. 19, P. 365, 1956.

10. Bert, C.W., "Dynamices of composite and sandwich panels - parts I and II,"(corrected title), Shock Vib. Dig., Vol. 8, No. 10, pp. 37-48 and Vol. 8, No. 11, pp. 15-24, 1976.

11. Bert, C.W., "Analysis of shell," in Analysis & Performance of Composites, Broutman, L.J. (ed.), Wiley, New York, pp. 207-258, 1980.

12. Love, A.E.H., "On the samll free vibrations and deformations of the elastic shells," Phil. Trans. Roy. Soc. (London), Ser. A, Vol. 17, pp. 491-546, 1888.

13. Ambartsumyan, S.A., "Calculation of laminated anisotropic shells," Izvestia Akademiia Nauk Armenskoi SSR, Ser. Fiz. Mat. Est. Tekh. Nauk., Vol. 6, No. 3, p. 15, 1953.

14. Ambartsumyan, S.A.,Theory of Anisotropic Shells, Moscow, 1961; English Translation, NASA TT F-118, May 1964.

15. Dong, S.B.,Pister, K.S. and Taylor,R.L., "On the theory of laminated anisotropic shells and plates," J. of Aero. Sci., Vol. 29, p. 969, 1962.

16. Cheng, S. and Ho, B.P.C., "Stability of heterogeneous anisotropic cylindrical shells under combined loading," AIAA J., Vol. 1, No. 4, p. 892, 1963.

17. Flugge, W., Stresses in Shells, Springer, Berlin, Germany, 1960.

18. Widera, G.E.O. and Chung, S.W., "A theory for nonhomogeneous anisotropic cylindrical shells," J. Appl. Math. & Phy., Vol. 21, p. 378, 1970.

19. Widera, G.E.O. and Logan, D.L., "Refined theories for nonhomogeneous anisotropic cylindrical shells: part I - derivation," J. Eng. Mech. Div., ASCE, Vol. 106, No. EM6, P. 1053, 1980.

20. Bert, C.W. and Reddy, V.S., "Cylindrical shells of bimodulus materil," J. Eng. Mech. Div., ASCE, Vol. 8, No. EM5, p. 675, 1982.

21. Gulati, S.T. and Essenberg, F., "Effects of anisotropy in axisymmetric cylinderical shells," J. Appl. Mech., Vol. 34, P. 650, 1967.

22. Zukas, J.A. and Vinson, J.R., "Laminated Transversely isotropic cylindrical shells," J. Appl. Mech., Vol. 38, p. 400, 1971.

23. Dong, S.B. and Tso, F.K.W., "On a laminated orthotropic shell theory including transverse shear deformation," J. Appl. Mech., Vol. 39, p. 1091, 1972.

24. Whitney, J.M. and Sun, C.T., "A higher order theory for extensional motion of laminated anisotropic shells and plates," J. Sound Vib., Vol. 30, p. 85, 1973.

25. Reddy, J.N., "Exact solution of moderately thick laminated shells," J. Eng. Mech., ASCE, Vol. 110, P. 794, 1984.

26. Dong, S.B., "Analysis of laminated shells of revolution," J. Eng. Mech. Div., Vol. 92, No. EM6, p. 135, 1966.

27. Dong, S.B. and Selna, L.G., "Natural vibrations of laminated orthotropic shells of revolution," J. Comp. Mater., Vol.4(1), p. 2, 1970.

28. Wilson, E.A. and Parsons, B., "The finite element analysis of filament-reinforced axisymmetric bodies," Fibre Science & Tech., Vol. 2, p. 155, 1969.

29. Schmit, L.A. and Monforton, G.R., "Finite element analysis of sandwich plate and laminate shells with laminates faces," AIAA J., Vol. 8, p. 1454, 1970.

30. Panda, S.C. and Natarajan, R., "Finite element analysis of aminated shells of revolution," Computer & Structures, Vol. 6, p. 61, 1976.

31. Shivakumar, K.N. and Krishna Murty, A.V. Krishna, "A high precision ring element for vibrations of laminated shells," J. Sound & Vib., Vol. 58, No. 3, P. 311, 1978.

32. Rao, K.P., "A rectangular anisotropic shallow thin shell finite element ," Comp. Meth. Appl. Mech. Eng., Vol. 15, p. 13, 1978.

33. Seide, P. and Chang, P. H. H., "Finite element analysis of laminated plates and shells," NASA CR-157106, 1978.

34. Venkatesh, A. and Rao, K.P., "A doubly curved quadrilateral finite element for the analysis of laminated anisotropic thin shell of revolution," Computer & Structures, Vol. 12, p. 825, 1980.

35. Hsu, H.S., Reddy, J.N. and Bert, C.W., "Thermoelasticity of circular cylindrical shells laminated of bimodulus composite materials," J. Thermal Stresses, Vol. 4, No. 2, p. 115, 1981.

36. Reddy, J.N., "Bending of laminated anisotropic shells by a shear deformable finite element," Fiber Sci. & Tech., Vol. 17, p. 9, 1982.

37. Chao, W.C. and Reddy, J.N., "Geometrically nonlinear analysis of layered composite plates and shells," Report No. VPI-E-83-10, Virginia Polytechnic Institute & State Univ., Blacksburg, VA.

38. Reddy, J.N. and Chandrashekhara, K., "Geometrically nonlinear transient analysis of laminated double curved shells," Intl. J. Nonlin. Mech., Vol. 20, No. 2, p. 79, 1985.

39. Noor, A.K. and Hartley, S.J., "Nonlinear shell analysis via mixed isoparametric elements," Computer & Structures, Vol. 7, p. 615, 1977

40. Noor, A.K. and Anderson, C.M., "Mixed isoparametric finite element models of laminated composite shells," Comp. Meth. Appl. Mech. Eng., Vol. 11, p. 255, 1977.

41. Noor, A. K., "Shear flexible finite element model of laminated composite plates and shells," NASA TN, D8044.

42. Chang, T.Y. and Sawamiphakdi K., "Large deformation analysis of laminated shells by finite element method," Computer & Structures, Vol. 13, pp. 331-340, 1981.

43. Chao W.C. and Reddy J.N., "Analysis of laminated composite shells using a degenerated 3D element," Int. J. Num. Meth. Eng., Vol. 20, pp. 1991-2007, 1984.

44. Liao, C.L, "An incremental total lagrangian formulation for general anisotropic shell-type structures," Ph.D. Thesis, VPI&SU, Blacksburg, VA, 1987.

45. Liao, C.L., Reddy, J.N. and Engelstad, S.P., "A solid-shell transition element for geometrically non-linear analysis of laminated composite structures," Int. J. Num. Meth. Eng., Vol. 26, pp. 1843-1854, 1988.

46. Reddy, J.N., "Bending of Imaninated anisotropic shells by a shear deformable finite element," Fibre Sci. Tech., Vol. 17, pp. 9-24, 1982.

47. Zienkiewicz, O.C., The Finite Element Method,McGraw-Hill, N.Y., 1977.

48. Greene, B.E., Strome, D.R. and Weikei, R.C., "Application of the stiffness method to the analysis of shell structure," Proc. Avi. Conf. Amer. Soc. Mech. Eng., Los Angeles, March 1961.

49. Ahmad, S., Iron, B.M. and Zienkiewicz, O.C., "Curved thick shell and membrane elements with particular reference to axi-symmetric problems," Proc. 2nd Conf. Matrix Methods in Structural Mechanics, Wright-Patterson A.F.Base, Ohio, 1968.

50. Ahmad, S., "Curved finite elements in the analysis of solid, shell and plate structures," Ph.D. Thesis, Univ. of Wales, Swansea, 1969.

51. Ahmad, S., Iron, B.M. and Zienkiewicz, O.C., "Analysis of thick and thin shell structures by curved elements," Int. J. Num. Meth. Eng., Vol. 2, pp. 419-451, 1970.

52. Bathe K.J. and Bolourchi, "A geometrical and material nonlinear plate and shell element," J. Computer & Structures, Vol. 11, pp. 23-48, 1980.

53. Pagano, N.J. and Pipes, B.R., "The influence of stacking sequence on laminate strength," J. Comp. Material, pp. 50-57, Jan. 1971.

54. Chao, W.C., "Geometrically nonlinear analysis of layered anisotropic plates and shells," PH.D. Thesis, VPI&SU, Blacksburg, VA 1983.

55. Bathe, K.J., Finite Element Procedures in Engineering Analysis, Southeast Book Co., 1982.

56. Bathe, K.J., "NONSAP - A nonlinear structure analysis program," Nuclear Eng. & Design, Vol. 29, pp. 266-293, 1974.

57. Jones, R.M., "Mechanics of composite materials," McGraw-Hill Book Co., 1975.

58. Fedrerick, D. and Chang, T.S., Continuum Mechanics, Scientific Publishers, Boston, 1965.

59. Roak, R.J. and Young W.C., Formulas for Stress and Strain, Fifth Ed., Mc-Graw-Hill Int. Book Comp., 1975.

60. "ABAQUS user's manual," Hibbit, Karlsson & Sorensen, Inc. Verson 4.6, 1987.

61. Timoshenko S. and Young D.H., Elements of Strength of Materials, 5th editon, 1968.

62. Reddy, J.N., Barbero, E.J. and Teply, J.L, "A generalized laminated theory for the analysis of composite laminates," Report No. VPI-E-88.17, Blacksburg, June 1988.

63. Cook, R.D. and Young, W.C., Advanced Mechanics of Materials, Macmillan Publishing Comp., New York, 1985.

64. Ahmad,S., Irons,B.M. and Zienkiewicz, O.C., "Analysis of thick and thin shell structures by curved finite elements," Int. J. Num. Meth. Eng., Vol. 2, pp. 419-451, 1970.

65. Zienkiewicz, O.C., Taylor, R.L. and Too, J.M., "Reduced integration technique in general analysis of plates and shells," Int. J. Num. Meth. Eng., Vol. 3, pp. 275-290, 1971.

66. Pawsey, S.F. and Clough, R.W., "Improved numerical integration of thick shell finite elements," Int. J. Num. Meth. Eng., Vol. 3, pp. 575-586, 1971.

67. Sander, G and Idelsohn, S., "A family of conforming finite elements for deep shell analysis," Int. J. Num. Meth. Eng., Vol. 18, pp.363-380, 1982.

68. Gibson, J.E., The Design of Cylinderical Shell Roofs, Spon, London, 1961.

69. Kiciman, O.K. and Popov, E.P., "A general finite element model for shells of arbitrary geometry," Comput. Meths. Appl. Mech. Engrg., Vol. 13, pp. 45-58, 1978.

70. Kawai, T. and Yoshimura, N., "Analysis of large deflection of plates by the finite element method," Int. J. Num. Meth. Eng., Vol. 1, pp. 123-133, 1969.

71. Liu, C.F., "Geometrically nonlinear analysis of composite laminates using a refined shear deformation shell theory," Ph.D. Thesis, VPI&SU, Blacksburg, VA, 1985.

72. Rao, K.P., "A rectangular laminated anisotropic shallow thin shell finite," Compt. Methods Appl. Mech. Eng., Vol. 15, pp. 13-33, 1978

73. Timoshenko, S. and Woinowsky-Krieger, S., Theory of Plates and Shells, 2nd Ed., 1959.

74. Chandrashekhara, K., "Geometric and material nonlinear analysis of laminated composite and shells," Ph.D. thesis, VPI&SU, Blacksburg, VA, 1985.

75. Sokolnikoff, I.S., Mathematical Theory of Elasticity, 2nd ed., McGraw-Hill, New York, 1956.

76. Pagano, N.J., "On the calculation of interlaminar normal stress in composite laminates," J. of Composite Material, Vol. 8, pp 65-82, 1974.

77. Meirovitch, L., Computational Method in Structural Dynamics, Sijthoff & Noordhoff, The Netherlands, 1980.

78. Pagano, N.J., "Exact solutions for rectangular bidirectional composites and sandwich plates," J.Composite Material., Vol. 4, pp. 20-24, 1970.

79. Bathe, K.J. and Cimento, A.P., "Some practical procedures for the solution of nonlinear finite element equations," J. Comp. Meth. Appl. Mech. & Eng., Vol. 22, pp. 59-85, 1980.

The vita has been removed from the scanned document